The circ_0002538/miR-138-5p/plasmolipin axis regulates Schwann cell migration and myelination in diabetic peripheral neuropathy

Yu-Tian Liu[1, #], Zhao Xu[1, #], Wei Liu[2], Sen Ren[1], He-Wei Xiong[1], Tao Jiang[1], Jing Chen[1], Yu Kang[1], Qian-Yun Li[1], Zi-Han Wu[1], Hans-GüNther Machens[3], Xiao-Fan Yang[1, *], Zhen-Bing Chen[1, *]

https://doi.org/10.4103/1673-5374.355979

Date of submission: February 2, 2022

Date of decision: March 18, 2022

Date of acceptance: August 2, 2022

Date of web publication: October 11, 2022

From the Contents

Graphical Abstract

circ_0002538 promotes PLLP expression by sponging miR-138-5p in Schwann cells

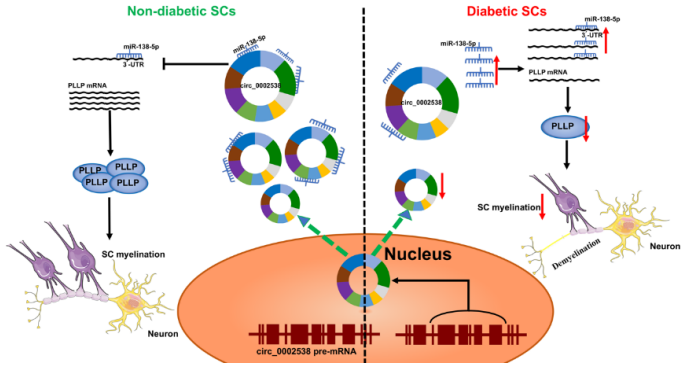

Abstract

Circular RNAs (circRNAs) play a vital role in diabetic peripheral neuropathy. However, their expression and function in Schwann cells in individuals with diabetic peripheral neuropathy remain poorly understood. Here, we performed protein profiling and circRNA sequencing of sural nerves in patients with diabetic peripheral neuropathy and controls. Protein profiling revealed 265 differentially expressed proteins in the diabetic peripheral neuropathy group. Gene Ontology indicated that differentially expressed proteins were mainly enriched in myelination and mitochondrial oxidative phosphorylation. A real-time polymerase chain reaction assay performed to validate the circRNA sequencing results yielded 11 differentially expressed circRNAs. circ_0002538 was markedly downregulated in patients with diabetic peripheral neuropathy. Further *in vitro* experiments showed that overexpression of circ_0002538 promoted the migration of Schwann cells by upregulating plasmolipin (PLLP) expression. Moreover, overexpression of circ_0002538 in the sciatic nerve in a streptozotocin-induced mouse model of diabetic peripheral neuropathy alleviated demyelination and improved sciatic nerve function. The results of a mechanistic experiment showed that circ_0002538 promotes PLLP expression by sponging miR-138-5p, while a lack of circ_0002538 led to a PLLP deficiency that further suppressed Schwann cell migration. These findings suggest that the circ_0002538/miR-138-5p/PLLP axis can promote the migration of Schwann cells in diabetic peripheral neuropathy patients, improving myelin sheath structure and nerve function. Thus, this axis is a potential target for therapeutic treatment of diabetic peripheral neuropathy.

Key Words: circ_0002538; circRNA sequencing; competing endogenous RNAs; demyelination; diabetic peripheral neuropathy; miR-138-5; myelination; plasmolipin; protein profiling; Schwann cells

Introduction

Diabetes mellitus is a major global health concern affecting more than 9% of the global population, and this is expected to increase over time (Feldman et al., 2019a). The most common complication of diabetes mellitus is diabetic peripheral neuropathy (DPN), which affects approximately 50% of people with diabetes during their lifetime (Pop-Busui et al., 2017). DPN is the key initiating factor of diabetic foot conditions that can lead to nontraumatic lower limb amputation, which can seriously reduce the quality of life and patient life expectancy (Feldman et al., 2019a; Selvarajah et al., 2019). DPN is characterized by pain, paresthesia, and loss of sensation, and is associated with axon atrophy, demyelination, weakened regenerative potential, and the loss of peripheral nerve fibers (Farmer et al., 2012). Although several therapeutic approaches have been introduced in clinical practice, the current DPN treatment has only been found to relieve some symptoms with limited effects (Singh et al., 2014). Current studies have found that the occurrence and development of DPN are largely caused by hyperglycemia, insulin deficiency, and dyslipidemia. However, the molecular mechanisms that lead to demyelination and neurological dysfunction remain unclear. Therefore, clarification of the molecular mechanism that promotes DPN initiation and development has important clinical significance and may lead to more effective treatments for DPN.

Circular RNAs (circRNAs) are a recently characterized type of noncoding RNA. They play a key role in the occurrence and development of many diseases and are highly evolutionarily conserved, stable, and tissue-specific (Zhang et al., 2019; Shi et al., 2020). circRNAs are involved in the modification of transcription or posttranscriptional gene expression, and their mode of action includes protein binding, translation, and microRNA (miRNA) sponges (Wang et al., 2020a). circRNA sequencing in spinal cord tissue and dorsal root ganglia of DPN mice revealed 135 and 15 differentially expressed circRNAs (Zhang et al., 2020; He et al., 2021), respectively, which were associated with the occurrence and development of neuronal abnormalities. However, the characteristics and functions of circRNAs in Schwann cells (SCs) in DPN remain unclear.

In the present study, we used circRNA sequencing and protein profiling analyses of nerve tissues from humans with or without DPN to explore the onset and developmental mechanisms of DPN. circ_0002538 is a circRNA derived from Kelch-like family member 8 (KLHL8) with downregulated expression in circRNA sequencing of nerves from patients with DPN, whose function has not previously been characterized. Moreover, we investigated the role of circ_0002538 in the development of DPN *in vitro* and *in vivo*.

[1]Department of Hand Surgery, Union Hospital, Tongji Medical College, Huazhong University of Science and Technology, Wuhan, Hubei Province, China; [2]Department of Geriatrics, Renmin Hospital of Wuhan University, Wuhan, Hubei Province, China; [3]Department of Plastic and Hand Surgery, Technical University of Munich, Munich, Germany

*Correspondence to: Zhen-Bing Chen, PhD, zbchen@hust.edu.cn; Xiao-Fan Yang, PhD, 2017xh0119@hust.edu.cn.

https://orcid.org/0000-0003-2828-866X (Zhen-Bing Chen); https://orcid.org/0000-0002-0997-0973 (Xiao-Fan Yang)

#Both authors contributed equally to this work.

Funding: *This work was supported by the National Natural Science Foundation of China, Nos. 81772094 (to ZBC), 81974289 (to ZBC); the Key Research and Development Program of Hubei Province, No. 2020BCB031 (to ZBC); and Natural Science Foundation of Hubei Province, No. 2020CFB433 (to YTL).*

How to cite this article: *Liu YT, Xu Z, Liu W, Ren S, Xiong HW, Jiang T, Chen J, Kang Y, Li QY, Wu ZH, Machens HG, Yang XF, Chen ZB (2023) The circ_0002538/miR-138-5p/plasmolipin axis regulates Schwann cell migration and myelination in diabetic peripheral neuropathy. Neural Regen Res 18(7):1591-1600.*

Methods

Ethics statement

This study was approved by the Ethics Committee of Tongji Medical College, Huazhong University of Science and Technology (approval No. IEC 2021-S085, approved on March 31, 2021), and informed consent was obtained from each patient. All animal study protocols were approved by the Animal Care Committee of Huazhong University of Science and Technology (No. 2020-S2665, approved on December 1, 2020). The timeline of the experiment was shown in **Figure 1**.

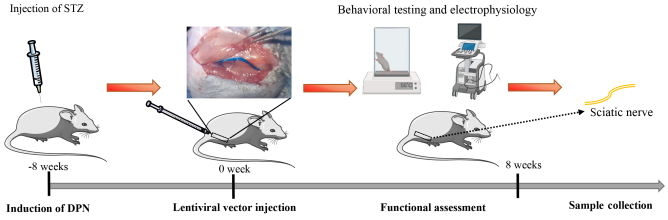

Figure 1 | **Schematic diagram illustrating the timeline of the experiment.**
DPN: Diabetic peripheral neuropathy; STZ: streptozotocin.

Patient tissue specimens

Sural nerve tissues and skin tissues were collected from 29 patients who underwent lower limb amputation at the Union Hospital and Liyuan Hospital of Huazhong University of Science and Technology from 2014 to 2020. The DPN diagnoses were based on a history of diabetes, typical symptoms, abnormal nerve conduction, and the exclusion of neuropathy with causes other than diabetes (Pop-Busui et al., 2017; Feldman et al., 2019b). For diabetic patients without nerve conduction data, we confirmed the diagnosis of DPN by performing a skin biopsy to assess intraepidermal nerve fiber density and utilizing transmission electron microscopy (HT7700, Hitachi, Hitachi, Japan) to confirm neuropathy in the peripheral nerves (Holland et al., 1997). Individuals diagnosed with the following diseases were excluded from the study: neuropathic deficits caused by other diseases, severe peripheral vascular disease, a history of major amputation, other serious chronic medical diseases, or alcohol and drug abuse.

Under a microscope, the epineurium of the sural nerve tissues in the distal calf was stripped, and the nerve bundles were drawn out and immediately snap-frozen in liquid nitrogen for further research. Skin tissues 10 cm above the lateral malleolus were collected for immunofluorescence staining of protein gene product 9.5. The intraepidermal nerve fiber density was calculated according to a previously described method (Vlcková-Moravcová et al., 2008).

Protein profiling analysis

Total proteins were extracted from three pairs of sural nerves from the patients with DPN and individuals without DPN using a protein lysis solution (4% sodium dodecyl sulfate, 100 mM Tris HCl, pH 7.6). We then performed proteomic profiling using the tandem mass tag labeling system (Thermo Fisher Scientific, Waltham, MA, USA). We used a Q Exactive Plus high-resolution mass spectrometer (Thermo Fisher Scientific) to perform tandem mass tag quantitative proteomic analysis, and the software programs Mascot 2.6 (Matrix Science, Boston, MA, USA) and Proteome Discoverer 2.1 (Thermo Fisher Scientific) for library identification and quantitative analysis, respectively (false discovery rate < 0.01).

Gene Ontology and Kyoto Encyclopedia of Genes and Genomes enrichment analysis

The differentially expressed proteins or mRNAs were further analyzed via Gene Ontology (GO) enrichment analysis and Kyoto Encyclopedia of Genes and Genomes (KEGG) analysis for functional prediction. We used GO analysis to annotate the cell components and biological processes based on the GO resource (http://www.geneontology.org), and pathway analysis to explore the enrichment of different pathways based on the KEGG database (http://www.genome.jp/kegg). The protein–protein interaction network analysis was based on the STRING database (https://string-db.org) and visualized using Cytoscape 3.7.2 (Shannon et al., 2003).

circRNA sequencing analysis

The sequencing libraries were constructed as described in a previous report (Lu et al., 2020). Briefly, the total RNA of the aforementioned three pairs of peripheral nerves was prepared using TRIzol reagent (Invitrogen, Carlsbad, CA, USA). The RNA integrity number was evaluated using the Agilent 2200 TapeStation (Agilent Technologies, Eugene, OR, USA), and all RNA samples with an RNA integrity number above 7.0 were subjected to further circRNA sequencing analysis. Before constructing the circRNA sequencing libraries, we used the Epicentre Ribo-Zero rRNA Removal Kit (Illumina, San Diego, CA, USA) to remove ribosomal RNA from the RNA samples, and incubated 40 U RNase R (Epicenter, Madison, WI, USA) with the total RNA at 37°C for 3 hours to remove linear RNA. The libraries were sequenced using the HiSeq-3000 sequencing platform, and we examined the differentially expressed circRNA between the sural nerves from patients with DPN and tissues from individuals without DPN using DESeq2 software (v 2.11.40.2; Bioconductor, Inc.).

Cell culture and treatments

We isolated the primary SCs from human sural nerves (three donors were randomly selected from each group), as previously described, to examine the impaired function of SCs from DPN patients (Wang et al., 2020b). Briefly, the sural nerves were cut into 5-mm-long sections after the epineurium had been stripped and predegenerated in SC culture medium for 10 days. Next, the nerve segments were cut into 2-mm^3 pieces and transferred to a mixture containing Dulbecco's modified Eagle's medium (Thermo Fisher Scientific), 10% fetal calf serum, 0.125% type IV collagenase (Sigma-Aldrich, St. Louis, MO, USA), 1.25 U/mL dispase II (Solaribo, Beijing, China), and 1% penicillin-streptomycin to digest for 18–20 hours. The cells were cultured in SC medium (ScienCell, Carlsbad, CA, USA). The SCs used in the other experiments were purchased from ScienCell Research Laboratories and cultured in SC medium containing 5% fetal calf serum. We added oxidized low-density lipoprotein (ox-LDL, BioVision, Exton, PA, USA) to the culture medium to mimic diabetic conditions. After growing to confluent or subconfluent cell layers, the SCs were cultured for another 6 days to examine plasmolipin (PLLP) expression as previously described (Gillen et al., 1996). SCs were identified via immunofluorescence staining with S100 calcium binding protein B and glial fibrillary acidic protein. HEK293 cells (ACC305, DMSZ, Braunschweig, Lower Saxony, Germany, RRID: CVCL_0045) were cultured in high glucose Dulbecco's modified Eagle's medium containing 10% fetal calf serum and 1% penicillin/streptomycin. The cells were cultured at 37°C in a humidified atmosphere containing 5% CO_2.

Real-time polymerase chain reaction

We extracted the total RNA from the sural nerves and cells using TRIzol reagent (TaKaRa, Kyoto, Japan). The genomic DNA was isolated using a TIANamp Genomic DNA Kit (TianGen Biotech, Beijing, China) according to the manufacturer's instructions. The RNA samples were then reverse transcribed into complementary DNA (cDNA) using the PrimeScript™ RT Reagent (TaKaRa, RR036A). We performed real-time polymerase chain reactions (RT-PCRs) using a 7500 Real-time PCR System (Applied Biosystems, Carlsbad, CA, USA) with the Universal SYBR Green Master Mix (4913914001; Roche, Shanghai, China). β-Actin was used as an internal control. The RT-PCR protocol was as follows: one cycle of 95°C for 10 minutes followed by 40 cycles of 95°C for 15 seconds and 60°C for 1 minute. Gene expression was quantified using the $2^{-\Delta\Delta Ct}$ method (Livak and Schmittgen, 2001). For circRNA, the total RNA was reverse transcribed to cDNA using the PrimeScript™ RT reagent kit (TaKaRa, RR037A). We used convergent and divergent primers to detect the expression of linear RNA and circRNA transcripts. The primers are shown in **Additional Table 1**.

Sanger sequencing

We conducted Sanger sequencing to verify the back-splicing position of circ_0002538. The total RNA was extracted from the SCs and reverse transcribed into cDNA. circ_0002538 was amplified with divergent primers and 2× Taq Master Mix (Vazyme, Nanjing, Jiangsu, China) using qPCR. The qPCR protocol was one cycle of 95°C for 5 minutes followed by 34 cycles of 95°C for 30 seconds, 52°C for 30 seconds, and 72°C for 30 seconds. Then, the base sequences of the products were determined using Sanger sequencing and compared with the data in circBase (http://circrna.org/).

Nuclear and cytoplasmic separation assay

To detect the cellular localization of circRNAs, we extracted RNA from nuclear and cytoplasmic fractions using a cytoplasmic and nuclear RNA isolation kit (Norgen Biotek, Ontario, Canada) according to the manufacturer's protocol. The relative expression levels of circ_0002538 in the nucleus and cytoplasm were detected via RT-PCR. We used GAPDH and U6 small nuclear RNA as internal controls.

Digestion with RNase R

For RNase R digestion, 10 μg of total RNA was incubated with 2 U/μg RNase R (BioVision, Milpitas, CA, USA) at 37°C for 30 minutes. RNAs treated with the same process without RNase R were the mock group. The expression levels of KLHL8 and circ_0002538 were determined via RT-PCR.

Plasmid construction and stable transfection

circ_0002538 cDNA was synthesized by Tsingke Biological Technology (Wuhan, China) and cloned into the GV689 vector (Shanghai GeneChem Co., Ltd., Shanghai, China) to construct overexpression plasmids. Short hairpin RNA (shRNA) for circ_0002538 was designed using the CircInteractome tool and cloned into the GV493 vector (Shanghai GeneChem Co., Ltd.) to construct silencing plasmids. The plasmids for the overexpression and knockdown of PLLP were designed and synthesized by Shanghai Gene Chemical Co., Ltd. Then, the constructed plasmids were packaged into lentivirals (LVs) by Shanghai Gene Chemical Co., Ltd. and cell transfection was performed according to the manufacturer's instructions. The transfected cells were incubated with 2 μg/mL of puromycin (BIOFOX, Nantong, China) for 5 days, and the surviving cells were used as stable transfectants.

Oligonucleotide transfection

miRNA mimics, miRNA inhibitors, and corresponding negative control oligonucleotides were synthesized by RiboBio (Guangzhou, China). The sequences used are listed in **Additional Table 2**. Transfection was carried out using a PECTTM CP Transfection kit (RiboBio) with a final concentration of 50 nM for miRNA mimics and 100 nM for miRNA inhibitors, according to the manufacturer's protocol.

Transwell assay
SC migration was determined using a Transwell chamber (8-μm pore size, Corning, Corning city, NY, USA) according to the manufacturer's protocol. Approximately 2×10^4 cells suspended in 200 μL of serum-free medium were added to the upper chamber, and a total of 650 μL of Schwann medium containing 5% fetal calf serum was added to the lower chamber as a chemical attractant. After a 24-hour incubation period, we evaluated cell migration by counting the number of migrated cells on the lower surface of the chamber in at least five random fields.

Western blot analysis
We tested the expression levels of PLLP protein in SCs and neural tissues via a western blot analysis. The protein was extracted using a radioimmunoprecipitation assay lysis buffer, supplemented with 1% protease inhibitor. Equal amounts of protein (30 μg) were separated in a 10% sodium dodecyl sulfate-polyacrylamide gel and then transferred to polyvinylidene fluoride membranes (Millipore, Darmstadt, Germany). The membranes were blocked in 5% (w/v) bovine serum albumin (Aladdin, Shanghai, China) before incubation with the primary antibodies at 4°C overnight. Then, the membranes were incubated with horseradish peroxidase-conjugated goat anti-rabbit secondary antibody (1:5000, Aspen Biotechnology Co., Ltd., Wuhan, China, Cat# AS1107) for 1 hour at room temperature and visualized using a BioSpectrum Imaging System (UVP, Upland, CA, USA) with the Immobilon ECL substrate kit (Millipore, Darmstadt, Germany). We used primary antibodies specific to PLLP (rabbit, 1:700, Cusabio, Houston, TX, USA, Cat# CSB-PA896501LA01HU). All tests were repeated three times, and the typical images were provided.

RNA pulldown assay
To detect the combination of circRNAs and miRNAs, we performed RNA pulldown assays with biotinylated probes according to the manufacturer's protocol (MCE, Shanghai, China, Cat# HY-K0208). In brief, the biotinylated probe or nonsense control probe (RiboBio) was incubated with M-280 streptavidin magnetic beads (MCE) at room temperature for 2 hours to generate probe-coated beads. Approximately 1×10^7 SCs were crosslinked with 1% paraformaldehyde and then neutralized with 1.25 M glycine. Next, these cells were harvested, lysed, and incubated with probe-coated magnetic beads at 4°C overnight. After being washed, the RNA complexes bound to the beads were eluted and extracted using an Rneasy Mini Kit (Qiagen, Hilden, Germany). Then, the abundance of circRNA or miRNA was evaluated via RT-PCR.

Dual-luciferase reporter assay
We predicted the binding sites of miR-138-5p targeting circ_0002538 and PLLP using RNAhybrid (Rehmsmeier et al., 2004) and TargetScan (McGeary et al., 2019), respectively. The wild-type or mut-circ_0002538 fragment was cloned into the downstream of the luciferase reporter gene of the pMIR-report vector (Promega, Madison, WI, USA), while wild-type or mut-PLLP fragment was inserted into the downstream of the hRluc (Renilla) reporter gene of the psi-check2 vector (Promega). The corresponding plasmid and miRNA mimic were cotransfected into HEK293T cells (5×10^4) seeded in a 12-well plate using Lipofectamine 2000 (Thermo Fisher Scientific). The firefly and Renilla luciferase activity of the cells was quantified using a Dual Luciferase Reporter System Kit (E1910, Promega) according to the manufacturer's instructions.

Prediction of miRNAs targeting circ_0002538 or PLLP
We made predictions regarding the miRNAs that target circ_0002538 or PLLP to ascertain the connection between circ_0002538 and PLLP. The prediction process was conducted by RiboBio (Guangzhou, China). For PLLP, miRNAs predicted by at least three databases (miRDB, miRTarBase, miRWalk, and TargetScan) were considered candidates (Dweep et al., 2011; McGeary et al., 2019; Chen and Wang, 2020; Huang et al., 2020). For circ_0002538, miRNAs predicted by at least two databases (RNAhybrid, miRanda, and TargetScan) were considered candidates (Rehmsmeier et al., 2004; McGeary et al., 2019). We used a Venn diagram to find the common miRNAs (Hulsen et al., 2008).

Induction of diabetes
Due to the high similarity to human and the stability in genes, mice were used to explore circ_0002538 function *in vivo* (Perlman, 2016). Sex is one factor influencing variations in diabetes induction. As estrogen interferes with streptozotocin (STZ) action, female animals are less sensitive to the diabetogenic action of STZ than male animals. Further, male mice are more commonly used in neuroscience research (Beery and Zucker, 2011). As a result, we chose to use male animals for our study. Compared with other age groups, rodents aged 8–9 weeks show maximal induction of diabetes (Goyal et al., 2016). Thus, we used rodents in this age group. The induction of diabetes was conducted as previously described (Wang et al., 2020b). Briefly, a total of 60 male (8-week-old) C57BL/6J mice (specific-pathogen-free level, SiPeiFu, Beijing, China, SCXK2019-0010) were intraperitoneally injected with STZ (Sigma-Aldrich) at a dose of 50 mg/kg for 5 consecutive days. Subsequently, 45 mice had fasting blood glucose levels of 16.7 mM or higher and were thus diagnosed with diabetes (Wang et al., 2020b). Forty mice with significantly increased mechanical and thermal thresholds were diagnosed with DPN (Fan et al., 2020). We randomly selected one side of the sciatic nerve to be injected with circ_0002538 (circ_0002538 group) and injected the other side with LV-vector (vehicle group, $n = 40$).

Surgery and lentiviral vector injection
We injected a LV-vector into the sciatic nerve of the mice with DPN, as previously described (Tannemaat et al., 2008). Briefly, after exposure and isolation of the sciatic nerve, 2.5 μL of lentiviral solution (6×10^6 TU LV-circ_0002538 or LV-GFP vector) was injected into the distal peroneal and tibial branches of the sciatic nerve through the epineurium using a 10-μL Hamilton syringe (Hamilton Co., Reno, NV, USA). Fast Green (Sigma-Aldrich) at a final concentration of 0.1% was added to the lentiviral solution to monitor the injection process and ensure that there was no obvious leakage. A 2.5-μL lentiviral solution containing 6×10^6 TU LV-sh-PLLP or LV-vector was injected into the sciatic nerve of normal mice to determine the role of PLLP. The epineurium at the injection site was repaired with 10-0 nylon sutures under an operating microscope (Xintian Medical Instrument Co., LTD, Zhenjiang, China).

Behavioral testing and electrophysiology
Eight weeks after diabetic induction, we assessed thermal and mechanical nociceptive thresholds via double-blind trials. Before the nociceptive behavior test, the mice were acclimated to the environment for at least half an hour. Mechanical allodynia was assessed using von Frey filaments (Danmic Aesthesio, Campbell, CA, USA), as described previously (Xu et al., 2015; Pan et al., 2019). A brisk withdrawal or flinching of the paw was considered a positive response. The inter-test interval between the two sides of the plantar hind paw was more than 15 minutes, and the 50% force withdrawal threshold was determined for the plantar hind paws using the "up-and-down" method (Chaplan et al., 1994). The thermal nociceptive threshold was assessed using the hot plate test (Masocha et al., 2016). A mouse was placed in a Plexiglas cylinder on a hot plate (Model 7280, Ugo Basile, Gemonio, Italy), and the time required for the stimulus to elicit behavioral changes (such as paw licking, stomping, and withdrawal of the hindpaw) was recorded.

At 8 weeks post-surgery, we evaluated the nerve conduction velocity of the sciatic nerve as a sign of DPN. The sciatic nerve conduction velocity was measured via orthodromic recording techniques, as described previously (Ii et al., 2005; Baum et al., 2016; Wang et al., 2020b). The sensory nerve conduction velocity and motor nerve conduction velocity were calculated using an electromyograph (Nicolet, Madison, WI, USA) according to a previous method (Ii et al., 2005).

Hematoxylin and eosin staining, immunofluorescence analysis
We conducted hematoxylin and eosin (HE) staining to evaluate the intraepidermal nerve fiber density of skin samples from diabetic and non-diabetic individuals. The samples were collected and fixed in paraformaldehyde (4%) within 2 hours of amputation, then dehydrated and embedded in paraffin. Four-micron-thick slices of skin were prepared and subjected to HE (Bioyear, Wuhan, China) to examine subcutaneous nerves in the skin.

We used protein gene product 9.5 to evaluate the number of subcutaneous nerves in the skin samples. Glial fibrillary acidic protein and S100 calcium binding protein B were used to characterize primary SCs extracted from the sural nerves. We used myelin protein zero (MPZ) to locate SCs in the sciatic nerves of the DPN mice. The mice were sacrificed 8 weeks after the operation, and the bioluminescence of green fluorescent protein (GFP)-expressing cells was detected via fluorescence microscopy (Olympus, Tokyo, Japan). Then, the sciatic nerve tissues were collected for morphological analysis. For immunofluorescence analyses, we incubated primary antibodies against protein gene product 9.5 (rabbit,1:300, Proteintech, Wuhan, China, Cat# 14730-1-AP, RRID: AB_2210497), glial fibrillary acidic protein (rabbit, 1:400, Abcam, Carlsbad, CA, USA, Cat# ab68428, RRID: AB_1209224), S100 calcium binding protein B (rabbit, 1:200, Abcam, Cat# ab52642, RRID: AB_882426), and MPZ (rabbit, 1:200, Abcam, Cat# ab183868, RRID: AB_2895675) overnight at 4°C. On the second day, we incubated goat anti-rabbit secondary antibody (Fluor® 488, 1:400, Abcam, Cat# ab150077) at 37°C for 1 hour. We used 2-(4-amidinophenyl)-6-indolecarbamidine dihydrochloride (Biosharp, Wuhan, China, Cat# BL105A) to stain the cell nuclei. Fifteen-micrometer-thick frozen sections of nerve tissues were stained with MPZ. Images were obtained using a fluorescence microscope (Olympus, Tokyo, Japan), with at least three visual fields for each sample.

Transmission electron microscopy
The collected nerves were cut into 5-mm long sections, prefixed in 2.5% glutaraldehyde for 30 minutes, and then postfixed in 1% osmium tettroxide for 1 hour. After dehydration and embedding in epoxy resin, ultrathin sections (60 μm) were prepared and stained with uranyl acetate and lead citrate. Images were captured under a transmission electron microscope (HT7700, Hitachi), and 15 random images were captured for each sample.

Statistical analysis
According to previous methods (Charan and Kantharia, 2013), we determined a minimum sample size of 35 mice. Considering the potential for unexpected death in the experiment and the failure of the STZ-induced diabetes model, we used a sample size of 60.

The data are expressed as the mean ± standard deviation (SD), median (interquartile range (IQR)), or number (%). *P* values were obtained using the paired *t*-test, independent-samples *t*-test, or Fisher's exact test (normal distribution) combined with the Mann-Whitney *U* test (nonnormal distribution) or one-way analysis of variance with Tukey's *post hoc* test (more than two groups). $P < 0.05$ was considered significant, and all statistical analyses were performed using Graphpad Prism 8.0 (GraphPad Software, San Diego, CA, USA, www.graphpad.com).

Results

Characteristics of patients and confirmation of DPN

Twenty-nine patients from two tertiary teaching hospitals were recruited for the study. The median age of the DPN group was 60.0 years (IQR: 56.0–67.0 years) and that of the non-DPN group was 63.5 years (IQR: 55.75–65.0 years). The calf skin and sural nerve were intact in all patients when undergoing amputation. Detailed patient information is provided in **Additional Table 3**. Because some of the patients had not undergone nerve conduction studies, which is the gold standard for diagnosing DPN, we attempted to verify the diagnosis using other indicators. HE staining revealed a decreased number of subcutaneous nerves in the skin of the lateral malleolus in the DPN group (**Additional Figure 1A** and **B**), which was confirmed by protein gene product 9.5 staining of axons (**Additional Figure 1C** and **D**). Furthermore, the numbers of axons and intact myelin sheaths were decreased in the nerves of the DPN group, as shown by transmission electron microscopy (**Additional Figure 1E** and **F**). We thus confirmed DPN in the collected diabetic peripheral nerves.

Impaired myelination and SC migration in the peripheral nerves of the DPN group

Protein profiling analyses were performed on three pairs of peripheral nerves in the DPN and non-DPN groups. A total of 5353 proteins were identified, and 265 proteins were significantly [$P < 0.05$, |fold change (FC)| ≥ 1.3] differentially expressed in the DPN group (**Additional Table 4**), as shown by the hierarchical cluster analysis (**Figure 2A**). GO cellular component analysis indicated that the differentially expressed proteins were mainly found in the mitochondrion and myelin sheath (**Figure 2B** and **Additional Table 5**). GO biological process analysis showed that 390 terms were significantly enriched, among which myelination was potentially related to DPN (**Figure 2C** and **Additional Table 6**). The proteins related to myelination were serine incorporator 5, PLLP, gap junction protein gamma 3, proteolipid protein 1, periaxin, and MPZ. GO molecular function analysis showed significant enrichment in G protein-coupled serotonin receptor binding and protein binding (**Figure 2D** and **Additional Table 7**). KEGG pathway analysis revealed that 77 pathways were significantly enriched, among which oxidative phosphorylation and the glucagon signaling pathways were potentially related to DPN (**Figure 2E** and **Additional Table 8**). **Figure 2F** shows a protein–protein interaction network constructed according to the differentially expressed proteins and showing the interactions among these proteins. These results indicate that abnormal myelination might play an important role in the pathogenesis of DPN.

Myelin is composed of SCs, which are indispensable for the physiological functions of peripheral nerves (Salzer, 2015). Previously, impaired SC migration was reported to contribute to the abnormal myelination and demyelination of peripheral nerves (Anliker et al., 2013; Yi et al., 2019). Thus, we compared the function of SCs from nerves in the DPN and control groups. The primary SCs isolated from the peripheral nerves exhibited a long spindle shape under an optical microscope (**Additional Figure 2A**). These were confirmed via positive immunofluorescence staining of S100 calcium binding protein B and glial fibrillary acidic protein (**Additional Figure 2B**). Cell migration assays showed significantly impaired migration of SCs derived from patients with DPN (**Figure 2G** and **H**).

Characterization of circ_0002538 and its function in SCs

We performed circRNA sequencing for the three pairs of peripheral nerves to uncover their characteristics in the development of DPN. In diabetic peripheral nerves, we identified a total of 15637 circRNAs. A total of 169 circRNAs showed significantly ($P < 0.01$, $q < 0.05$, readings ≥ 50, FC ≥ 2) dysregulated expression in the DPN group: 116 circRNAs had significantly downregulated expression and 53 circRNAs had significantly upregulated expression (**Additional Table 9**). The differentially expressed circRNAs (DEcircRNAs) were directly displayed by hierarchical cluster analysis (**Figure 3A**). The DEcircRNAs were verified using RT-PCR, and the results showed that six circRNAs with downregulated expression and five with upregulated expression were confirmed in the DPN group (**Figure 3B** and **C**). These DEcircRNAs may play an important role in the pathogenesis of DPN.

To further investigate the function of DEcircRNAs in DPN, we focused on circRNA circ_0002538, which showed a 2.14-FC decrease in expression in the DPN group compared with the non-DPN group. circ_0002538 is formed by head-to-tail splicing of exon 2 of the KLHL8 gene, which is located on chromosome 4 (q22.1) (**Figure 3D**). Sanger sequencing verified the head-to-tail splicing, which was consistent with the data in circBase (**Figure 3D**). circ_0002538 could be amplified by RT-PCR using divergent primers in cDNA but not in genomic DNA (**Figure 3E**). circ_0002538 was barely altered after incubation with RNase R comparing to the mock group (**Figure 3F**), which further confirmed that circ_0002538 has a loop structure.

We confirmed that circ_0002538 expression was decreased in DPN tissues (**Figure 3C**). Then, we transfected LV-circ_0002538-shRNA into SCs to simulate the pathological process of SCs during DPN. shRNA significantly reduced circ_0002538 expression without affecting the KLHL8 mRNA expression (**Figure 3G**). We chose sh-circ_0002538 #2 in the following experiments because it had a high inhibitory efficiency compared with the other shRNAs. Migration assays revealed that the knockdown of circ_0002538 impeded the migration of SCs (**Figure 3H** and **I**). We further validated the effects of circ_0002538 in the circ_0002538-overexpressing SCs. The expression level of circ_0002538 in these stable overexpression cells was substantially increased, while there was no change in the KLHL8 mRNA level (**Additional Figure 3A**). Migration assays revealed that the overexpression of circ_0002538 increased the number of SCs that migrated to the lower chamber (**Additional Figure 3B** and **C**). These findings indicate that circ_0002538 was involved in regulating SC migration *in vitro*.

Overexpression of circ_0002538 improves the neuropathic phenotype and symptoms of DPN

To further assess the role of circ_0002538 in DPN *in vivo*, we injected circ_0002538 LV into mice with DPN (**Figure 4A**). We used a fluorescence microscope to examine GFP-positive cells in the sciatic nerve at the 8th week after surgery, and found that injection of the LV-vector led to long-term transgene expression in the sciatic nerve (**Figure 4B**). RT-PCR revealed that circ_0002538 expression in the circ_0002538 group was higher than that in the vector group (**Figure 4C**). Immunofluorescence showed that GFP-positive cells also expressed MPZ protein in the circ_0002538 overexpression group, indicating that circ_0002538 was stably expressed in SCs (**Figure 4D**).

To further examine the effect of circ_0002538 on the signs and symptoms of DPN *in vivo*, we conducted behavioral tests and neurophysiological measurements. Compared with the control vector group, the circ_0002538 group showed improved thermal and mechanical thresholds (**Figure 4E** and **F**). Electrophysiological records showed that compared with those of the control group, the sensory and motor nerve conduction velocities of the circ_0002538 group were significantly increased (**Figure 4G** and **H**). These results demonstrated that the upregulation of circ_0002538 expression improved the function of the sciatic nerve in diabetic mice with DPN. Transmission electron microscopy revealed that the percentage of abnormal myelin sheaths, which manifested as myelin infoldings, vacuolization, and uneven thickness, increased in the DPN group but significantly decreased in the circ_0002538 group (**Figure 4I** and **J**). These results suggest that the overexpression of circ_0002538 ameliorated the symptoms of DPN by improving myelination.

Overexpression of circ_0002538 increases PLLP expression

To examine the effect of circ_0002538 on myelination-related proteins, we detected the expression of serine incorporator 5, PLLP, gap junction protein gamma 3, proteolipid protein 1, periaxin, and MPZ in the circ_0002538-overexpressing SCs because protein profiling indicated that these molecules are dysregulated in DPN. RT-PCR showed that circ_0002538 regulated the expression of PLLP, gap junction protein gamma 3, and proteolipid protein 1, and PLLP showed the greatest FC (**Figure 5A**). Western blotting further revealed that knocking down circ_0002538 led to the downregulation of PLLP expression (**Figure 5B** left). Accordingly, the overexpression of circ_0002538 increased PLLP protein expression in SCs (**Figure 5B** right). These results confirmed that circ_0002538 could regulate the expression of PLLP.

To simulate diabetic conditions, we added ox-LDL to the culture medium. RT-PCR revealed decreased PLLP expression in the ox-LDL-cultured SCs. We used 100-μg/mL ox-LDL in the following experiments because it produced a more significant effect (**Figure 5C** and **D**). RT-PCR showed that the overexpression of circ_0002538 increased PLLP expression in the SCs cultured with ox-LDL. This was further confirmed by western blotting (**Figure 5E** and **F**). We also investigated PLLP expression in the nerve tissues from the patients with DPN via western blots. PLLP expression was significantly downregulated in the nerve tissues of the patients with DPN compared with those without DPN (**Figure 5G** and **H**). In addition, the administration of circ_0002538 LV significantly increased the expression of PLLP in the sciatic nerve of the mice with DPN compared with the administration of control LV (**Figure 5I** and **J**). These results indicated that circ_0002538 could regulate the expression of PLLP *in vitro* and *in vivo*.

PLLP regulates SC migration and myelination

To further verify the role of PLLP in SCs, we transfected a lentiviral vector containing the PLLP gene into SCs. RT-PCR showed that the PLLP overexpression cells had significantly increased PLLP expression, which was further confirmed by the western blotting results (**Figure 6A** and **B**). We performed a mRNA-sequencing analysis of the SCs transduced with the LV carrying either PLLP or the control vector. A total of 23448 mRNAs were identified, and 1671 mRNAs met the filtering criteria ($P < 0.05$, FC ≥ 2) (**Additional Table 10**). The filtered mRNAs were further analyzed using GO analysis for functional prediction (**Additional Tables 11–13**). GO biological process analysis showed that the filtered mRNAs were significantly enriched in neutrophil migration, regulation of neutrophil migration, positive regulation of neutrophil migration, and positive regulation of leukocyte migration, indicating that PLLP might be related to cell migration (**Additional Figure 4A**). Transwell assays confirmed that the overexpression of PLLP significantly increased SC migration (**Figure 6C** and **D**). We further validated the role of PLLP by knocking it down. RT-PCR revealed that PLLP expression was decreased in PLLP knockdown SCs (**Figure 6E**). Transwell assays showed that the knockdown of PLLP effectively inhibited SC migration (**Figure 6F** and **G**). These results indicate that PLLP affects SC migration.

To verify the effect of PLLP on peripheral nerve myelination *in vivo*, we injected sh-PLLP LV into the mouse sciatic nerve. Western blotting revealed that PLLP was decreased in the PLLP knockdown group compared with the control vector group (**Figure 6H** and **I**). The ratio of myelin abnormalities was strongly increased in the PLLP knockdown group, as shown by transmission electron microscopy (**Figure 6J** and **K**). These results indicate that PLLP might regulate myelination in peripheral nerves.

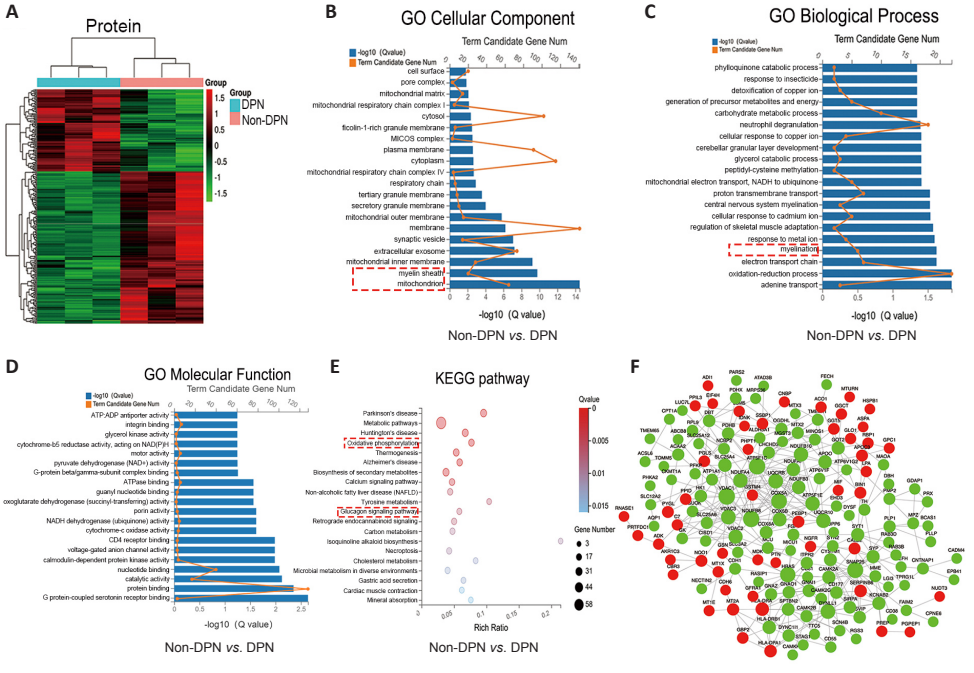

Figure 2 | **Protein profiling analysis and the detection of SC function in DPN.**
(A) Hierarchical clustering analyses of differentially expressed proteins in the non-DPN *vs.* DPN group (n = 3). (B) GO cellular component analysis of differentially expressed proteins. The red dotted box highlights the cellular components of interest. (C) GO biological process analysis of differentially expressed proteins. The red dotted box highlights the biological processes of interest. (D) GO molecular function analysis of differentially expressed proteins. (E) KEGG pathway analysis of differentially expressed proteins. The red dotted box highlights the pathways of interest. (F) The PPI network based on the STRING database showed the interactions between differentially expressed proteins. The green and red nodes represent proteins with decreased and increased expression, respectively. (G, H) Transwell assays indicated that the migrating number of SCs in the diabetic group was lower compared with that in the non-diabetic group. Scale bars: 100 μm. All bar graphs represent the average of three independent replicates, and the error bars are the SD. ***P < 0.001, *vs.* non-diabetic (independent-sample t-test). DPN: Diabetic peripheral neuropathy; GO: Gene Ontology; KEGG: Kyoto Encyclopedia of Genes and Genomes; PPI: protein-protein interaction.

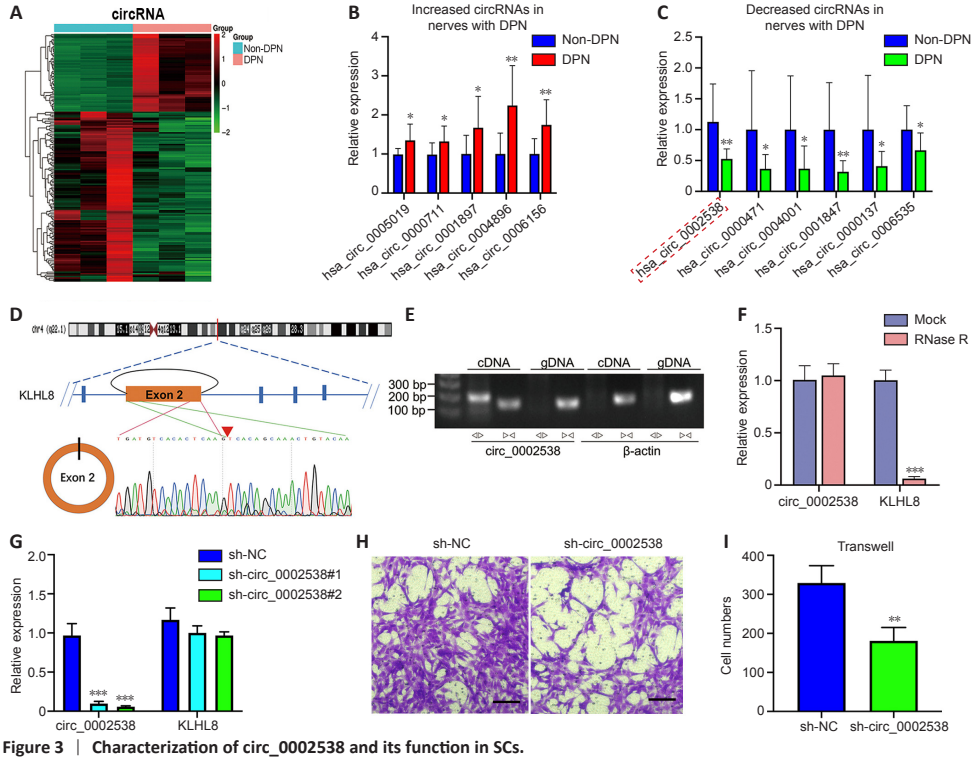

Figure 3 | **Characterization of circ_0002538 and its function in SCs.**
(A) Hierarchical clustering analyses of DEcircRNAs (n = 3). (B, C) RT-PCR verified five circRNAs with upregulated expression and six circRNAs with downregulated expression, and the results were consistent with the RNA-seq data (n = 12). The red dotted box highlights the circRNA of interest. Y-axis: Fold changes in circRNA expression compared with the non-diabetic group. *P < 0.05, **P < 0.01, *vs.* non-diabetic group (independent-sample t-test). (D) Schematic diagram showing that circ_0002538 was formed by the circularization of KLHL8 exon 2. The red arrow represents the "head-to-tail" splicing site of circ_0002538, confirmed by Sanger sequencing. (E) We used divergent primers and convergent primers to amplify circ_0002538 in cDNA and gDNA. We used β-actin as a negative control. (F) circ_0002538 and KLHL8 mRNA in SCs were detected via RT-PCR after incubation with or without RNase R. Y-axis: fold changes in RNA expression compared with the mock group. ***P < 0.001, *vs.* mock group (independent-sample t-test). (G) circ_0002538 and KLHL8 mRNA levels were evaluated in the sh-circ_0002538-transfected SCs via RT-PCR. Y-axis: fold changes in RNA expression compared with the sh-NC group. ***P < 0.001, *vs.* sh-NC group. (H, I) The migrating number of SCs in the sh-circ_0002538 group was lower than that in the sh-NC group in the Transwell assays. **P < 0.01, *vs.* sh-NC group (independent-sample t-test). Scale bars: 100 μm. All bar graphs represent the average of at least three independent replicates, and the error bars are the SD. cDNA: Complementary DNA; DPN: diabetic peripheral neuropathy; gDNA: genomic DNA; KLHL8: Kelch-like family member 8; sh-circ_0002538: short hairpin RNA for circ_0002538; sh-NC: normal control for short hairpin RNA.

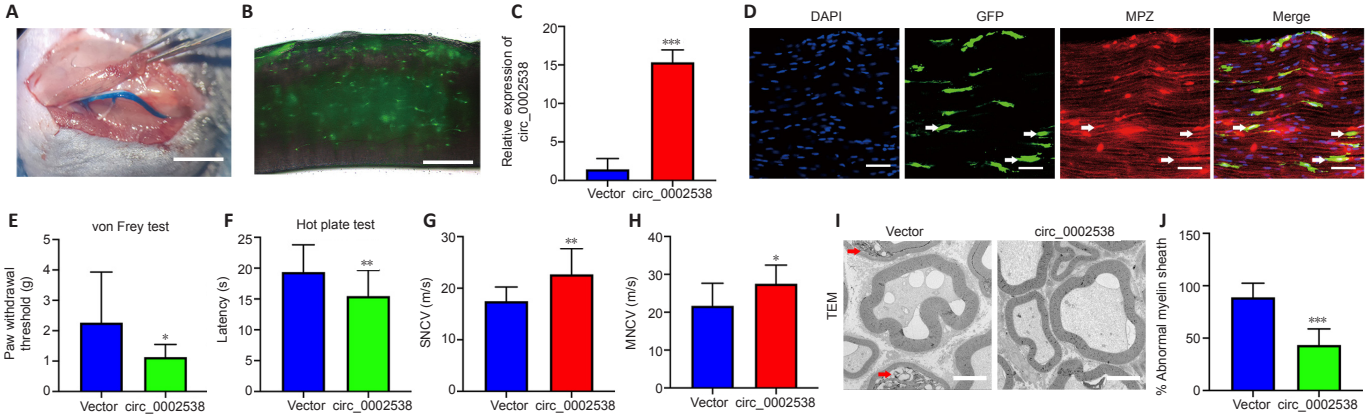

Figure 4 | **Overexpression of circ_0002538 improves demyelination and symptoms of DPN.**
(A) Intraoperative images showing the sciatic nerve after the injection of lentiviral solution. Scale bar: 1500 μm. (B) Eight weeks after the injection of lentiviral solution. We observed green fluorescence in the sciatic nerve under a fluorescence microscope. Scale bar: 200 μm. (C) Eight weeks after the injection of LV-circ_0002538, we examined the mRNA expression level of circ_0002538 in the sciatic nerve via RT-PCR (n = 4). Y-axis: fold changes in circ_0002538 expression compared with the vector side. (D) Immunofluorescence staining of MPZ showed that GFP$^+$ cells also expressed MPZ. The arrows indicate the co-localized regions. (E, F) Eight weeks after the injection of lentiviral solution, the mechanical (E) and thermal (F) nociceptive thresholds were evaluated in the circ_0002538 group and the vector group (n = 20). (G, H) SNCV and MNCV were measured in the circ_0002538 group and the control group (n = 20). (I) The number of abnormal myelin sheaths in the circ_0002538 group, detected by transmission electron microscopy, was lower than that in the vector group (n = 4). Arrows indicate abnormal myelin sheaths. Scale bars: 5 μm. (J) Quantification of the ratio of myelin abnormalities in I. The data are given as the mean ± SD. $^*P < 0.05$, $^{**}P < 0.01$, $^{***}P < 0.001$, *vs.* vector side (paired t-test). DAPI: 2-(4-Amidinophenyl)-6-indolecarbamidine dihydrochloride; GFP: green fluorescent protein; MNCV: motor nerve conduction velocity; MPZ: myelin protein zero; SNCV: sensory nerve conduction velocity; TEM: transmission electron microscope.

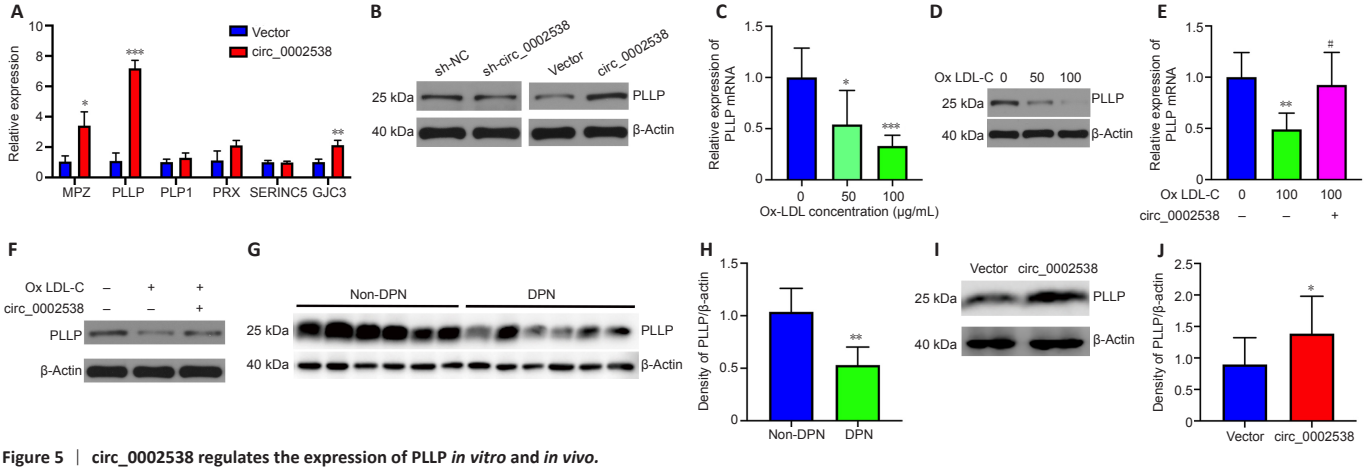

Figure 5 | **circ_0002538 regulates the expression of PLLP *in vitro* and *in vivo*.**
(A) We examined the mRNA expression of the myelination-related genes SERINC5, PLLP, GJC3, PLP1, PRX, and MPZ in the circ_0002538-overexpressing SCs. Y-axis: fold changes in mRNA expression compared with the vector group. $^*P < 0.05$, $^{**}P < 0.01$, $^{***}P < 0.001$, *vs.* vector group (independent-sample t-test). (B) We used western blot analysis to evaluate the effect of circ_0002538 on PLLP in SCs. (C, D) We examined PLLP expression in the SCs cultured in ox-LDL via RT-PCR and western blotting. Y-axis: fold changes in PLLP mRNA expression compared with the 0 μg/mL group. $^*P < 0.05$, $^{***}P < 0.001$, *vs.* 0 μg/mL group (one-way analysis of variance and Tukey's *post hoc* test). (E, F) We evaluated the effect of circ_0002538 on PLLP in SCs cultured with ox-LDL via RT-PCR and western blotting. Y-axis: fold changes in PLLP mRNA expression compared with the control group. $^{**}P < 0.01$, *vs.* control group; $^{\#}P < 0.05$, *vs.* SCs cultured in ox-LDL (one-way analysis of variance and Tukey's *post hoc* test). (G, H) We tested PLLP protein expression in peripheral nerve tissues from patients with or without DPN via western blotting (n = 6). Y-axis: Fold changes in PLLP protein expression normalized to β-actin compared with the vector group. $^{**}P < 0.01$ (independent-sample t-test). (I) The overexpression of circ_0002538 increased the protein expression level of PLLP in the sciatic nerve of mice with DPN (n = 3). (J) Quantification of PLLP by the densitometry of protein bands. $^*P < 0.05$, *vs.* vector group (paired t-test). All bar graphs represent the average of three independent replicates, and the data are given as the mean ± SD. DPN: Diabetic peripheral neuropathy; GJC3: gap junction protein gamma 3; MPZ: myelin protein zero; ox-LDL-C: oxidized low-density lipoprotein cholesterol; PLLP: plasmolipin; PLP1: proteolipid protein 1; PRX: periaxin; SERINC5: serine incorporator 5; sh-circ_0002538: short hairpin RNA for circ_0002538; sh-NC: normal control for short hairpin RNA.

circ_0002538 serves as a sponge for miR-138-5p in SCs

The most common function of circRNAs is to act as sponges for miRNAs, thus regulating downstream target genes. We located circ_0002538 in cellular components via nuclear and cytoplasmic separation experiments. RT-PCR analysis showed that circ_0002538 was predominantly localized in the cytoplasm (**Figure 7A**), indicating that it might target specific miRNAs to regulate PLLP expression. Forty-eight candidate miRNAs were predicted to bind to PLLP and 130 candidate miRNAs were predicted to bind to circ_0002538 (**Additional Tables 14** and **15**). After overlapping the candidate miRNAs of PLLP and the candidate miRNAs of circ_0002538, only two miRNAs (miR-138-5p and miR-3714) were found (**Figure 7B**). We conducted pulldown assays using the biotinylated circ_0002538 probe to verify the interaction between circ_0002538 and the two candidate miRNAs. The circ_0002538 probe effectively pulled down circ_0002538 (**Figure 7C**), and miR-138-5p was significantly enriched in the circ_0002538 probe sponge complex, while miR-3714 was not significantly enriched (**Figure 7D**). RT-PCR and agarose gel electrophoresis confirmed that the miR-138-5p probe could prominently pull down circ_0002538 (**Figure 7E** and **F**). We further verified this interaction using a dual-luciferase reporter assay. A schematic model showed the putative binding site of circ_0002538 and miR-138-5p (**Figure 7G**). Luciferase reporter assays demonstrated that miR-138-5p decreased the luciferase activity of HEK293T cells in the wild-type circ_0002538 group but had no effect in the mutant group (**Figure 7H**), demonstrating the direct binding between circ_0002538 and miR-138-5p in SCs. Taken together, these data demonstrate that circ_0002538 acts as a miRNA sponge for miR-138-5p in SCs.

miR-138-5p inhibits the migration of SCs by targeting PLLP

To investigate the function of miR-138-5p, we transfected miR-138-5p mimic or inhibitor into SCs. In the migration assays, the number of SCs that migrated to the lower chamber was significantly reduced after transfection with the miR-138-5p mimics. In contrast, the miR-138-5p inhibitor enhanced SC migration (**Figure 8A** and **B**). Then, we used a dual-luciferase reporter assay to determine whether miR-138-5p could bind to PLLP to regulate its expression. **Figure 8C** shows the predicted binding sites and mutated sites of miR-138-5p on the 3′UTR of PLLP. The overexpression of miR-138-5p significantly weakened the relative Rluc activity of the wild-type plasmids but not the mutant plasmids (**Figure 8D**), suggesting that miR-138-5p could directly bind to the PLLP 3′UTR and block its activity. Western blot analysis further demonstrated that the miR-138-5p mimics significantly reduced PLLP protein expression, while the miR-138-5p inhibitors increased PLLP protein expression (**Figure 8E**). These results revealed that miR-138-5p could strongly suppress SC migration by targeting PLLP.

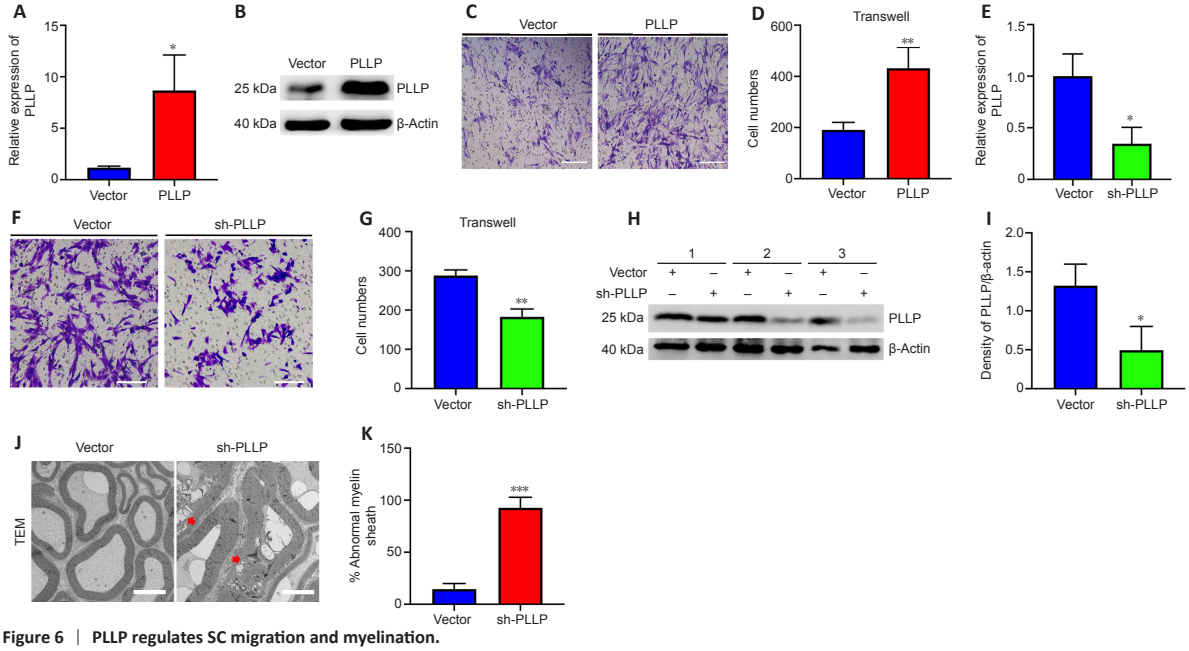

Figure 6 | **PLLP regulates SC migration and myelination.**
(A, B) RT-PCR and western blotting showed that PLLP expression was increased in the SCs transfected with LV-PLLP. *Y*-axis: fold changes in mRNA expression compared with the vector group. $*P < 0.05$, *vs*. vector group (independent-sample *t*-test). (C, D) Transwell assays revealed that the number of migrating SCs in the PLLP group was greater than that in the vector group. $**P < 0.01$, *vs*. vector group (independent-sample *t*-test). Scale bars: 100 μm. (E) RT-PCR analysis showed that the mRNA expression of PLLP was decreased in PLLP knockdown SCs. *Y*-axis: fold changes in mRNA expression compared with the vector group. $*P < 0.05$, *vs*. vector group (independent-sample *t*-test). (F, G) The number of migrating SCs in the sh-PLLP group was low compared with that in the vector group in the Transwell assays. $**P < 0.01$, *vs*. vector group (independent-sample *t*-test). Scale bars: 100 μm. (H) Eight weeks after the injection of LV-vector or LV-sh-PLLP, PLLP expression was examined via western blotting ($n = 3$). (I) Quantification of PLLP by the densitometry of protein bands. $*P < 0.05$, *vs*. vector group (paired *t*-test). (J) The number of abnormal myelin sheaths in the sh-PLLP group, measured via transmission electron microscopy, was higher than that in the vector group ($n = 4$). Arrows point to abnormal myelin sheaths. Scale bars: 5 μm. (K) Quantification of the ratio of myelin abnormalities in J. The data are given as the mean ± SD. $**P < 0.01$, *vs.* vector group (paired *t*-test). LV: Lentivirus; PLLP: plasmolipin; sh-PLLP: short hairpin RNA for PLLP; TEM: transmission electron microscope.

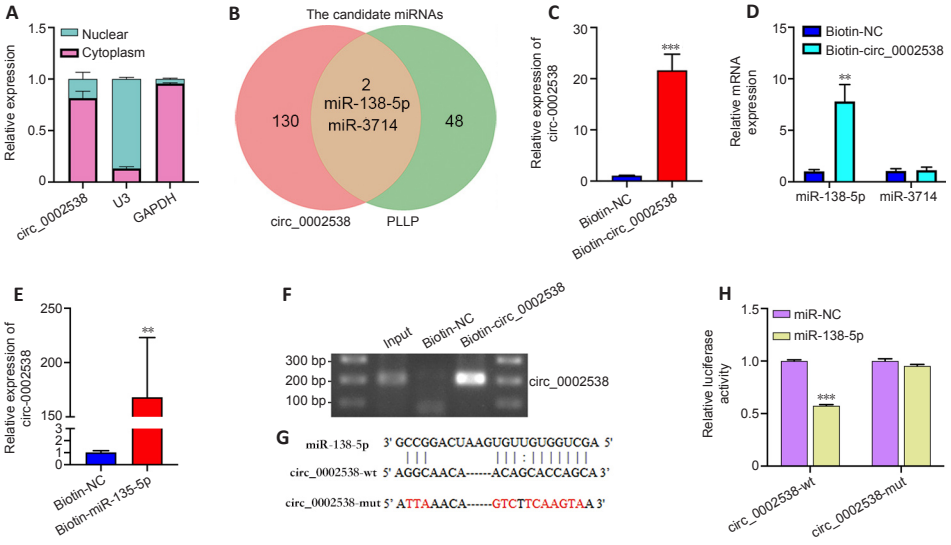

Figure 7 | **circ_0002538 acts as a sponge for miR-138-5p in SCs.**
(A) Nuclear and cytoplasmic separation assays detecting the localization of circ_0002538 in SCs. Y-axis: proportion of nuclear and cytoplasmic RNA to total RNA. (B) Venn diagram showing the overlap of circ_0002538 candidate miRNAs and PLLP candidate miRNAs. (C) circ_0002538 was pulled down in SC lysates by the biotin-circ_0002538 probe and detected via RT-PCR. The relative level of circ_0002538 was normalized to the input. *Y*-axis: fold changes in circ_0002538 expression compared with the biotin-NC group. $***P < 0.001$, *vs.* Biotin-NC group (independent-sample *t*-test). (D) miR-138-5p was pulled down by the biotin-circ_0002538 probe, while miR-3714 was not, as shown by the RT-PCR. *Y*-axis: fold changes in miRNAs expression compared with the biotin-NC group. $**P < 0.01$, *vs*. Biotin-NC group (independent-sample *t*-test). (E, F) circ_0002538 was pulled down in SC lysates by the biotin-miR-138-5p probe, as shown by RT-PCR. The relative level of circ_0002538 was normalized to the input. *Y*-axis: fold changes in circ_0002538 expression compared with the biotin-NC group. $**P < 0.01$, *vs*. Biotin-NC group (independent-sample *t*-test). (G) The miR-138-5p binding site of circ_0002538 was predicted via RNAhybrid. The mutant sequences are marked in red. (H) Dual-luciferase reporter assays of HEK293T cells cotransfected with miR-138-5p mimics, circ_0002538 wild-type (circ_0002538-wt), or circ_0002538 mutant type (circ_0002538-mut) plasmids. *Y*-axis: relative luciferase activity compared with the miR-NC + circ_0002538-wt group. $***P < 0.001$, *vs*. miR-NC group (one-way analysis of variance and Tukey's *post hoc* test). All bar graphs represent the average of three independent replicates, and the error bars are the SD. GAPDH: Glyceraldehyde-3-phosphate dehydrogenase; mut: mutant type; NC: normal control; PLLP: plasmolipin; U3: small nucleolar U3 RNA; wt: wild-type.

miR-138-5p reverses the effect of circ_0002538 on SCs

We demonstrated that circ_0002538 could sponge miR-138-5p and that miR-138-5p could inhibit SC migration by targeting PLLP. Subsequently, we explored whether circ_0002538 could regulate PLLP through miR-138-5p. The SCs cotransfected with the miR-138-5p mimics and circ_0002538 exhibited decreased migration compared with the SCs transfected with circ_0002538 only (**Figure 9A** and **B**), which indicated that ectopic expression of miR-138-5p could partially eliminate the promoting effect of circ_0002538. Western blot analysis showed that the SCs cotransfected with the miR-138-5p mimic and circ_0002538 exhibited reduced PLLP expression compared with the SCs transfected with circ_0002538 only (**Figure 9C** and **D**). The above results demonstrated that circ_0002538 regulated SC migration in part by sponging miR-138-5p and subsequently influencing PLLP expression.

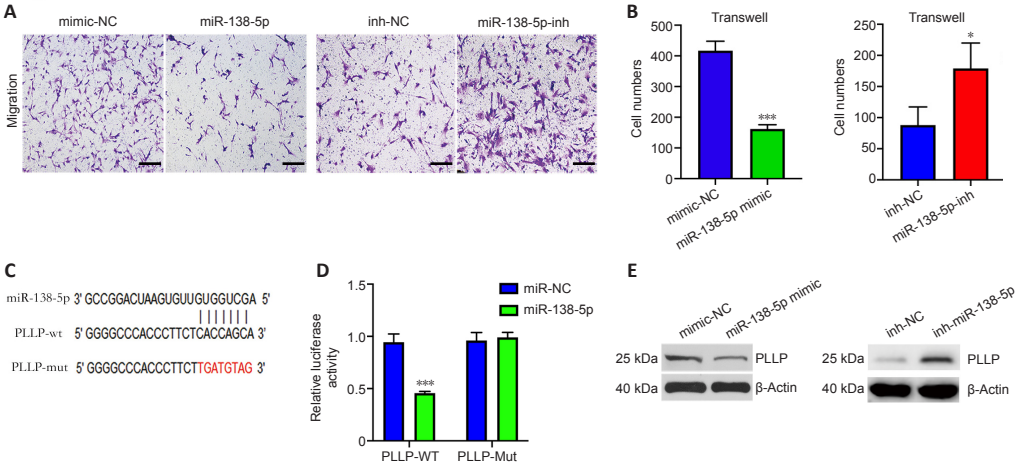

Figure 8 | **miR-138-5p inhibits SC migration by targeting PLLP.**
(A) The number of migrating SCs in the miR-138-5p group was less than that in the mimic-NC group via the Transwell assays. Further, the number of migrating SCs in the miR-138-5p-inh group was more than that in the inh-NC group. Scale bars: 100 μm. (B) Quantification of the number of migrating cells in A. **P* < 0.05, ****P* < 0.001, *vs.* mimic-NC or inh-NC group (independent-sample *t*-test). (C) The potential binding site of miR-138-5p on the 3'UTR of PLLP mRNA. The mutant sequences are marked in red. (D) Dual-luciferase reporter assays of HEK293T cells cotransfected with miR-138-5p mimics, PLLP wild-type (PLLP-wt), or PLLP-mutant type (PLLP-mut) plasmids. *Y*-axis: Relative luciferase activity compared with the miR-NC + PLLP-Wt group. ****P* < 0.001, *vs.* miR-NC group (one-way analysis of variance and Tukey's *post hoc* test). (E) We tested PLLP expression via western blotting in the SCs transfected with miR-138-5p mimics or miR-138-5p inhibitor. All bar graphs represent the average of three independent replicates, and the error bars are the SD. inh: Inhibitor; mut: mutant type; NC: normal control; PLLP: plasmolipin; wt: wild-type.

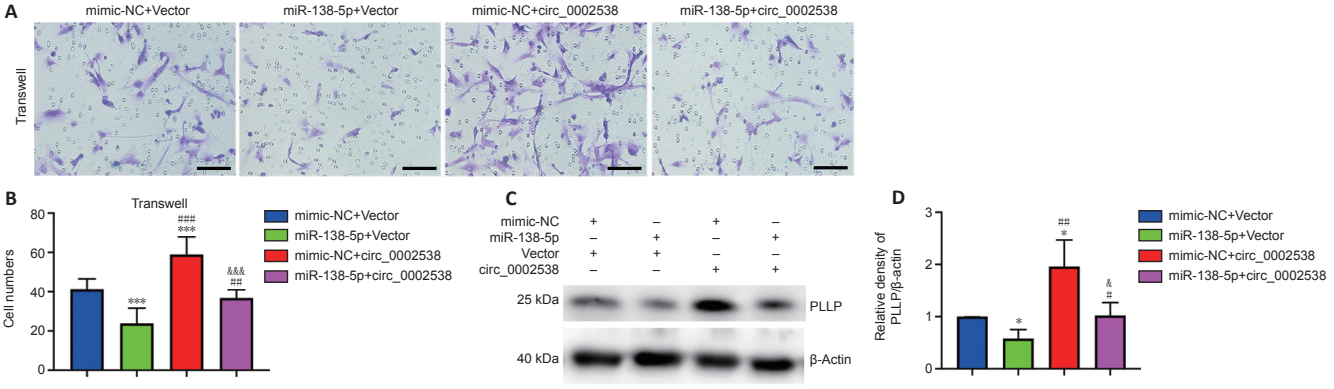

Figure 9 | **miR-138-5p reverses the circ_0002538-mediated promotion of SCs.**
(A) Transwell analysis revealed that circ_0002538 promoted SC migration, but its effect was partially neutralized by the overexpression of miR-138-5p. Scale bars: 100 μm. (B) Quantification of the number of migrating cells in (A). All bar graphs represent the average of three independent replicates, and error bars are the SD. ****P* < 0.001, *vs.* mimic-NC + vector group; ##*P* < 0.01, ###*P* < 0.001, *vs.* miR-138-5p + vector group; &&&*P* < 0.001, *vs.* mimic-NC + circ_0002538 group (one-way analysis of variance and Tukey's *post hoc* test). (C) Western blot analyses showed that the overexpression of circ_0002538 increased PLLP protein expression, while the ectopic expression of miR-138-5p could partially eliminate this effect. (D) Quantification of PLLP by the densitometry of protein bands. **P* < 0.05, *vs.* mimic-NC + vector group; #*P* < 0.05, ##*P* < 0.01, *vs.* miR-138-5p + vector group; &*P* < 0.05, *vs.* mimic-NC + circ_0002538 group (one-way analysis of variance and Tukey's *post hoc* test). PLLP: Plasmolipin; NC: normal control.

Discussion

DPN is the most common complication of diabetes, and thus represents a major burden to healthcare systems and society worldwide (Selvarajah et al., 2019). Few studies have been used circRNA sequencing to study the etiology of human DPN. Although nontraumatic amputations are mainly caused by DPN, the actual number of calf amputations each year is not high, limiting the availability of sural nerve samples from individuals with DPN. We collected peripheral nerve tissues from individuals with or without DPN and performed circRNA sequencing and protein profiling. We verified the results of circRNA sequencing and further showed that circ_0002538 could ameliorate symptoms in diabetic mice with DPN by promoting the migration and myelination of SCs. Therefore, our data indicate that the overexpression of circ_0002538 may be a promising treatment for patients with DPN.

Transcriptomic alterations often occur during the pathogenesis and progression of diseases. Previous studies have identified hundreds of differentially expressed genes in patients with static or progressive diabetic neuropathy that are functionally enriched in pathways, including the regulation of axonogenesis and lipid metabolism (Hur et al., 2011). A microarray analysis of the dorsal root ganglia of diabetic rats found that DE mRNAs with downregulated expression were significantly enriched in various biological processes, including myelination, peripheral nervous system myelination, axon guidance, and the regulation of axon production (Guo et al., 2018). Further, aberrantly expressed mRNAs in SCs isolated from the sciatic nerves of diabetic rats were enriched in downregulated biological processes related to myelination, axonogenesis, and axon development (Wang et al., 2020b). In this study, we identified 265 proteins with dysregulated expression in peripheral nerves from DPN patients that were enriched in myelination. SCs provide protection and nutritional support to enable myelinated axons to maintain normal physiological functions, and impaired SC function eventually leads to axonal loss (Dey et al., 2013). Therefore, we focused on the influence of SCs on DPN. We evaluated the function of SCs from patients with diabetes and found that these SCs had reduced migration, consistent with the results of previous studies (Gumy et al., 2008; Jia et al., 2018).

Although circRNAs were originally thought to be byproducts of abnormal splicing events (Cocquerelle et al., 1993), recent studies have shown that certain circRNAs are involved in some important physiological processes. However, the role of circRNAs in the SCs of DPN has rarely been examined, especially in human DPN. Zhang et al. (2020) reported 15 DEcircRNAs in the dorsal root ganglia between wild-type mice and mice with diabetes mellitus. Liu et al. (2019) reported that mmu_circRNA_006636 could relieve high glucose-induced apoptosis and autophagy in RSC96 cells. In our study, 116 circRNAs had downregulated expression and 53 circRNAs had upregulated expression in DPN. Among them, 11 circRNAs were verified, of which circ_0000711 and circ_0006156 were previously reported to play important roles in tumors (Li et al., 2018; Hong et al., 2019; Chen et al., 2020; He et al., 2020), but none were found to be involved in neuropathy. The functions of most verified DEcircRNAs are still unclear. Therefore, more research is needed to explore the potential roles of noncoding RNAs in human DPN.

One of the most common and important functions of circRNAs is to act as competing endogenous RNAs that sequester miRNAs through their binding sites and then modulate the activity of miRNAs on their target genes (Salmena et al., 2011). Although the function of circ_0002538 has not previously been characterized, we found decreased circ_0002538 expression in the nerves of patients with DPN. Further, we found that the overexpression of circ_0002538 improved the symptoms of DPN in diabetic mice. Transmission electron microscopy demonstrated that the administration of circ_0002538 decreased

the number of damaged myelin sheaths in DPN, indicating that circ_0002538 might help repair damaged myelin sheaths by improving myelination. According to the GO biological process analysis, the proteins with dysregulated expression identified using protein profiling were significantly enriched in the myelination process, indicating that circ_0002538 improved DPN by regulating myelination-related proteins. The expression of myelination-related proteins was detected in the circ_0002538-overexpressing SCs, which demonstrated that circ_0002538 could regulate the expression of PLLP. Based on the computational predictions and experimental validation of candidate miRNAs binding circ_0002538 and PLLP, we selected miR-138-5p for the construction of competing endogenous RNAs. The circ_0002538-miR-138-5p-PLLP axis was demonstrated using RNA pulldown assays, dual luciferase assays, and a mouse model of DPN. We further verified that circ_0002538 could competitively adsorb miR-138-5p to antagonize its suppression of PLLP.

DPN is involved in deleterious changes in peripheral nerves, such as myelin damage (Cermenati et al., 2012). The myelin sheath is a multilayer membrane produced by SCs that allows efficient transmission of nerve impulses. PLLP has been found to assemble myelin membrane precursor domains via its ability to attract liquid-ordered lipids between the Golgi complex and plasma membrane (Yaffe et al., 2015), and PLLP expression was found to be elevated in nerve stumps following axotomy (Bosse et al., 2003). However, the characteristics and functions of PLLP have not been examined in DPN. In our research, we found that PLLP regulated the migration of SCs, which is an important step preceding myelination and remyelination of the peripheral nervous system (Anliker et al., 2013). Impaired or delayed SC migration contributes to abnormal myelination and demyelination of peripheral nerves (Anliker et al., 2013; Yi et al., 2019). These data are consistent with our finding that silencing PLLP can lead to impaired SC migration and peripheral nerve demyelination in mice. PLLP expression was decreased in diabetic mice with DPN. The increased expression of PLLP, mediated by the overexpression of circ_0002538, improved demyelination. Therefore, we concluded that circ_0002538 and PLLP might play important roles in DPN, and thus might be useful in the development of treatments for demyelinating diseases.

This study had several limitations. First, the number of nerve samples used for sequencing and verification was relatively small. Second, to minimize the influence of other cells, we only used nerve bundles for sequencing and subsequent verification. However, we still cannot completely exclude the influence of other components in peripheral nerves, such as axons, fibroblasts, endothelial cells, and inflammatory cells. Their effects on DPN are the subjects of further research. Third, as circRNAs can interact with different proteins or be translated in a way that mediates their biological roles, further research is needed to identify more circRNAs related to the pathogenesis of DPN. Finally, although we validated the protective effects of circ_0002538 in mice and found an improvement in the neuropathic phenotype and symptoms of DPN, the therapeutic effects on humans need to be verified.

In conclusion, this study reported the results of circRNA sequencing and protein profiling of peripheral nerves from individuals with DPN. As a result, we verified 11 DEcircRNAs in the DPN and control groups. Furthermore, our study demonstrated that circ_0002538 expression was downregulated in patients with DPN and that increased expression of circ_0002538 improved the symptoms of diabetic mice with DPN. Mechanistically, circ_0002538 regulated SC migration and myelination, at least in part, through the miR-138-5p/PLLP axis. Collectively, our study illuminated the key role of the circ_0002538/miR-138-5p/PLLP axis in DPN. Our results provide new insight into the mechanisms and potential treatments for DPN.

Author contributions: *Study design: YTL, ZX, HGM, ZBC; sample collection: YTL, ZX, SR, HWX, WL, TJ, JC, XFY, YK, QYL, ZHW; data verify the sequencing: YTL, ZX, SR, HWX, WL; cell experiments: YTL, ZX, WL, TJ, JC; animal data collection and analysis: YTL, ZX, XFY, YK, ZHW, QYL; manuscript draft and review: YTL, ZX, XFY, HGM, ZBC. All authors approved the final version of the manuscript.*

Conflicts of interest: *The authors declare no competing interests.*

Availability of data and materials: *All data generated or analyzed during this study are included in this published article and its supplementary information files.*

Additional files:

Additional Table 1: *Primers used in this study.*

Additional Table 2: *Nucleic acid sequences used in this study.*

Additional Table 3: *Basic characteristics of patients included in the study.*

Additional Table 4: *The differentially expressed proteins analyzed in this study were selected from the results of protein profiling analysis with fold change (FC) > 1.3 and P < 0.05.*

Additional Table 5: *GO cellular component analysis of differentially expressed proteins.*

Additional Table 6: *GO biological process analysis of differentially expressed proteins.*

Additional Table 7: *GO molecular function analysis of differentially expressed proteins.*

Additional Table 8: *KEGG pathway analysis of differentially expressed proteins.*

Additional Table 9: *The DEcircRNAs analyzed in this study were selected from the results of circRNA sequencing analysis with FC > 2.0, P<0.01, q < 0.05 and readings ≥ 50.*

Additional Table 10: *The differentially expressed mRNAs analyzed in this study were selected from the results of mRNA sequencing analysis.*

Additional Table 11: *GO biological process analysis of filtered mRNAs.*

Additional Table 12: *GO cellular component analysis of filtered mRNAs.*

Additional Table 13: *GO molecular function analysis of filtered mRNAs.*

Additional Table 14: *Candidate miRNAs binding to circ_0002538 predicted by RNAhybrid, miRanda and TargetScan.*

Additional Table 15: *The candidate miRNAs binding to PLLP predicted by miRDB, miRTarBase, miRWalk and TargetScan.*

Additional Figure 1: *Confirmation of DPN in the collected peripheral nerve tissues.*

Additional Figure 2: *Identification of SCs isolated from sural nerves of patients.*

Additional Figure 3: *Overexpression of circ_0002538 promoted SC migration.*

Additional Figure 4: *The filtered mRNAs in the mRNA sequencing results of the PLLP-overexpressing SCs and the control SCs were further analyzed with GO enrichment analysis.*

References

Anliker B, Choi JW, Lin ME, Gardell SE, Rivera RR, Kennedy G, Chun J (2013) Lysophosphatidic acid (LPA) and its receptor, LPA1, influence embryonic schwann cell migration, myelination, and cell-to-axon segregation. Glia 61:2009-2022.

Baum P, Kosacka J, Estrela-Lopis I, Woidt K, Serke H, Paeschke S, Stockinger M, Klöting N, Blüher M, Dorn M, Classen J, Thiery J, Bechmann I, Toyka KV, Nowicki M (2016) The role of nerve inflammation and exogenous iron load in experimental peripheral diabetic neuropathy (PDN). Metabolism 65:391-405.

Beery AK, Zucker I (2011) Sex bias in neuroscience and biomedical research. Neurosci Biobehav Rev 35:565-572.

Bosse F, Hasse B, Pippirs U, Greiner-Petter R, Müller HW (2003) Proteolipid plasmolipin: localization in polarized cells, regulated expression and lipid raft association in CNS and PNS myelin. J Neurochem 86:508-518.

Cermenati G, Abbiati F, Cermenati S, Brioschi E, Volonterio A, Cavaletti G, Saez E, De Fabiani E, Crestani M, Garcia-Segura LM, Melcangi RC, Caruso D, Mitro N (2012) Diabetes-induced myelin abnormalities are associated with an altered lipid pattern: protective effects of LXR activation. J Lipid Res 53:300-310.

Chaplan SR, Bach FW, Pogrel JW, Chung JM, Yaksh TL (1994) Quantitative assessment of tactile allodynia in the rat paw. J Neurosci Methods 53:55-63.

Charan J, Kantharia ND (2013) How to calculate sample size in animal studies? J Pharmacol Pharmacother 4:303-306.

Chen KH, Pan JF, Chen ZX, Pan D, Gao T, Huang M, Huang JN (2020) Effects of hsa_circ_0000711 expression level on proliferation and apoptosis of hepatoma cells. Eur Rev Med Pharmacol Sci 24:4161-4171.

Chen Y, Wang X (2020) miRDB: an online database for prediction of functional microRNA targets. Nucleic Acids Res 48:D127-131.

Cocquerelle C, Mascrez B, Hétuin D, Bailleul B (1993) Mis-splicing yields circular RNA molecules. FASEB J 7:155-160.

Dey I, Midha N, Singh G, Forsyth A, Walsh SK, Singh B, Kumar R, Toth C, Midha R (2013) Diabetic Schwann cells suffer from nerve growth factor and neurotrophin-3 underproduction and poor associability with axons. Glia 61:1990-1999.

Dweep H, Sticht C, Pandey P, Gretz N (2011) miRWalk--database: prediction of possible miRNA binding sites by "walking" the genes of three genomes. J Biomed Inform 44:839-847.

Fan B, Li C, Szalad A, Wang L, Pan W, Zhang R, Chopp M, Zhang ZG, Liu XS (2020) Mesenchymal stromal cell-derived exosomes ameliorate peripheral neuropathy in a mouse model of diabetes. Diabetologia 63:431-443.

Farmer KL, Li C, Dobrowsky RT (2012) Diabetic peripheral neuropathy: should a chaperone accompany our therapeutic approach? Pharmacol Rev 64:880-900.

Feldman EL, Callaghan BC, Pop-Busui R, Zochodne DW, Wright DE, Bennett DL, Bril V, Russell JW, Viswanathan V (2019a) Diabetic neuropathy. Nat Rev Dis Primers 5:41.

Feldman EL, Callaghan BC, Pop-Busui R, Zochodne DW, Wright DE, Bennett DL, Bril V, Russell JW, Viswanathan V (2019b) Diabetic neuropathy. Nat Rev Dis Primers 5:42.

Gillen C, Gleichmann M, Greiner-Petter R, Zoidl G, Kupfer S, Bosse F, Auer J, Müller HW (1996) Full-lenth cloning, expression and cellular localization of rat plasmolipin mRNA, a proteolipid of PNS and CNS. Eur J Neurosci 8:405-414.

Goyal SN, Reddy NM, Patil KR, Nakhate KT, Ojha S, Patil CR, Agrawal YO (2016) Challenges and issues with streptozotocin-induced diabetes- A clinically relevant animal model to understand the diabetes pathogenesis and evaluate therapeutics. Chem Biol Interact 244:49-63.

Gumy LF, Bampton ET, Tolkovsky AM (2008) Hyperglycaemia inhibits Schwann cell proliferation and migration and restricts regeneration of axons and Schwann cells from adult murine DRG. Mol Cell Neurosci 37:298-311.

Guo G, Liu Y, Ren S, Kang Y, Duscher D, Machens HG, Chen Z (2018) Comprehensive analysis of differentially expressed microRNAs and mRNAs in dorsal root ganglia from streptozotocin-induced diabetic rats. PLoS One 13:e0202696.

He J, Wang HB, Huang JJ, Zhang L, Li DL, He WY, Xiong QM, Qin ZS (2021) Diabetic neuropathic pain induced by streptozotocin alters the expression profile of non-coding RNAs in the spinal cord of mice as determined by sequencing analysis. Exp Ther Med 22:775.

He YX, Ju H, Li N, Jiang YF, Zhao WJ, Song TT, Ren WH (2020) Association between hsa_circ_0006156 expression and incidence of gastric cancer. Eur Rev Med Pharmacol Sci 24:3030-3036.

Holland NR, Stocks A, Hauer P, Cornblath DR, Griffin JW, McArthur JC (1997) Intraepidermal nerve fiber density in patients with painful sensory neuropathy. Neurology 48:708-711.

Hong Y, Qin H, Li Y, Zhang Y, Zhuang X, Liu L, Lu K, Li L, Deng X, Liu F, Shi S, Liu G (2019) FNDC3B circular RNA promotes the migration and invasion of gastric cancer cells via the regulation of E-cadherin and CD44 expression. J Cell Physiol 234:19895-19910.

Huang HY, Lin YC, Li J, Huang KY, Shrestha S, Hong HC, Tang Y, Chen YG, Jin CN, Yu Y, Xu JT, Li YM, Cai XX, Zhou ZY, Chen XH, Pei YY, Hu L, Su JJ, Cui SD, Wang F, et al. (2020) miRTarBase 2020: updates to the experimentally validated microRNA-target interaction database. Nucleic Acids Res 48:D148-154.

Hulsen T, de Vlieg J, Alkema W (2008) BioVenn- a web application for the comparison and visualization of biological lists using area-proportional Venn diagrams. BMC Genomics 9:488.

Hur J, Sullivan KA, Pande M, Hong Y, Sima AA, Jagadish HV, Kretzler M, Feldman EL (2011) The identification of gene expression profiles associated with progression of human diabetic neuropathy. Brain 134:3222-3235.

Ii M, Nishimura H, Kusano KF, Qin G, Yoon YS, Wecker A, Asahara T, Losordo DW (2005) Neuronal nitric oxide synthase mediates statin-induced restoration of vasa nervorum and reversal of diabetic neuropathy. Circulation 112:93-102.

Jia L, Chopp M, Wang L, Lu X, Szalad A, Zhang ZG (2018) Exosomes derived from high-glucose-stimulated Schwann cells promote development of diabetic peripheral neuropathy. FASEB J 32:fj201800597R.

Li J, Ni S, Zhou C, Ye M (2018) The expression profile and clinical application potential of hsa_circ_0000711 in colorectal cancer. Cancer Manag Res 10:2777-2784.

Liu Y, Chen X, Yao J, Kang J (2019) Circular RNA ACR relieves high glucose-aroused RSC96 cell apoptosis and autophagy via declining microRNA-145-3p. J Cell Biochem doi: 10.1002/jcb.29568.

Livak KJ, Schmittgen TD (2001) Analysis of relative gene expression data using real-time quantitative PCR and the 2(-Delta Delta C(T)) method. Methods 25:402-408.

Lu S, Zhu N, Guo W, Wang X, Li K, Yan J, Jiang C, Han S, Xiang H, Wu X, Liu Y, Xiong H, Chen L, Gong Z, Luo F, Hou W (2020) RNA-Seq revealed a circular RNA-microRNA-mRNA regulatory network in hantaan virus infection. Front Cell Infect Microbiol 10:97.

Masocha W, Kombian SB, Edafiogho IO (2016) Evaluation of the antinociceptive activities of enaminone compounds on the formalin and hot plate tests in mice. Sci Rep 6:21582.

McGeary SE, Lin KS, Shi CY, Pham TM, Bisaria N, Kelley GM, Bartel DP (2019) The biochemical basis of microRNA targeting efficacy. Science 366:eaav1741.

Pan Z, Li GF, Sun ML, Xie L, Liu D, Zhang Q, Yang XX, Xia S, Liu X, Zhou H, Xue ZY, Zhang M, Hao LY, Zhu LJ, Cao JL (2019) MicroRNA-1224 splicing circularRNA-Filip1l in an Ago2-dependent manner regulates chronic inflammatory pain via targeting Ubr5. J Neurosci 39:2125-2143.

Perlman RL (2016) Mouse models of human disease: An evolutionary perspective. Evol Med Public Health 2016:170-176.

Pop-Busui R, Boulton AJ, Feldman EL, Bril V, Freeman R, Malik RA, Sosenko JM, Ziegler D (2017) Diabetic neuropathy: a position statement by the American Diabetes Association. Diabetes Care 40:136-154.

Rehmsmeier M, Steffen P, Hochsmann M, Giegerich R (2004) Fast and effective prediction of microRNA/target duplexes. RNA 10:1507-1517.

Salmena L, Poliseno L, Tay Y, Kats L, Pandolfi PP (2011) A ceRNA hypothesis: the Rosetta Stone of a hidden RNA language? Cell 146:353-358.

Salzer JL (2015) Schwann cell myelination. Cold Spring Harb Perspect Biol 7:a020529.

Selvarajah D, Kar D, Khunti K, Davies MJ, Scott AR, Walker J, Tesfaye S (2019) Diabetic peripheral neuropathy: advances in diagnosis and strategies for screening and early intervention. Lancet Diabetes Endocrinol 7:938-948.

Shannon P, Markiel A, Ozier O, Baliga NS, Wang JT, Ramage D, Amin N, Schwikowski B, Ideker T (2003) Cytoscape: a software environment for integrated models of biomolecular interaction networks. Genome Res 13:2498-2504.

Shi L, Sun BL, Zhang SY, Zhang YQ (2020) Biological function of circular RNA and its role in tissue repair. Zhongguo Zuzhi Gongcheng Yanjiu 24:2770-2774.

Singh R, Kishore L, Kaur N (2014) Diabetic peripheral neuropathy: current perspective and future directions. Pharmacol Res 80:21-35.

Tannemaat MR, Eggers R, Hendriks WT, de Ruiter GC, van Heerikhuize JJ, Pool CW, Malessy MJ, Boer GJ, Verhaagen J (2008) Differential effects of lentiviral vector-mediated overexpression of nerve growth factor and glial cell line-derived neurotrophic factor on regenerating sensory and motor axons in the transected peripheral nerve. Eur J Neurosci 28:1467-1479.

Vlcková-Moravcová E, Bednarík J, Dusek L, Toyka KV, Sommer C (2008) Diagnostic validity of epidermal nerve fiber densities in painful sensory neuropathies. Muscle Nerve 37:50-60.

Wang A, Toma MA, Ma J, Li D, Vij M, Chu T, Wang J, Li X, Xu Landén N (2020a) Circular RNA hsa_circ_0084443 is upregulated in diabetic foot ulcer and modulates keratinocyte migration and proliferation. Adv Wound Care (New Rochelle) 9:145-160.

Wang C, Xu X, Chen J, Kang Y, Guo J, Duscher D, Yang X, Guo G, Ren S, Xiong H, Yuan M, Jiang T, Machens HG, Chen Z, Chen Y (2020b) The construction and analysis of lncRNA-miRNA-mRNA competing endogenous RNA network of Schwann cells in diabetic peripheral neuropathy. Front Bioeng Biotechnol 8:490.

Xu ZZ, Kim YH, Bang S, Zhang Y, Berta T, Wang F, Oh SB, Ji RR (2015) Inhibition of mechanical allodynia in neuropathic pain by TLR5-mediated A-fiber blockade. Nat Med 21:1326-1331.

Yaffe Y, Hugger I, Yassaf IN, Shepshelovitch J, Sklan EH, Elkabetz Y, Yeheskel A, Pasmanik-Chor M, Benzing C, Macmillan A, Gaus K, Eshed-Eisenbach Y, Peles E, Hirschberg K (2015) The myelin proteolipid plasmolipin forms oligomers and induces liquid-ordered membranes in the Golgi complex. J Cell Sci 128:2293-2302.

Yi S, Liu Q, Wang X, Qian T, Wang H, Zha G, Yu J, Wang P, Gu X, Chu D, Li S (2019) Tau modulates Schwann cell proliferation, migration and differentiation following peripheral nerve injury. J Cell Sci 132:jcs222059.

Zhang HH, Zhang Y, Wang X, Yang P, Zhang BY, Hu S, Xu GY, Hu J (2020) Circular RNA profile in diabetic peripheral neuropathy: analysis of coexpression networks of circular RNAs and mRNAs. Epigenomics 12:843-857.

Zhang SB, Lin SY, Liu M, Liu CC, Ding HH, Sun Y, Ma C, Guo RX, Lv YY, Wu SL, Xu T, Xin WJ (2019) CircAnks1a in the spinal cord regulates hypersensitivity in a rodent model of neuropathic pain. Nat Commun 10:4119.

C-Editor: Zhao M; S-Editors: Yu J, Li CH; L-Editors: Yu J, Song LP; T-Editor: Jia Y

Additional Table 1: Primers used in this study

Name	Sequence (5'-3')
circRNA	
hsa_circ_0004001	Forward: TGACGAACATCACAGTACATTGG
	Reverse: AAGGTGCGTTCATCACGTTTT
hsa_circ_0001847	Forward: ACAATCAGATGGCACCAGGGA
	Reverse: TCCAAGCCCCTTTGAGTCCAT
hsa_circ_0000137	Forward: TTGAGGCTGTTGTTCAGAGTGT
	Reverse: ACAGAGTCATCCCCAGAAGCA
hsa_circ_0005019	Forward: CTGGAGCCTGGTGAGAACTT
	Reverse: CAGATGTGTCAGAACCCTCACT
hsa_circ_0000711	Forward: AGGTAGCCGAGGGGCAGTAA
	Reverse: GTGGTAAGCAAAGTGGTGTGGT
hsa_circ_0001897	Forward: GCTGGCCTTGGGAGGTTATTTA
	Reverse: GCCCACTGTCATCCAAGAAGAA
hsa_circ_0004896	Forward: CTAACCACCGCCGAGAACGA
	Reverse: TGTCACCTGGGCGGAAACTC
hsa_circ_0006156	Forward: AAGGGCCATAGTGGTGGAAGT
	Reverse: GCTTGGGGGATAACACTCAGGA
hsa_circ_0000471	Forward: CACACAAAGACCTCCTCCTCC
	Reverse: GCTTGTTTTGCTGTACCCATCT
hsa_circ_0001647	Forward: GTCTGAGTTTACCTGAAAGGGATA
	Reverse: ATGCCTGTACTTCATCACCTG
hsa_circ_0087960	Forward: GTAGTTCTGGGGCGTGTTCA
	Reverse: TAGGTGGATGGGGAGCTTCA
hsa_circ_0004374	Forward: ACACCAGCATACTTTGCCTCA
	Reverse: CACATTTAGGACAGCGCAGC
hsa_circ_0020433	Forward: ACAAAGTCATCGCTGCCAAAG
	Reverse: CGGCTGAAAGGGAATGAAATGC
hsa_circ_0024604	Forward: AAAAGGCAACAACAGCACCAGC
	Reverse: CAAAACCCACTCAACTGCCATTGT
hsa_circ_0005615	Forward: ACCCTTTACCTGGAGCAAACCA
	Reverse: TTTGGAGCTGAAACGATGGTGAC
hsa_circ_0040823	Forward: ATCGGAGAAGACGGACAGGT
	Reverse: AGTCGGATTCTGTGATGCCA
hsa_circ_0007715	Forward: ACGGAGGCTCCAGAGACTACTA
	Reverse: TTGTCTGACGACTTGCCTGC
hsa_circ_0003781	Forward: TGAGTACGACCCCGAGGACA
	Reverse: CTCATCGGTGGCAGCGTAGT
hsa_circ_0001824	Forward: AAGTGACGGGATCCGGAAAG
	Reverse: TCAGCAGCCAGTTTTTCAATGT
hsa_circ_0002882	Forward: GGGAGAGTTTGGAGCTGTGAT
	Reverse: TCCTTCAGCTCTTCACTGATGC
hsa_circ_0001819	Forward: CCTGGTAGGACAAGCGACTCTC
	Reverse: GCAGCATGATTTGGTCCCAC
hsa_circ_0008394	Forward: TGAACACTAGTCTGAATGTATACCG
	Reverse: ACGAATGAAGCCTCGTGTGG
hsa_circ_0006535	Forward: CATGCTGAGCTTTGCCAGAGAC
	Reverse: GCAATCTCCTGTTGGCTGGC
hsa_circ_0002538	Forward: AAAAGGCAACAACAGCACCAGC
	Reverse: CAAAACCCACTCAACTGCCATTGT
hsa_circ_0002538 convergent	Forward: ACCTTCTGCCTTCTCTCTACCCT
	Reverse: GCTGTTGTTGCCTTTTCCCCTT

mRNA (5'-3')	
SERINC5	Forward: GGAGGCTTGGTTTTGATGGCA
	Reverse: CCGAGTGTGGCTGTCGATTTT
GJC3	Forward: TTGTGCTTCTGGGTTTGGGGA
	Reverse: TGGGAGGCTATCGGTTGCTTT
PLP1	Forward: CATCACCTATGCCCTGACCGT
	Reverse: AGGCAATAGACTGGCAGGTGG
PRX	Forward: GGTGGCCAAGCTGAACATCCA
	Reverse: AGGAGAACTCGACGTCAACAGG
MPZ	Forward: AGAGGAGGCTCAGTGCTATGG
	Reverse: CAGCTTTGGTGCTTCTGCTGT
KLHL8	Forward: CGTGGAGGAGTTGGCTCTGTT
	Reverse: CCTGCTCTTCGCTGACCCATT
GAPDH	Forward: ATCCACAGTCTTCTGGGTGGC
	Reverse: TCCTGGAACAGCAAAACAAGGC
PLLP	Forward: CTTTAACATCAGCGCCACCGTT
	Reverse: ACCAAACACGCAAAGAACGAGG
β-Actin	Forward: CAGCCTTCCTTCCTGGGCAT
	Reverse: GGGCAGTGATCTCCTTCTGCAT
β-Actin-divergent	Forward: AAATCGTGCGTGACATTAAGGAGA
	Reverse: CATACCCCTCGTAGATGGGCA
U3	Forward: TGTAGAGCACCGAAAACCACG
	Reverse: CAGCCAAGCAACGCCAGA
miRNA (5'-3')	
hsa-miR-138-5p	AGCTGGTGTTGTGAATCAGG
miR-3714	GAAGGCAGCAGTGCTCCCCTGT
U6	Forward: CTCGCTTCGGCAGCACA
	Reverse: AACGCTTCACGAATTTGCGT
miR-138-5p stem-loop	RT: GTCGTATCCAGTGCAGGGTCCGAGGTATTCGCACTGGATACGACCGGCCT
	Forward: GCGAGCTGGTGTTGTGAATC
	Reverse: AGTGCAGGGTCCGAGGTATT
U6 stem-loop RT	RT: GTCGTATCGACTGCAGGGTCCGAGGTATTCGCAGTCGATACGACAAAATATG
	Forward: AGCACATATACTAAAATTGGAACGAT
	Reverse: ACTGCAGGGTCCGAGGTATT

circRNAs: circular RNAs; SERINC5: serine incorporator 5; PLLP: plasmolipin; GJC3: gap junction protein gamma 3; PLP1: proteolipid protein 1; PRX: periaxin; MPZ: myelin protein zero; KLHL8: Kelch-like family member 8; GAPDH: glyceraldehyde-3-phosphate dehydrogenase; U3: small nucleolar U3 RNA.

Additional Table 2. Nucleic acid sequences used in this study

Nucleic acid	Sequences (5'-3')
sh NC	Sense: TTCTCCGAACGTGTCACGT
	Antisense: ACGTGACACGTTCGGAGAA
sh1 circ_0002538	Sense: GTCACACTCAAGTCACAGCAA
	Antisense: TTGCTGTGACTTGAGTGTGAC
sh2 circ_0002538	Sense: ACTCAAGTCACAGCAAACTGT
	Antisense: ACAGTTTGCTGTGACTTGAGT
biotin-miR NC	TTTGTACTACACAAAAGTACTG
biotin-miR-138-5p mimic	AGCTGGTGTTGTGAATCAGGCCG
biotin-circ_0002538 NC	GAACTCTGTGATGTCACACTCAAGTCACAGCAAACTGTACAATGGCAG
biotin-circ_0002538	CTGCCATTGTACAGTTTGCTGTGACTTGAGTGTGACATCACAGAGTTC
mimics NC	Sense: UUUGUACUACACAAAAGUACUG
	Antisense: AAACAUGAUGUGUUUUCAUGAC
miR-138-5p mimics	Sense: AGCUGGUGUUGUGAAUCAGGCCG
	Antisense: UCGACCACAACACUUAGUCCGGC
Inhibitor miR-NC	CAGUACUUUUGUGUAGUACAAA
Inhibitor miR-138-5p	AGCTGGTGTTGTGAATCAGG

NC: Normal control; sh circ_0002538: short hairpin RNA for circ_0002538; sh NC: normal control for short hairpin RNA.

Additional Table 3. Basic characteristics of patients included in the study

Variables	Non-diabetic donators	Diabetic donators	*P*-value
Number	14	15	NA
Age (yr)	63.5 (55.75-65.0)	60.0 (56.0-67.0)	0.78
Female [*n* (%)]	4 (29)	4 (27)	NA
BMI (kg/m^2)	24.22 (23.35-26.23)	24.36 (23.1-25.265)	0.55
SBP (mmHg)	133.5 (123.75-140)	138 (126-150.5)	0.27
DBP (mmHg)	78.5 (73.5-84.25)	82 (70.5-88)	0.82
FBG (mM)	5.8 (5.49-6.345)	11.3 (8.1-14.375)	<0.0001
HbA1c (%)	NA	7.2 (6.8-7.35)	NA
Total cholesterol (mM)	4.165 (3.52-4.72)	3.66 (3.14-5.32)	0.61
Triglyceride (mM)	1.29 (1.09-1.565)	1.39 (1.11-1.56)	0.91
Creatinine (μM)	67.4 (47.4-76.5)	71.8 (67.3-96.2)	0.07
BUN (mM)	5.27 (3.56-6.27)	5.49 (4.15-7.29)	0.31
HDL-C (mM)	1.09 (0.765-1.16)	0.79 (0.72-0.87)	0.40
LDL-C (mM)	2.69 (1.96-3)	2.56 (1.58-3.93)	0.42

Data are median (IQR) or number (%), unless otherwise specified. *P*-values comparing patients with or without DPN were obtained by the independent-samples *t*-test or Fisher's exact test. BMI: Body mass index; BUN: blood urea nitrogen; DBP: diastolic blood pressure; FBG: fasting blood glucose; HbA1c: glycated hemoglobin; HDL-C: high-density lipoprotein cholesterol; IQR: interquartile range; LDL-C: low-density lipoprotein cholesterol; NA: not applicable; SBP: systolic blood pressure.

Additional Table 5 GO cellular component analysis of differentially expressed proteins

GO_C Term ID	GO_C Term Desc	GO_C Term Level1	GO_C Term Level2	Term Candidate Gene Num	Total Candidate Gene Num	Term Gene Num	Total Gene Num	Rich Ratio	P value	Q value
GO:0005739	mitochondrion	cellular_component	organelle	64	255	1926	25187	0.033229	9.47E-18	3.36E-15
GO:0043209	myelin sheath	cellular_component	cell part	20	255	246	25187	0.081301	9.73E-13	1.73E-10
GO:0005743	mitochondrial inner membrane	cellular_component	organelle	28	255	565	25187	0.049558	5.14E-12	6.08E-10
GO:0070062	extracellular exosome	cellular_component	organelle	73	255	3513	25187	0.02078	7.01E-10	6.22E-08
GO:0008021	synaptic vesicle	cellular_component	organelle	14	255	162	25187	0.08642	1.21E-09	8.61E-08
GO:0016020	membrane	cellular_component	membrane	141	255	9539	25187	0.014781	1.08E-08	6.37E-07
GO:0005741	mitochondrial outer membrane	cellular_component	organelle	15	255	244	25187	0.061475	3.24E-08	1.64E-06
GO:0030667	secretory granule membrane	cellular_component	organelle	10	255	144	25187	0.069444	2.22E-06	9.85E-05
GO:0070821	tertiary granule membrane	cellular_component	organelle	8	255	97	25187	0.082474	6.57E-06	2.59E-04
GO:0070469	respiratory chain	cellular_component	membrane	6	255	61	25187	0.098361	3.54E-05	0.001256
GO:0005751	mitochondrial respiratory chain	cellular_component	organelle	4	255	22	25187	0.181818	6.50E-05	0.002099
GO:0005737	cytoplasm	cellular_component	cell part	115	255	8450	25187	0.013609	7.81E-05	0.002309
GO:0005886	plasma membrane	cellular_component	membrane	91	255	6315	25187	0.01441	9.80E-05	0.002676
GO:0061617	MICOS complex	cellular_component	organelle	3	255	10	25187	0.3	1.17E-04	0.002961
GO:0101003	ficolin-1-rich granule membrane	cellular_component	organelle	6	255	78	25187	0.076923	1.42E-04	0.003356
GO:0005829	cytosol	cellular_component	cell part	102	255	7429	25187	0.01373	2.03E-04	0.004498
GO:0005747	mitochondrial respiratory chain	cellular_component	organelle	5	255	60	25187	0.083333	3.55E-04	0.007407
GO:0005759	mitochondrial matrix	cellular_component	membrane-enclosed lumen	14	255	481	25187	0.029106	4.27E-04	0.008414
GO:0046930	pore complex	cellular_component	membrane	3	255	18	25187	0.166667	7.48E-04	0.013972
GO:0009986	cell surface	cellular_component	cell	20	255	900	25187	0.022222	9.01E-04	0.015988
GO:0000275	mitochondrial proton-transporting ATP synthase complex, catalytic core F(1)	cellular_component	organelle	2	255	5	25187	0.4	0.001001	0.016916
GO:0048471	perinuclear region of cytoplasm	cellular_component	cell part	20	255	914	25187	0.021882	0.001085	0.01751
GO:0005768	endosome	cellular_component	organelle	17	255	724	25187	0.023481	0.001211	0.017915
GO:0045202	synapse	cellular_component	synapse	17	255	723	25187	0.023513	0.001193	0.017915
GO:0001401	mitochondrial sorting and assembly machinery complex	cellular_component	organelle	2	255	6	25187	0.333333	0.001491	0.019776
GO:0031225	anchored component of membrane	cellular_component	membrane	7	255	165	25187	0.042424	0.001504	0.019776
GO:0045261	proton-transporting ATP synthase complex, catalytic core F(1)	cellular_component	membrane	2	255	6	25187	0.333333	0.001491	0.019776
GO:0030054	cell junction	cellular_component	cell junction	21	255	1016	25187	0.020669	0.001652	0.020218
GO:0030666	endocytic vesicle membrane	cellular_component	organelle	6	255	123	25187	0.04878	0.001609	0.020218
GO:0042584	chromaffin granule membrane	cellular_component	organelle	2	255	7	25187	0.285714	0.002073	0.023744
GO:0045254	pyruvate dehydrogenase complex	cellular_component	cell part	2	255	7	25187	0.285714	0.002073	0.023744
GO:0044306	neuron projection terminus	cellular_component	cell part	3	255	26	25187	0.115385	0.002245	0.024901
GO:0030315	T-tubule	cellular_component	cell part	4	255	55	25187	0.072727	0.002334	0.025113
GO:0043190	ATP-binding cassette (ABC) transporter complex	cellular_component	membrane	2	255	8	25187	0.25	0.002746	0.027854
GO:1990246	uniplex complex	cellular_component	organelle	2	255	8	25187	0.25	0.002746	0.027854
GO:0030424	axon	cellular_component	cell part	12	255	466	25187	0.025751	0.002996	0.028964
GO:0042645	mitochondrial nucleoid	cellular_component	membrane-enclosed lumen	4	255	59	25187	0.067797	0.003019	0.028964
GO:0030658	transport vesicle membrane	cellular_component	organelle	5	255	98	25187	0.05102	0.003233	0.030206
GO:0042734	presynaptic membrane	cellular_component	membrane	5	255	100	25187	0.05	0.003527	0.032102
GO:0008091	spectrin	cellular_component	organelle	2	255	10	25187	0.2	0.004355	0.037706
GO:0032592	integral component of mitochondrial membrane	cellular_component	organelle	2	255	10	25187	0.2	0.004355	0.037706
GO:0043005	neuron projection	cellular_component	cell part	12	255	496	25187	0.024194	0.004908	0.041487
GO:0005921	gap junction	cellular_component	cell junction	3	255	35	25187	0.085714	0.005285	0.042658
GO:0014731	spectrin-associated cytoskeleton	cellular_component	organelle	2	255	11	25187	0.181818	0.005287	0.042658
GO:0005834	heterotrimeric G-protein complex	cellular_component	membrane	3	255	36	25187	0.083333	0.005723	0.045144
GO:0043204	perikaryon	cellular_component	cell part	6	255	160	25187	0.0375	0.005897	0.045509
GO:0009898	cytoplasmic side of plasma membrane	cellular_component	membrane	4	255	76	25187	0.052632	0.007447	0.05508
GO:0031982	vesicle	cellular_component	organelle	7	255	220	25187	0.031818	0.007313	0.05508
GO:0005586	collagen type III trimer	cellular_component	extracellular region part	1	255	1	25187	1	0.010124	0.061968
GO:0009295	nucleoid	cellular_component	nucleoid	1	255	1	25187	1	0.010124	0.061968
GO:0020003	symbiont-containing vacuole	cellular_component	organelle	1	255	1	25187	1	0.010124	0.061968
GO:0020005	symbiont-containing vacuole membrane	cellular_component	organelle	1	255	1	25187	1	0.010124	0.061968
GO:0031305	integral component of mitochondrial inner membrane	cellular_component	organelle	3	255	44	25187	0.068182	0.010005	0.061968
GO:0033017	sarcoplasmic reticulum membrane	cellular_component	organelle	3	255	43	25187	0.069767	0.009392	0.061968
GO:0034358	plasma lipoprotein particle	cellular_component	extracellular region part	1	255	1	25187	1	0.010124	0.061968
GO:0034466	chromaffin granule lumen	cellular_component	organelle	1	255	1	25187	1	0.010124	0.061968
GO:0099189	postsynaptic spectrin-associated cytoskeleton	cellular_component	organelle	1	255	1	25187	1	0.010124	0.061968
GO:1990031	pinceau fiber	cellular_component	cell part	1	255	1	25187	1	0.010124	0.061968
GO:0005614	interstitial matrix	cellular_component	extracellular region part	2	255	16	25187	0.125	0.011158	0.064935
GO:0016471	vacuolar proton-transporting V-type ATPase complex	cellular_component	organelle	2	255	16	25187	0.125	0.011158	0.064935
GO:0099738	cell cortex region	cellular_component	cell part	2	255	16	25187	0.125	0.011158	0.064935

GO:0031226	intrinsic component of plasma membrane	cellular_component	membrane	3	255	47	25187	0.06383	0.011981	0.068601
GO:0005740	mitochondrial envelope	cellular_component	organelle	2	255	17	25187	0.117647	0.012562	0.070785
GO:0030672	synaptic vesicle membrane	cellular_component	organelle	4	255	90	25187	0.044444	0.013298	0.073764
GO:0005750	mitochondrial respiratory chain	cellular_component	organelle	2	255	20	25187	0.1	0.017204	0.092537
GO:0015629	actin cytoskeleton	cellular_component	organelle	8	255	321	25187	0.024922	0.017011	0.092537
GO:0005922	connexin complex	cellular_component	membrane	2	255	22	25187	0.090909	0.020641	0.096417
GO:0005954	calcium- and calmodulin-dependent protein kinase complex	cellular_component	cell part	1	255	2	25187	0.5	0.020146	0.096417
GO:0008076	voltage-gated potassium channel complex	cellular_component	membrane	4	255	99	25187	0.040404	0.018269	0.096417
GO:0009353	mitochondrial oxoglutarate dehydrogenase complex	cellular_component	membrane-enclosed lumen	1	255	2	25187	0.5	0.020146	0.096417
GO:0019008	molybdopterin synthase complex	cellular_component	cell part	1	255	2	25187	0.5	0.020146	0.096417
GO:0032473	cytoplasmic side of mitochondrial outer membrane	cellular_component	organelle	1	255	2	25187	0.5	0.020146	0.096417
GO:0060987	lipid tube	cellular_component	protein-containing complex	1	255	2	25187	0.5	0.020146	0.096417
GO:0097180	serine protease inhibitor complex	cellular_component	protein-containing complex	1	255	2	25187	0.5	0.020146	0.096417
GO:0098688	parallel fiber to Purkinje cell synapse	cellular_component	synapse	2	255	22	25187	0.090909	0.020641	0.096417
GO:0099160	postsynaptic intermediate filament cytoskeleton	cellular_component	organelle	1	255	2	25187	0.5	0.020146	0.096417
GO:0005868	cytoplasmic dynein complex	cellular_component	organelle	2	255	23	25187	0.086957	0.022458	0.103542
GO:0010008	endosome membrane	cellular_component	membrane	8	255	340	25187	0.023529	0.023063	0.104967
GO:0031201	SNARE complex	cellular_component	membrane	3	255	62	25187	0.048387	0.02503	0.112479
GO:0034361	very-low-density lipoprotein particle	cellular_component	extracellular region part	2	255	25	25187	0.08	0.026281	0.116623
GO:0031410	cytoplasmic vesicle	cellular_component	organelle	14	255	776	25187	0.018041	0.027302	0.119657
GO:0005945	6-phosphofructokinase complex	cellular_component	cell part	1	255	3	25187	0.333333	0.030068	0.120195
GO:0016021	integral component of membrane	cellular_component	membrane	86	255	7102	25187	0.012109	0.030133	0.120195
GO:0020018	ciliary pocket membrane	cellular_component	organelle	1	255	3	25187	0.333333	0.030068	0.120195
GO:0043296	apical junction complex	cellular_component	cell junction	2	255	26	25187	0.076923	0.028284	0.120195
GO:0045177	apical part of cell	cellular_component	cell	4	255	113	25187	0.035398	0.028042	0.120195
GO:0060201	clathrin-sculpted acetylcholine transport vesicle membrane	cellular_component	organelle	1	255	3	25187	0.333333	0.030068	0.120195
GO:0098560	cytoplasmic side of late endosome membrane	cellular_component	membrane	1	255	3	25187	0.333333	0.030068	0.120195
GO:0099503	secretory vesicle	cellular_component	organelle	1	255	3	25187	0.333333	0.030068	0.120195
GO:0034774	secretory granule lumen	cellular_component	organelle	5	255	172	25187	0.02907	0.031036	0.122421
GO:0005753	mitochondrial proton-transporting ATP synthase complex	cellular_component	organelle	2	255	28	25187	0.071429	0.032467	0.122613
GO:0005783	endoplasmic reticulum	cellular_component	organelle	27	255	1831	25187	0.014746	0.031832	0.122613
GO:0016459	myosin complex	cellular_component	organelle	3	255	68	25187	0.044118	0.031747	0.122613
GO:0034704	calcium channel	cellular_component	membrane	2	255	28	25187	0.071429	0.032467	0.122613
GO:0030425	dendrite	cellular_component	cell part	11	255	582	25187	0.0189	0.035725	0.132106
GO:0098685	Schaffer collateral - CA1 synapse	cellular_component	synapse	4	255	122	25187	0.032787	0.035692	0.132106
GO:0005846	nuclear cap binding complex	cellular_component	cell part	1	255	4	25187	0.25	0.039889	0.134861
GO:0016529	sarcoplasmic reticulum	cellular_component	organelle	3	255	74	25187	0.040541	0.03931	0.134861
GO:0030027	lamellipodium	cellular_component	cell part	6	255	245	25187	0.02449	0.039092	0.134861
GO:0030478	actin cap	cellular_component	organelle	1	255	4	25187	0.25	0.039889	0.134861
GO:0034518	RNA cap binding complex	cellular_component	protein-containing complex	1	255	4	25187	0.25	0.039889	0.134861
GO:0034686	integrin alphav-beta8 complex	cellular_component	membrane	1	255	4	25187	0.25	0.039889	0.134861
GO:0042588	zymogen granule	cellular_component	organelle	1	255	4	25187	0.25	0.039889	0.134861
GO:0060203	clathrin-sculpted glutamate transport vesicle membrane	cellular_component	organelle	1	255	4	25187	0.25	0.039889	0.134861
GO:0098559	cytoplasmic side of early endosome membrane	cellular_component	membrane	1	255	4	25187	0.25	0.039889	0.134861
GO:0042613	MHC class II protein complex	cellular_component	membrane	3	255	76	25187	0.039474	0.042016	0.140714
GO:0045121	membrane raft	cellular_component	membrane	7	255	317	25187	0.022082	0.043252	0.1435
GO:0031307	integral component of mitochondrial outer membrane	cellular_component	organelle	2	255	33	25187	0.060606	0.043886	0.144256
GO:0005947	mitochondrial alpha-ketoglutarate dehydrogenase complex	cellular_component	membrane-enclosed lumen	1	255	5	25187	0.2	0.049611	0.151825
GO:0014704	intercalated disc	cellular_component	cell junction	3	255	81	25187	0.037037	0.049178	0.151825
GO:0016342	catenin complex	cellular_component	membrane	2	255	35	25187	0.057143	0.048812	0.151825
GO:0033557	Slx1-Slx4 complex	cellular_component	membrane-enclosed lumen	1	255	5	25187	0.2	0.049611	0.151825
GO:0070032	synaptobrevin 2-SNAP-25-syntaxin-1a-complexin I complex	cellular_component	membrane	1	255	5	25187	0.2	0.049611	0.151825
GO:0070083	clathrin-sculpted monoamine transport vesicle membrane	cellular_component	organelle	1	255	5	25187	0.2	0.049611	0.151825
GO:0098857	membrane microdomain	cellular_component	membrane	1	255	5	25187	0.2	0.049611	0.151825
GO:1990726	Lsm1-7-Pat1 complex	cellular_component	protein-containing complex	1	255	5	25187	0.2	0.049611	0.151825

Additional Table 8 KEGG pathway analysis of differentially expressed proteins

KEGG Pathway Term ID	KEGG Pathway Term Desc	KEGG Pathway Term Level1	KEGG Pathway Term Level2	Term Candidate Gene Num	Total Candidate Gene Num	Term Gene Num	Total Gene Num	Rich Ratio	P value	Q value
5012	Parkinson's disease	Human Diseases	Neurodegenerative diseases	20	187	209	15870	0.09569	5.64E-13	1.60E-10
1100	Metabolic pathways	Metabolism	Global and overview maps	58	187	1923	15870	0.03016	4.81E-12	6.81E-10
5016	Huntington's disease	Human Diseases	Neurodegenerative diseases	19	187	283	15870	0.06714	1.03E-09	9.72E-08
190	Oxidative phosphorylation	Metabolism	Energy metabolism	15	187	195	15870	0.07692	1.04E-08	7.33E-07
4714	Thermogenesis	Organismal Systems	Environmental adaptation	17	187	318	15870	0.05346	2.27E-07	1.28E-05
5010	Alzheimer's disease	Human Diseases	Neurodegenerative diseases	15	187	256	15870	0.05859	3.76E-07	1.77E-05
1110	Biosynthesis of secondary metabolites	Metabolism	Global and overview maps	21	187	558	15870	0.03763	2.73E-06	1.10E-04
4020	Calcium signaling pathway	Environmental Information Processing	Signal transduction	12	187	256	15870	0.04688	5.27E-05	0.00186
4932	Non-alcoholic fatty liver disease (NAFLD)	Human Diseases	Endocrine and metabolic diseases	11	187	250	15870	0.044	1.89E-04	0.00594
350	Tyrosine metabolism	Metabolism	Amino acid metabolism	5	187	48	15870	0.10417	2.44E-04	0.00629
4922	Glucagon signaling pathway	Organismal Systems	Endocrine system	8	187	138	15870	0.05797	2.30E-04	0.00629
4723	Retrograde endocannabinoid signaling	Organismal Systems	Nervous system	9	187	180	15870	0.05	2.86E-04	0.00675
1200	Carbon metabolism	Metabolism	Global and overview maps	9	187	189	15870	0.04762	4.10E-04	0.00892
950	Isoquinoline alkaloid biosynthesis	Metabolism	Biosynthesis of other secondary metabolites	3	187	14	15870	0.21429	5.33E-04	0.01005
4217	Necroptosis	Cellular Processes	Cell growth and death	10	187	236	15870	0.04237	4.97E-04	0.01005
4979	Cholesterol metabolism	Organismal Systems	Digestive system	5	187	60	15870	0.08333	6.96E-04	0.01231
1120	Microbial metabolism in diverse environments	Metabolism	Global and overview maps	10	187	250	15870	0.04	7.77E-04	0.01267
4971	Gastric acid secretion	Organismal Systems	Digestive system	6	187	93	15870	0.06452	8.06E-04	0.01267
4260	Cardiac muscle contraction	Organismal Systems	Circulatory system	6	187	97	15870	0.06186	0.001	0.01497
4978	Mineral absorption	Organismal Systems	Digestive system	5	187	66	15870	0.07576	0.00108	0.01522
4728	Dopaminergic synapse	Organismal Systems	Nervous system	8	187	177	15870	0.0452	0.0012	0.01616
4725	Cholinergic synapse	Organismal Systems	Nervous system	7	187	145	15870	0.04828	0.00166	0.02136
1130	Biosynthesis of antibiotics	Metabolism	Global and overview maps	11	187	327	15870	0.03364	0.00175	0.02154
4730	Long-term depression	Organismal Systems	Nervous system	5	187	75	15870	0.06667	0.00191	0.0225
360	Phenylalanine metabolism	Metabolism	Amino acid metabolism	3	187	22	15870	0.13636	0.0021	0.02284
4218	Cellular senescence	Cellular Processes	Cell growth and death	10	187	287	15870	0.03484	0.00218	0.02284
4921	Oxytocin signaling pathway	Organismal Systems	Endocrine system	8	187	194	15870	0.04124	0.00214	0.02284
5031	Amphetamine addiction	Human Diseases	Substance dependence	5	187	86	15870	0.05814	0.00347	0.03401
5216	Thyroid cancer	Human Diseases	Cancers: Specific types	4	187	53	15870	0.07547	0.00348	0.03401
4720	Long-term potentiation	Organismal Systems	Nervous system	5	187	88	15870	0.05682	0.00383	0.03593
4916	Melanogenesis	Organismal Systems	Endocrine system	6	187	127	15870	0.04724	0.00394	0.03593
4022	cGMP-PKG signaling pathway	Environmental Information Processing	Signal transduction	8	187	228	15870	0.03509	0.00569	0.05033
4514	Cell adhesion molecules (CAMs)	Environmental Information Processing	Signaling molecules and interaction	9	187	279	15870	0.03226	0.00591	0.05068
790	Folate biosynthesis	Metabolism	Metabolism of cofactors and vitamins	3	187	33	15870	0.09091	0.00677	0.05544
3320	PPAR signaling pathway	Organismal Systems	Endocrine system	5	187	101	15870	0.0495	0.00686	0.05544
4216	Ferroptosis	Cellular Processes	Cell growth and death	4	187	65	15870	0.06154	0.00723	0.0568
4911	Insulin secretion	Organismal Systems	Endocrine system	5	187	104	15870	0.04808	0.00774	0.0592
4621	NOD-like receptor signaling pathway	Organismal Systems	Immune system	8	187	247	15870	0.03239	0.00904	0.06734
4972	Pancreatic secretion	Organismal Systems	Digestive system	5	187	111	15870	0.04505	0.0101	0.07331
4745	Phototransduction - fly	Organismal Systems	Sensory system	3	187	39	15870	0.07692	0.01078	0.07625
30	Pentose phosphate pathway	Metabolism	Carbohydrate metabolism	3	187	41	15870	0.07317	0.01236	0.08032
52	Galactose metabolism	Metabolism	Carbohydrate metabolism	3	187	41	15870	0.07317	0.01236	0.08032
4212	Longevity regulating pathway - worm	Organismal Systems	Aging	5	187	117	15870	0.04274	0.01249	0.08032
5034	Alcoholism	Human Diseases	Substance dependence	7	187	208	15870	0.03365	0.01174	0.08032
4912	GnRH signaling pathway	Organismal Systems	Endocrine system	5	187	118	15870	0.04237	0.01292	0.08125
4713	Circadian entrainment	Organismal Systems	Environmental adaptation	5	187	120	15870	0.04167	0.01381	0.08497
480	Glutathione metabolism	Metabolism	Metabolism of other amino acids	4	187	79	15870	0.05063	0.01413	0.08507
5230	Central carbon metabolism in cancer	Human Diseases	Cancers: Overview	4	187	81	15870	0.04938	0.01536	0.09059
4360	Axon guidance	Organismal Systems	Development	7	187	223	15870	0.03139	0.01665	0.09474
4925	Aldosterone synthesis and secretion	Organismal Systems	Endocrine system	5	187	126	15870	0.03968	0.01674	0.09474
51	Fructose and mannose metabolism	Metabolism	Carbohydrate metabolism	3	187	47	15870	0.06383	0.01786	0.09536
4371	Apelin signaling pathway	Environmental Information Processing	Signal transduction	6	187	175	15870	0.03429	0.0176	0.09536
4721	Synaptic vesicle cycle	Organismal Systems	Nervous system	4	187	84	15870	0.04762	0.01734	0.09536
4261	Adrenergic signaling in cardiomyocytes	Organismal Systems	Circulatory system	6	187	185	15870	0.03243	0.02245	0.11763
250	Alanine, aspartate and glutamate metabolism	Metabolism	Amino acid metabolism	3	187	52	15870	0.05769	0.02333	0.12003
10	Glycolysis / Gluconeogenesis	Metabolism	Carbohydrate metabolism	4	187	94	15870	0.04255	0.02506	0.12664
4640	Hematopoietic cell lineage	Organismal Systems	Immune system	6	187	194	15870	0.03093	0.02751	0.1366
20	Citrate cycle (TCA cycle)	Metabolism	Carbohydrate metabolism	3	187	58	15870	0.05172	0.03095	0.14129
71	Fatty acid degradation	Metabolism	Lipid metabolism	3	187	57	15870	0.05263	0.0296	0.14129
4066	HIF-1 signaling pathway	Environmental Information Processing	Signal transduction	5	187	148	15870	0.03378	0.03089	0.14129
4726	Serotonergic synapse	Organismal Systems	Nervous system	5	187	147	15870	0.03401	0.03012	0.14129
5214	Glioma	Human Diseases	Cancers: Specific types	4	187	100	15870	0.04	0.03054	0.14129
1230	Biosynthesis of amino acids	Metabolism	Global and overview maps	4	187	104	15870	0.03846	0.03455	0.15501
4974	Protein digestion and absorption	Organismal Systems	Digestive system	4	187	105	15870	0.0381	0.0356	0.15501
5030	Cocaine addiction	Human Diseases	Substance dependence	3	187	61	15870	0.04918	0.0352	0.15501

330	Arginine and proline metabolism	Metabolism	Amino acid metabolism	3	187	63	15870	0.04762	0.03819	0.15716
340	Histidine metabolism	Metabolism	Amino acid metabolism	2	187	27	15870	0.07407	0.03997	0.15716
520	Amino sugar and nucleotide sugar metabolism	Metabolism	Carbohydrate metabolism	3	187	64	15870	0.04688	0.03973	0.15716
4012	ErbB signaling pathway	Environmental Information Processing	Signal transduction	4	187	109	15870	0.0367	0.03999	0.15716
4727	GABAergic synapse	Organismal Systems	Nervous system	4	187	108	15870	0.03704	0.03886	0.15716
5110	Vibrio cholerae infection	Human Diseases	Infectious diseases: Bacterial	3	187	62	15870	0.04839	0.03668	0.15716
5166	HTLV-I infection	Human Diseases	Infectious diseases: Viral	10	187	447	15870	0.02237	0.03928	0.15716
4722	Neurotrophin signaling pathway	Organismal Systems	Nervous system	5	187	160	15870	0.03125	0.04105	0.15728
4970	Salivary secretion	Organismal Systems	Digestive system	4	187	110	15870	0.03636	0.04113	0.15728
4015	Rap1 signaling pathway	Environmental Information Processing	Signal transduction	7	187	273	15870	0.02564	0.04316	0.16287
1212	Fatty acid metabolism	Metabolism	Global and overview maps	3	187	69	15870	0.04348	0.0479	0.17797
4614	Renin-angiotensin system	Organismal Systems	Endocrine system	2	187	30	15870	0.06667	0.04842	0.17797

KEGG: Kyoto Encyclopedia of Genes and Genomes.

Additional Table 9 The DEcircRNAs analyzed in this study were selected from the results of circRNA sequencing analysis

circName	gene symbol	CZL-FC-B	FFL-FQ-B	YYC-FC-B	CCK-FC	WCF-FC-BX	CZG-FC-BS	log2(Fold_change)	p-value	q-value	circBase	Web
hsa_circ:chr11:120276827-120278532	*ARHGEF12*	319	435	636	9234	2564	4666	2.710491179	1.26E-10	2.22E-08	hsa_circ_0024604	http://www.circbase.org/cgi-bin/singlerecord.cgi?id=hsa_circ_0024604
hsa_circ:chr9:134381501-134381840	*POMT1*	330	683	739	8179	4331	6055	2.598539216	2.77E-20	6.19E-17	hsa_circ_0001897	http://www.circbase.org/cgi-bin/singlerecord.cgi?id=hsa_circ_0001897
hsa_circ:chr10:128806996-128810638	*DOCK1*	80	136	217	1933	1163	1073	2.468022558	9.41E-15	6.13E-12	hsa_circ_0020433	http://www.circbase.org/cgi-bin/singlerecord.cgi?id=hsa_circ_0020433
hsa_circ:chr13:24823615-24826000	*SPATA13*	63	90	66	1552	398	310	2.347737447	2.78E-06	0.000109	hsa_circ_0003040	http://www.circbase.org/cgi-bin/singlerecord.cgi?id=hsa_circ_0003040
hsa_circ:chr16:68155890-68160513	*ENSG00000261864.1,NFATC3*	140	127	170	1522	1492	944	2.331800087	3.09E-14	1.79E-11	hsa_circ_0000711	http://www.circbase.org/cgi-bin/singlerecord.cgi?id=hsa_circ_0000711
hsa_circ:chr15:101775287-101775782	*CHSY1*	113	161	107	2302	673	706	2.278883636	1.92E-05	0.000503	hsa_circ_0005019	http://www.circbase.org/cgi-bin/singlerecord.cgi?id=hsa_circ_0005019
hsa_circ:chr19:1271328-1272050	*CIRBP*	115	273	289	2890	1394	1281	2.184967412	8.65E-11	1.73E-08	hsa_circ_0007715	http://www.circbase.org/cgi-bin/singlerecord.cgi?id=hsa_circ_0007715
hsa_circ:chr3:171965323-171969331	*FNDC3B*	358	1139	926	8645	4811	4483	2.039068321	3.77E-06	0.000138	hsa_circ_0006156	http://www.circbase.org/cgi-bin/singlerecord.cgi?id=hsa_circ_0006156
hsa_circ:chr5:171482592-171484477	*STK10*	86	172	117	1260	705	793	2.001937464	8.13E-08	5.36E-06	hsa_circ_0001555	http://www.circbase.org/cgi-bin/singlerecord.cgi?id=hsa_circ_0001555
hsa_circ:chr1:14042036-14075982	*PRDM2*	82	83	105	809	562	480	1.919088074	9.56E-08	6.13E-06	NA	NA
hsa_circ:chr16:88061089-88071617	*BANP*	169	147	192	1461	1166	846	1.906629396	4.70E-10	6.56E-08	hsa_circ_0040823	http://www.circbase.org/cgi-bin/singlerecord.cgi?id=hsa_circ_0040823
hsa_circ:chr10:99196948-99197507	*EXOSC1*	172	254	482	2531	1820	1364	1.872337049	2.45E-10	3.76E-08	hsa_circ_0004896	http://www.circbase.org/cgi-bin/singlerecord.cgi?id=hsa_circ_0004896
hsa_circ:chr15:41036245-41037457	*RMDN3*	70	133	158	1171	517	624	1.838657173	1.16E-06	5.33E-05	hsa_circ_0004942	http://www.circbase.org/cgi-bin/singlerecord.cgi?id=hsa_circ_0004942
hsa_circ:chr15:93540187-93541851	*CHD2*	60	55	125	426	490	464	1.794259793	2.85E-05	0.000704	hsa_circ_0000655	http://www.circbase.org/cgi-bin/singlerecord.cgi?id=hsa_circ_0000655
hsa_circ:chr16:68155890-68157024	*ENSG00000261864.1,NFATC3*	133	99	174	1039	779	652	1.764900392	1.28E-07	7.93E-06	hsa_circ_0005615	http://www.circbase.org/cgi-bin/singlerecord.cgi?id=hsa_circ_0005615
hsa_circ:chr19:41754419-41754725	*AXL*	211	297	597	3127	1340	1883	1.741241582	6.40E-08	4.27E-06	hsa_circ_0002882	http://www.circbase.org/cgi-bin/singlerecord.cgi?id=hsa_circ_0002882
hsa_circ:chr8:131164982-131181313	*ASAP1*	542	363	544	4679	1996	2298	1.71720344	2.15E-08	1.69E-06	hsa_circ_0001824	http://www.circbase.org/cgi-bin/singlerecord.cgi?id=hsa_circ_0001824
hsa_circ:chr16:11114050-11154879	*CLEC16A*	57	63	55	435	309	308	1.712257159	0.000168	0.002957	hsa_circ_0000672	http://www.circbase.org/cgi-bin/singlerecord.cgi?id=hsa_circ_0000672
hsa_circ:chr21:48063447-48064400	*PRMT2*	143	220	351	1972	1321	843	1.711577476	5.98E-08	4.07E-06	hsa_circ_0003781	http://www.circbase.org/cgi-bin/singlerecord.cgi?id=hsa_circ_0003781
hsa_circ:chr22:34157358-34252790	*LARGE1*	110	143	250	1555	527	832	1.708406728	5.51E-06	0.000187	hsa_circ_0063019	http://www.circbase.org/cgi-bin/singlerecord.cgi?id=hsa_circ_0063019
hsa_circ:chr9:131271155-131277918	*GLE1*	75	101	141	1006	413	462	1.706348705	1.24E-05	0.000357	hsa_circ_0002675	http://www.circbase.org/cgi-bin/singlerecord.cgi?id=hsa_circ_0002675
hsa_circ:chr12:57059988-57064148	*PTGES3*	69	86	84	589	276	526	1.702531372	0.00013	0.00244	hsa_circ_0027089	http://www.circbase.org/cgi-bin/singlerecord.cgi?id=hsa_circ_0027089
hsa_circ:chr21:46275125-46281186	*PTTG1IP*	357	285	333	2777	1239	1859	1.698755826	1.32E-07	8.12E-06	hsa_circ_0001200	http://www.circbase.org/cgi-bin/singlerecord.cgi?id=hsa_circ_0001200
hsa_circ:chr6:43023283-43024183	*MRPL2*	57	66	131	629	367	418	1.69182392	3.44E-05	0.000814	hsa_circ_0001608	http://www.circbase.org/cgi-bin/singlerecord.cgi?id=hsa_circ_0001608
hsa_circ:chr12:123983091-123984083	*RILPL1*	236	520	520	3230	1977	1984	1.666769005	1.52E-08	1.25E-06	hsa_circ_0007552	http://www.circbase.org/cgi-bin/singlerecord.cgi?id=hsa_circ_0007552
hsa_circ:chr1:154207067-154207767	*UBAP2L*	104	216	266	1431	644	1087	1.640288416	8.60E-06	0.00027	NA	NA
hsa_circ:chr14:103918255-103923549	*MARK3*	157	139	150	1321	530	727	1.617693132	1.54E-05	0.000426	hsa_circ_0033475	http://www.circbase.org/cgi-bin/singlerecord.cgi?id=hsa_circ_0033475
hsa_circ:chr1:27269151-27269556	*NUDC*	256	302	550	2609	1519	1684	1.595422136	6.40E-09	5.99E-07	hsa_circ_0005087	http://www.circbase.org/cgi-bin/singlerecord.cgi?id=hsa_circ_0005087
hsa_circ:chr3:153912433-153935747	*ARHGEF26*	73	92	85	526	246	556	1.584230606	0.000715	0.008975	NA	NA
hsa_circ:chr12:124904503-124915333	*NCOR2*	88	118	162	1099	509	376	1.544679115	7.38E-05	0.001525	hsa_circ_0029308	http://www.circbase.org/cgi-bin/singlerecord.cgi?id=hsa_circ_0029308
hsa_circ:chr1:215759838-215768813	*KCTD3*	146	310	261	1709	765	1238	1.531205242	2.13E-05	0.000548	hsa_circ_0005521	http://www.circbase.org/cgi-bin/singlerecord.cgi?id=hsa_circ_0005521
hsa_circ:chr15:41361768-41362745	*INO80*	87	91	116	621	421	468	1.527105285	5.26E-05	0.00115	hsa_circ_0007489	http://www.circbase.org/cgi-bin/singlerecord.cgi?id=hsa_circ_0007489
hsa_circ:chr3:119222379-119222868	*TIMMDC1*	628	987	1512	7770	4093	3672	1.486728502	8.43E-09	7.53E-07	hsa_circ_0008394	http://www.circbase.org/cgi-bin/singlerecord.cgi?id=hsa_circ_0008394
hsa_circ:chr11:124517261-124518071	*SIAE*	145	58	148	631	502	583	1.46585348	0.000785	0.009691	hsa_circ_0000367	http://www.circbase.org/cgi-bin/singlerecord.cgi?id=hsa_circ_0000367
hsa_circ:chr8:103372299-103373854	*UBR5*	700	859	1621	6211	4483	4183	1.449358147	7.72E-10	1.01E-07	hsa_circ_0001819	http://www.circbase.org/cgi-bin/singlerecord.cgi?id=hsa_circ_0001819
hsa_circ:chr19:47767860-47768203	*CCDC9*	671	1253	1708	7592	4454	4462	1.379543586	7.66E-08	5.07E-06	hsa_circ_0000944	http://www.circbase.org/cgi-bin/singlerecord.cgi?id=hsa_circ_0000944
hsa_circ:chr12:120592774-120593523	*GCN1*	254	214	353	1843	877	1084	1.356950971	1.22E-05	0.000355	hsa_circ_0000448	http://www.circbase.org/cgi-bin/singlerecord.cgi?id=hsa_circ_0000448

hsa_circ:chr3:47139445-47147610	*SETD2*	355	449	487	2582	2034	1387	1.354151656	2.39E-07	1.36E-05	hsa_circ_0001290	http://www.circbase.org/cgi-bin/singlerecord.cgi?id=hsa_circ_0001290
hsa_circ:chr14:23378692-23380612	*RBM23*	667	977	1913	7053	3121	5100	1.342548268	7.29E-06	0.000234	hsa_circ_0000524	http://www.circbase.org/cgi-bin/singlerecord.cgi?id=hsa_circ_0000524
hsa_circ:chr8:131164982-131193126	*ASAP1*	416	319	408	2441	1681	1141	1.297037309	1.40E-05	0.000395	hsa_circ_0008934	http://www.circbase.org/cgi-bin/singlerecord.cgi?id=hsa_circ_0008934
hsa_circ:chr20:47570093-47580435	*ARFGEF2*	154	158	286	1158	673	740	1.293570365	5.27E-05	0.001151	hsa_circ_0003998	http://www.circbase.org/cgi-bin/singlerecord.cgi?id=hsa_circ_0003998
hsa_circ:chr15:80412670-80415142	*ZFAND6*	527	568	743	3469	1985	2536	1.284851683	4.57E-07	2.43E-05	hsa_circ_0000643	http://www.circbase.org/cgi-bin/singlerecord.cgi?id=hsa_circ_0000643
hsa_circ:chr2:160025761-160027316	*TANC1*	180	223	267	1150	1009	737	1.277151485	1.78E-05	0.000475	hsa_circ_0056810	http://www.circbase.org/cgi-bin/singlerecord.cgi?id=hsa_circ_0056810
hsa_circ:chr3:196118684-196120490	*UBXN7*	142	174	237	1046	654	651	1.255873553	6.77E-05	0.001419	hsa_circ_0005051	http://www.circbase.org/cgi-bin/singlerecord.cgi?id=hsa_circ_0005051
hsa_circ:chr18:9524592-9525849	*RALBP1*	1003	1152	2868	10330	4744	5270	1.235638445	1.91E-05	0.000502	hsa_circ_0005158	http://www.circbase.org/cgi-bin/singlerecord.cgi?id=hsa_circ_0005158
hsa_circ:chr11:108137898-108138069	*ATM*	179	204	289	1390	602	838	1.228247142	0.000216	0.003586	hsa_circ_0007694	http://www.circbase.org/cgi-bin/singlerecord.cgi?id=hsa_circ_0007694
hsa_circ:chr9:33971649-33973235	*UBAP2*	657	1419	1442	5858	4652	3689	1.195953494	6.18E-06	0.000205	hsa_circ_0001851	http://www.circbase.org/cgi-bin/singlerecord.cgi?id=hsa_circ_0001851
hsa_circ:chr2:72958136-72960247	*EXOC6B*	287	311	549	2065	941	1492	1.170419692	0.000174	0.003028	hsa_circ_0001030	http://www.circbase.org/cgi-bin/singlerecord.cgi?id=hsa_circ_0001030
hsa_circ:chr3:56600622-56601081	*CCDC66*	322	286	510	1987	1398	1019	1.138112107	4.21E-05	0.000963	hsa_circ_0001312	http://www.circbase.org/cgi-bin/singlerecord.cgi?id=hsa_circ_0001312
hsa_circ:chr3:197592294-197593090	*LRCH3*	194	209	359	1218	729	916	1.113625109	0.000336	0.005019	hsa_circ_0008439	http://www.circbase.org/cgi-bin/singlerecord.cgi?id=hsa_circ_0008439
hsa_circ:chr2:168920010-168986268	*STK39*	275	623	721	3239	1381	1516	1.077885846	0.000968	0.011373	hsa_circ_0005882	http://www.circbase.org/cgi-bin/singlerecord.cgi?id=hsa_circ_0005882
hsa_circ:chr2:209209835-209212747	*PIKFYVE*	221	327	371	1433	1151	829	1.054921911	0.000252	0.004053	hsa_circ_0001097	http://www.circbase.org/cgi-bin/singlerecord.cgi?id=hsa_circ_0001097
hsa_circ:chr2:153431650-153437563	*FMNL2*	556	825	1057	3816	2604	2419	1.038670032	1.03E-05	0.000312	NA	NA
hsa_circ:chr5:142434004-142437312	*ARHGAP26*	527	543	586	456	476	468	-1.063382894	0.000916	0.010935	hsa_circ_0074371	http://www.circbase.org/cgi-bin/singlerecord.cgi?id=hsa_circ_0074371
hsa_circ:chr11:46098305-46113774	*PHF21A*	928	1052	1333	995	1093	678	-1.084886764	4.59E-05	0.001024	hsa_circ_0000296	http://www.circbase.org/cgi-bin/singlerecord.cgi?id=hsa_circ_0000296
hsa_circ:chr5:65284463-65290692	*ERBIN*	794	640	1888	996	1003	629	-1.087183343	0.000669	0.00854	hsa_circ_0001492	http://www.circbase.org/cgi-bin/singlerecord.cgi?id=hsa_circ_0001492
hsa_circ:chr8:62593527-62596747	*ASPH*	1413	1936	2315	2148	1127	1320	-1.146691876	3.42E-06	0.000127	hsa_circ_0084615	http://www.circbase.org/cgi-bin/singlerecord.cgi?id=hsa_circ_0084615
hsa_circ:chr3:157839892-157841780	*RSRC1*	333	362	550	331	321	292	-1.186546656	0.000256	0.004091	hsa_circ_0001355	http://www.circbase.org/cgi-bin/singlerecord.cgi?id=hsa_circ_0001355
hsa_circ:chr4:128995615-128999117	*LARP1B*	288	242	369	301	240	148	-1.247937024	0.000787	0.009699	hsa_circ_0001438	http://www.circbase.org/cgi-bin/singlerecord.cgi?id=hsa_circ_0001438
hsa_circ:chr11:77394755-77404656	*RSF1*	541	609	1027	614	535	430	-1.254991191	5.89E-06	0.000197	hsa_circ_0000344	http://www.circbase.org/cgi-bin/singlerecord.cgi?id=hsa_circ_0000344
hsa_circ:chr10:32197100-32199491	*ARHGAP12*	850	564	874	589	560	521	-1.289193851	3.98E-05	0.000919	hsa_circ_0000231	http://www.circbase.org/cgi-bin/singlerecord.cgi?id=hsa_circ_0000231
hsa_circ:chr8:48308936-48320523	*SPIDR*	236	385	371	384	177	187	-1.289993629	0.000696	0.008758	hsa_circ_0001798	http://www.circbase.org/cgi-bin/singlerecord.cgi?id=hsa_circ_0001798
hsa_circ:chr9:16727795-16738483	*BNC2*	502	322	648	342	400	297	-1.303581784	0.000208	0.003485	hsa_circ_0008732	http://www.circbase.org/cgi-bin/singlerecord.cgi?id=hsa_circ_0008732
hsa_circ:chr2:9083316-9098771	*MBOAT2*	783	991	1306	839	729	587	-1.329282379	1.20E-07	7.47E-06	hsa_circ_0007334	http://www.circbase.org/cgi-bin/singlerecord.cgi?id=hsa_circ_0007334
hsa_circ:chr12:120995085-120995485	*RNF10*	402	505	580	284	487	231	-1.373430304	0.000227	0.003722	hsa_circ_0028899	http://www.circbase.org/cgi-bin/singlerecord.cgi?id=hsa_circ_0028899
hsa_circ:chr10:71243447-71244971	*TSPAN15*	201	543	588	248	341	258	-1.395283832	0.000598	0.007849	hsa_circ_0002758	http://www.circbase.org/cgi-bin/singlerecord.cgi?id=hsa_circ_0002758
hsa_circ:chr12:70193989-70195501	*RAB3IP*	633	939	1455	742	555	598	-1.445561613	1.99E-07	1.16E-05	hsa_circ_0000419	http://www.circbase.org/cgi-bin/singlerecord.cgi?id=hsa_circ_0000419
hsa_circ:chr2:24357989-24369956	*FAM228B*	389	521	717	494	268	297	-1.44910951	3.08E-06	0.000118	hsa_circ_0000982	http://www.circbase.org/cgi-bin/singlerecord.cgi?id=hsa_circ_0000982
hsa_circ:chr17:57430576-57430887	*YPEL2*	415	523	518	393	331	243	-1.45137057	4.95E-06	0.000171	hsa_circ_0005600	http://www.circbase.org/cgi-bin/singlerecord.cgi?id=hsa_circ_0005600
hsa_circ:chr17:30310018-30315516	*SUZ12*	246	265	363	238	191	140	-1.459103606	5.79E-05	0.00125	hsa_circ_0002629	http://www.circbase.org/cgi-bin/singlerecord.cgi?id=hsa_circ_0002629
hsa_circ:chr2:191523884-191537878	*NAB1*	218	174	400	157	215	115	-1.468917338	0.000695	0.008753	hsa_circ_0002024	http://www.circbase.org/cgi-bin/singlerecord.cgi?id=hsa_circ_0002024
hsa_circ:chr3:196118684-196129890	*UBXN7*	5879	6433	9687	4835	5200	3721	-1.473332214	1.01E-11	2.63E-09	hsa_circ_0001380	http://www.circbase.org/cgi-bin/singlerecord.cgi?id=hsa_circ_0001380
hsa_circ:chr6:82920531-82922510	*IBTK*	217	163	457	157	235	97	-1.528497514	0.000981	0.011495	hsa_circ_0002041	http://www.circbase.org/cgi-bin/singlerecord.cgi?id=hsa_circ_0002041
hsa_circ:chr15:62299507-62306191	*VPS13C*	557	1016	942	555	472	491	-1.536923666	4.72E-07	2.48E-05	hsa_circ_0000607	http://www.circbase.org/cgi-bin/singlerecord.cgi?id=hsa_circ_0000607

hsa_circ:chr2:240929491-240946787	*NDUFA10*	240	263	316	182	160	151	-1.556620967	3.99E-05	0.00092	hsa_circ_0001118	http://www.circbase.org/cgi-bin/singlerecord.cgi?id=hsa_circ_0001118
hsa_circ:chr17:63739186-63746842	*CEP112*	231	220	285	166	144	133	-1.563739774	7.63E-05	0.001566	hsa_circ_0002910	http://www.circbase.org/cgi-bin/singlerecord.cgi?id=hsa_circ_0002910
hsa_circ:chr4:87685746-87689129	*PTPN13*	448	382	838	275	361	301	-1.569552881	8.09E-06	0.000257	hsa_circ_0007948	http://www.circbase.org/cgi-bin/singlerecord.cgi?id=hsa_circ_0007948
hsa_circ:chr15:76152219-76165909	*UBE2Q2*	235	303	372	306	132	126	-1.578701729	6.23E-05	0.001327	NA	NA
hsa_circ:chr1:107866904-107867544	*NTNG1*	135	227	433	108	134	177	-1.586753878	0.000925	0.011016	hsa_circ_0002286	http://www.circbase.org/cgi-bin/singlerecord.cgi?id=hsa_circ_0002286
hsa_circ:chr8:25265499-25266456	*DOCK5*	197	155	386	178	114	128	-1.591595366	0.000197	0.003357	hsa_circ_0007618	http://www.circbase.org/cgi-bin/singlerecord.cgi?id=hsa_circ_0007618
hsa_circ:chr8:42812237-42819617	*HOOK3*	504	280	548	203	331	231	-1.595558057	8.55E-05	0.00172	hsa_circ_0006376	http://www.circbase.org/cgi-bin/singlerecord.cgi?id=hsa_circ_0006376
hsa_circ:chr5:145634506-145638156	*RBM27*	142	174	323	118	147	90	-1.603683599	0.000366	0.005392	hsa_circ_0006087	http://www.circbase.org/cgi-bin/singlerecord.cgi?id=hsa_circ_0006087
hsa_circ:chr20:35532560-35533906	*SAMHD1*	147	285	320	138	151	131	-1.611456748	0.000156	0.002811	hsa_circ_0060221	http://www.circbase.org/cgi-bin/singlerecord.cgi?id=hsa_circ_0060221
hsa_circ:chr14:80163973-80271533	*NRXN3*	466	706	1022	368	437	392	-1.61911495	3.73E-07	2.03E-05	hsa_circ_0032812	http://www.circbase.org/cgi-bin/singlerecord.cgi?id=hsa_circ_0032812
hsa_circ:chr1:9991949-9994918	*LZIC*	929	1146	1706	803	821	508	-1.629900769	5.59E-10	7.54E-08	hsa_circ_0000014	http://www.circbase.org/cgi-bin/singlerecord.cgi?id=hsa_circ_0000014
hsa_circ:chr17:49340635-49346265	*UTP18*	546	322	588	343	252	248	-1.638251504	3.23E-06	0.000122	hsa_circ_0002789	http://www.circbase.org/cgi-bin/singlerecord.cgi?id=hsa_circ_0002789
hsa_circ:chr13:21305980-21306260	*EEF1AKMT1*	208	172	572	194	172	138	-1.642222482	0.000137	0.002537	hsa_circ_0003285	http://www.circbase.org/cgi-bin/singlerecord.cgi?id=hsa_circ_0003285
hsa_circ:chr12:109509417-109511337	*USP30*	207	316	495	265	189	114	-1.661513009	1.53E-05	0.000425	hsa_circ_0028094	http://www.circbase.org/cgi-bin/singlerecord.cgi?id=hsa_circ_0028094
hsa_circ:chr21:34804484-34805178	*IFNGR2*	359	487	801	379	249	268	-1.663057865	1.47E-07	8.93E-06	hsa_circ_0001185	http://www.circbase.org/cgi-bin/singlerecord.cgi?id=hsa_circ_0001185
hsa_circ:chr18:51797730-51800460	*POLI*	333	147	305	141	138	156	-1.67484072	0.000324	0.004882	hsa_circ_0007180	http://www.circbase.org/cgi-bin/singlerecord.cgi?id=hsa_circ_0007180
hsa_circ:chr18:39607407-39629569	*PIK3C3*	149	149	203	115	93	73	-1.675462109	0.000252	0.004052	hsa_circ_0007765	http://www.circbase.org/cgi-bin/singlerecord.cgi?id=hsa_circ_0007765
hsa_circ:chr1:155646339-155649303	*YY1AP1*	2356	3540	5429	1894	2148	1856	-1.685354126	3.27E-11	7.30E-09	hsa_circ_0014606	http://www.circbase.org/cgi-bin/singlerecord.cgi?id=hsa_circ_0014606
hsa_circ:chr10:17746430-17747740	*STAM*	169	183	371	100	101	161	-1.691618912	0.000374	0.005482	hsa_circ_0008311	http://www.circbase.org/cgi-bin/singlerecord.cgi?id=hsa_circ_0008311
hsa_circ:chr4:17963526-17974508	*LCORL*	167	212	161	137	123	55	-1.695139251	0.00062	0.008076	hsa_circ_0069285	http://www.circbase.org/cgi-bin/singlerecord.cgi?id=hsa_circ_0069285
hsa_circ:chr7:156758964-156759786	*NOM1*	198	174	224	111	148	67	-1.71930518	0.000266	0.004207	hsa_circ_0004210	http://www.circbase.org/cgi-bin/singlerecord.cgi?id=hsa_circ_0004210
hsa_circ:chr21:16386665-16415895	*NRIP1*	714	326	806	421	311	273	-1.725063678	2.17E-06	9.04E-05	hsa_circ_0004771	http://www.circbase.org/cgi-bin/singlerecord.cgi?id=hsa_circ_0004771
hsa_circ:chr8:52773405-52773806	*PCMTD1*	208	300	498	198	84	223	-1.729606809	0.000145	0.002661	hsa_circ_0001801	http://www.circbase.org/cgi-bin/singlerecord.cgi?id=hsa_circ_0001801
hsa_circ:chr17:28011581-28030080	*SSH2*	323	364	556	123	269	224	-1.731580628	4.70E-05	0.001042	hsa_circ_0000754	http://www.circbase.org/cgi-bin/singlerecord.cgi?id=hsa_circ_0000754
hsa_circ:chr6:69943182-69949118	*ADGRB3*	323	457	1022	389	312	213	-1.734214663	8.51E-07	4.11E-05	hsa_circ_0076952	http://www.circbase.org/cgi-bin/singlerecord.cgi?id=hsa_circ_0076952
hsa_circ:chr1:67356837-67371058	*WDR78*	1412	2109	2693	1131	1452	672	-1.736691757	1.60E-09	1.91E-07	hsa_circ_0006677	http://www.circbase.org/cgi-bin/singlerecord.cgi?id=hsa_circ_0006677
hsa_circ:chr13:61013822-61041513	*TDRD3*	355	326	514	135	245	212	-1.758880801	1.71E-05	0.000465	hsa_circ_0003441	http://www.circbase.org/cgi-bin/singlerecord.cgi?id=hsa_circ_0003441
hsa_circ:chr15:59204762-59209198	*SLTM*	1416	1922	2225	1377	835	741	-1.771539504	1.54E-13	7.28E-11	hsa_circ_0000605	http://www.circbase.org/cgi-bin/singlerecord.cgi?id=hsa_circ_0000605
hsa_circ:chr16:69729039-69729282	*NFAT5*	143	149	213	146	66	60	-1.778319789	0.000239	0.00388	hsa_circ_0006845	http://www.circbase.org/cgi-bin/singlerecord.cgi?id=hsa_circ_0006845
hsa_circ:chr9:123593609-123595734	*PSMD5*	174	282	304	227	84	98	-1.780625243	5.56E-05	0.001203	hsa_circ_0088300	http://www.circbase.org/cgi-bin/singlerecord.cgi?id=hsa_circ_0088300
hsa_circ:chr12:50488220-50490755	*SMARCD1*	115	118	198	105	58	60	-1.781723407	0.00039	0.005678	hsa_circ_0006535	http://www.circbase.org/cgi-bin/singlerecord.cgi?id=hsa_circ_0006535
hsa_circ:chr11:61133517-61135470	*TMEM138*	189	146	182	135	81	64	-1.7955221	0.000178	0.003096	hsa_circ_0002058	http://www.circbase.org/cgi-bin/singlerecord.cgi?id=hsa_circ_0002058
hsa_circ:chr11:74500671-74528759	*RNF169*	110	121	172	64	54	78	-1.808809005	0.000729	0.0091	hsa_circ_0006705	http://www.circbase.org/cgi-bin/singlerecord.cgi?id=hsa_circ_0006705
hsa_circ:chr18:12999420-13019205	*CEP192*	221	102	184	70	115	72	-1.815986154	0.000885	0.010634	hsa_circ_0000831	http://www.circbase.org/cgi-bin/singlerecord.cgi?id=hsa_circ_0000831
hsa_circ:chr1:65830318-65831879	*DNAJC6*	295	481	347	160	205	189	-1.834491757	6.26E-06	0.000207	hsa_circ_0002454	http://www.circbase.org/cgi-bin/singlerecord.cgi?id=hsa_circ_0002454
hsa_circ:chr6:42571326-42574389	*UBR2*	112	163	185	66	99	58	-1.836536466	0.00037	0.005439	hsa_circ_0003177	http://www.circbase.org/cgi-bin/singlerecord.cgi?id=hsa_circ_0003177
hsa_circ:chr6:163876311-163899928	*QKI*	1657	1249	1307	782	652	692	-1.859275235	1.03E-09	1.30E-07	hsa_circ_0005328	http://www.circbase.org/cgi-bin/singlerecord.cgi?id=hsa_circ_0005328

hsa_circ:chr1:46105882-46108171	*GPBP1L1*	328	293	612	254	169	167	-1.860555838	1.06E-07	6.68E-06	hsa_circ_0008774	http://www.circbase.org/cgi-bin/singlerecord.cgi?id=hsa_circ_0008774
hsa_circ:chr13:41400642-41411021	*TPTE2P5*	245	394	782	293	190	169	-1.887843272	3.14E-07	1.74E-05	hsa_circ_0030049	http://www.circbase.org/cgi-bin/singlerecord.cgi?id=hsa_circ_0030049
hsa_circ:chr14:73614503-73614814	*PSEN1*	320	237	641	234	190	134	-1.887868333	7.37E-07	3.65E-05	hsa_circ_0003848	http://www.circbase.org/cgi-bin/singlerecord.cgi?id=hsa_circ_0003848
hsa_circ:chr7:77214860-77230123	*PTPN12*	495	455	833	414	225	217	-1.897059838	1.89E-09	2.20E-07	hsa_circ_0003764	http://www.circbase.org/cgi-bin/singlerecord.cgi?id=hsa_circ_0003764
hsa_circ:chr1:155408118-155429689	*ASH1L*	328	269	304	285	97	92	-1.897198961	2.31E-05	0.000588	hsa_circ_0003247	http://www.circbase.org/cgi-bin/singlerecord.cgi?id=hsa_circ_0003247
hsa_circ:chr11:130130751-130131824	*ZBTB44*	608	571	848	383	334	251	-1.89787129	5.36E-11	1.13E-08	hsa_circ_0002484	http://www.circbase.org/cgi-bin/singlerecord.cgi?id=hsa_circ_0002484
hsa_circ:chr1:8601273-8617582	*RERE*	290	681	464	171	272	208	-1.931936853	3.90E-06	0.000142	hsa_circ_0002158	http://www.circbase.org/cgi-bin/singlerecord.cgi?id=hsa_circ_0002158
hsa_circ:chr4:3088666-3109150	*HTT*	404	453	842	234	347	162	-1.957630898	8.89E-08	5.81E-06	hsa_circ_0001392	http://www.circbase.org/cgi-bin/singlerecord.cgi?id=hsa_circ_0001392
hsa_circ:chr4:88116476-88116842	*KLHL8*	1033	1215	1827	722	706	411	-1.963351471	9.68E-14	5.22E-11	hsa_circ_0002538	http://www.circbase.org/cgi-bin/singlerecord.cgi?id=hsa_circ_0002538
hsa_circ:chr2:61749746-61761038	*XPO1*	959	665	1209	544	502	253	-1.984531006	4.67E-10	6.56E-08	hsa_circ_0001017	http://www.circbase.org/cgi-bin/singlerecord.cgi?id=hsa_circ_0001017
hsa_circ:chr17:57808782-57816308	*VMP1*	361	318	726	154	211	214	-1.988030719	4.03E-07	2.19E-05	hsa_circ_0006508	http://www.circbase.org/cgi-bin/singlerecord.cgi?id=hsa_circ_0006508
hsa_circ:chr7:35707044-35712888	*HERPUD2*	340	387	699	234	218	163	-1.993507775	1.99E-09	2.28E-07	hsa_circ_0001696	http://www.circbase.org/cgi-bin/singlerecord.cgi?id=hsa_circ_0001696
hsa_circ:chr2:72945232-72960247	*EXOC6B*	1431	2095	3069	1431	1054	480	-2.001467344	1.03E-11	2.63E-09	hsa_circ_0009043	http://www.circbase.org/cgi-bin/singlerecord.cgi?id=hsa_circ_0009043
hsa_circ:chr6:13579683-13584457	*SIRT5*	146	288	318	129	100	97	-2.004710089	2.56E-06	0.000103	hsa_circ_0007218	http://www.circbase.org/cgi-bin/singlerecord.cgi?id=hsa_circ_0007218
hsa_circ:chr4:25334805-25335610	*ZCCHC4*	156	207	280	133	77	73	-2.022388568	2.96E-06	0.000115	hsa_circ_0001398	http://www.circbase.org/cgi-bin/singlerecord.cgi?id=hsa_circ_0001398
hsa_circ:chr5:176370336-176385155	*UIMC1*	461	772	1120	353	216	351	-2.106445561	5.79E-10	7.74E-08	hsa_circ_0001558	http://www.circbase.org/cgi-bin/singlerecord.cgi?id=hsa_circ_0001558
hsa_circ:chrX:84322133-84329397	*APOOL*	145	198	269	118	83	53	-2.112907281	2.78E-06	0.000109	NA	NA
hsa_circ:chr17:40652725-40653322	*ATP6V0A1*	254	223	372	146	113	90	-2.113586009	5.38E-08	3.71E-06	hsa_circ_0008179	http://www.circbase.org/cgi-bin/singlerecord.cgi?id=hsa_circ_0008179
hsa_circ:chr9:86293356-86301070	*UBQLN1*	189	163	310	107	79	80	-2.115649688	1.13E-06	5.25E-05	hsa_circ_0087357	http://www.circbase.org/cgi-bin/singlerecord.cgi?id=hsa_circ_0087357
hsa_circ:chr1:24840804-24841057	*RCAN3*	206	210	329	183	56	77	-2.123426738	4.46E-06	0.000158	hsa_circ_0003553	http://www.circbase.org/cgi-bin/singlerecord.cgi?id=hsa_circ_0003553
hsa_circ:chr2:203329532-203332412	*BMPR2*	484	444	797	269	218	201	-2.125658637	6.93E-12	1.84E-09	hsa_circ_0003218	http://www.circbase.org/cgi-bin/singlerecord.cgi?id=hsa_circ_0003218
hsa_circ:chr19:5604594-5604947	*SAFB2*	442	373	995	333	227	158	-2.128204396	1.52E-09	1.83E-07	hsa_circ_0000880	http://www.circbase.org/cgi-bin/singlerecord.cgi?id=hsa_circ_0000880
hsa_circ:chr1:231672959-231678357	*TSNAX,TSNAX-DISC1*	201	158	286	100	97	62	-2.140515735	1.59E-06	6.94E-05	hsa_circ_0004834	http://www.circbase.org/cgi-bin/singlerecord.cgi?id=hsa_circ_0004834
hsa_circ:chr15:65471272-65472542	*CLPX*	299	355	497	176	139	139	-2.146513558	5.34E-10	7.32E-08	hsa_circ_0004374	http://www.circbase.org/cgi-bin/singlerecord.cgi?id=hsa_circ_0004374
hsa_circ:chr9:96233423-96261168	*FAM120A*	197	224	255	107	106	60	-2.162766439	6.63E-07	3.31E-05	hsa_circ_0001875	http://www.circbase.org/cgi-bin/singlerecord.cgi?id=hsa_circ_0001875
hsa_circ:chr1:155408118-155408859	*ASH1L*	364	271	580	97	204	141	-2.190087424	4.80E-07	2.52E-05	hsa_circ_0000137	http://www.circbase.org/cgi-bin/singlerecord.cgi?id=hsa_circ_0000137
hsa_circ:chr15:52073241-52075025	*TMOD2*	437	1044	1579	504	311	321	-2.194525839	1.25E-10	2.21E-08	hsa_circ_0005566	http://www.circbase.org/cgi-bin/singlerecord.cgi?id=hsa_circ_0005566
hsa_circ:chr9:86294690-86301070	*UBQLN1*	151	147	200	56	78	50	-2.242152547	8.23E-06	0.00026	hsa_circ_0008207	http://www.circbase.org/cgi-bin/singlerecord.cgi?id=hsa_circ_0008207
hsa_circ:chr2:148730308-148733544	*ORC4*	365	388	689	135	252	126	-2.242823654	1.62E-08	1.33E-06	hsa_circ_0001074	http://www.circbase.org/cgi-bin/singlerecord.cgi?id=hsa_circ_0001074
hsa_circ:chr10:112356156-112358048	*SMC3*	491	172	529	212	188	62	-2.264025134	3.61E-06	0.000134	hsa_circ_0000260	http://www.circbase.org/cgi-bin/singlerecord.cgi?id=hsa_circ_0000260
hsa_circ:chr13:28748409-28752072	*PAN3*	183	153	260	88	65	62	-2.294869535	4.05E-07	2.19E-05	hsa_circ_0004372	http://www.circbase.org/cgi-bin/singlerecord.cgi?id=hsa_circ_0004372
hsa_circ:chr4:170523159-170523829	*NEK1*	176	347	97	96	63	79	-2.306289829	5.38E-05	0.001169	NA	NA
hsa_circ:chr18:19345733-19359646	*MIB1*	323	351	426	217	120	77	-2.315777256	1.85E-09	2.18E-07	hsa_circ_0000835	http://www.circbase.org/cgi-bin/singlerecord.cgi?id=hsa_circ_0000835
hsa_circ:chr17:1264386-1265302	*YWHAE*	262	157	384	85	136	57	-2.321810669	1.49E-06	6.58E-05	hsa_circ_0007643	http://www.circbase.org/cgi-bin/singlerecord.cgi?id=hsa_circ_0007643
hsa_circ:chr3:119222379-119236162	*TIMMDC1*	210	263	481	60	167	80	-2.342166994	1.90E-06	8.04E-05	hsa_circ_0001330	http://www.circbase.org/cgi-bin/singlerecord.cgi?id=hsa_circ_0001330
hsa_circ:chr9:113734353-113735838	*LPAR1*	2936	4423	8134	1906	1654	1478	-2.365204654	2.86E-21	1.12E-17	hsa_circ_0087960	http://www.circbase.org/cgi-bin/singlerecord.cgi?id=hsa_circ_0087960
hsa_circ:chr13:33091994-33101669	*N4BP2L2*	2837	2329	4577	940	1585	707	-2.369990899	7.91E-09	7.15E-07	hsa_circ_0000471	http://www.circbase.org/cgi-bin/singlerecord.cgi?id=hsa_circ_0000471
hsa_circ:chr16:69404386-69406258	*TERF2*	498	542	898	247	245	159	-2.374102438	1.49E-14	8.94E-12	NA	NA

hsa_circ:chr18:76953183-76974038	*ATP9B*	252	454	450	113	102	158	-2.391382487	1.05E-08	9.19E-07	hsa_circ_0003275	http://www.circbase.org/cgi-bin/singlerecord.cgi?id=hsa_circ_0003275
hsa_circ:chr13:61013822-61034674	*TDRD3*	244	203	403	115	104	65	-2.395858265	5.94E-09	5.69E-07	hsa_circ_0004245	http://www.circbase.org/cgi-bin/singlerecord.cgi?id=hsa_circ_0004245
hsa_circ:chr12:12397196-12397589	*LRP6*	188	294	547	165	98	62	-2.473349321	5.41E-09	5.28E-07	hsa_circ_0000378	http://www.circbase.org/cgi-bin/singlerecord.cgi?id=hsa_circ_0000378
hsa_circ:chr2:201721405-201721708	*CLK1*	309	194	574	194	85	64	-2.506600637	2.21E-08	1.72E-06	hsa_circ_0004001	http://www.circbase.org/cgi-bin/singlerecord.cgi?id=hsa_circ_0004001
hsa_circ:chr6:144858718-144860579	*UTRN*	582	657	729	197	171	234	-2.508556777	1.32E-13	6.45E-11	hsa_circ_0001647	http://www.circbase.org/cgi-bin/singlerecord.cgi?id=hsa_circ_0001647
hsa_circ:chr9:33953283-33963789	*UBAP2*	347	516	608	128	222	97	-2.509558617	2.45E-10	3.76E-08	hsa_circ_0001847	http://www.circbase.org/cgi-bin/singlerecord.cgi?id=hsa_circ_0001847
hsa_circ:chr2:9083316-9114564	*MBOAT2*	372	604	682	185	198	106	-2.583299781	1.02E-13	5.31E-11	NA	NA
hsa_circ:chr3:119222379-119232566	*TIMMDC1*	424	751	949	204	277	109	-2.644168253	9.51E-13	3.54E-10	hsa_circ_0066875	http://www.circbase.org/cgi-bin/singlerecord.cgi?id=hsa_circ_0066875
hsa_circ:chr6:79770195-79770535	*PHIP*	194	377	456	69	136	68	-2.660814144	6.00E-09	5.69E-07	hsa_circ_0003810	http://www.circbase.org/cgi-bin/singlerecord.cgi?id=hsa_circ_0003810
hsa_circ:chr7:158552177-158557544	*ESYT2*	666	659	1374	205	250	196	-2.794191361	1.93E-18	2.51E-15	hsa_circ_0001776	http://www.circbase.org/cgi-bin/singlerecord.cgi?id=hsa_circ_0001776
hsa_circ:chr2:167304122-167328955	*SCN7A*	456	1950	1151	123	303	386	-2.832543078	0.000396	0.005733	NA	NA
hsa_circ:chr8:71071740-71075089	*NCOA2*	342	417	675	121	154	57	-2.914152365	1.76E-13	8.09E-11	hsa_circ_0001810	http://www.circbase.org/cgi-bin/singlerecord.cgi?id=hsa_circ_0001810
hsa_circ:chr4:144464662-144465125	*SMARCA5*	5007	5266	8372	1224	1054	1807	-2.924894033	1.23E-13	6.19E-11	hsa_circ_0001445	http://www.circbase.org/cgi-bin/singlerecord.cgi?id=hsa_circ_0001445
hsa_circ:chr17:67151160-67152066	*ABCA10*	327	365	1210	184	153	73	-2.95426875	2.63E-12	7.90E-10	NA	NA
hsa_circ:chr8:71126138-71128999	*NCOA2*	243	465	708	116	107	69	-3.050636317	1.82E-15	1.43E-12	NA	NA
hsa_circ:chr1:48821342-48825442	*SPATA6*	1753	2831	3554	736	508	480	-3.050955648	2.72E-37	4.25E-33	hsa_circ_0008202	http://www.circbase.org/cgi-bin/singlerecord.cgi?id=hsa_circ_0008202
hsa_circ:chr10:61844360-61845011	*ANK3*	397	537	1227	154	115	95	-3.31743446	4.15E-21	1.30E-17	NA	NA
hsa_circ:chr6:139264650-139265759	*REPS1*	420	387	825	82	91	98	-3.322250921	4.80E-19	9.39E-16	hsa_circ_0004368	http://www.circbase.org/cgi-bin/singlerecord.cgi?id=hsa_circ_0004368
hsa_circ:chr11:18312989-18314523	*HPS5*	462	281	521	56	61	87	-3.405443326	5.65E-15	3.84E-12	hsa_circ_0000280	http://www.circbase.org/cgi-bin/singlerecord.cgi?id=hsa_circ_0000280
hsa_circ:chr12:121220458-121222396	*SPPL3*	427	685	958	59	80	87	-3.918139861	1.22E-25	9.58E-22	hsa_circ_0003472	http://www.circbase.org/cgi-bin/singlerecord.cgi?id=hsa_circ_0003472

Additional Table 12 GO cellular component analysis of filtered mRNAs

ONTOLOGY	GOID	Description	GeneRatio	BgRatio	pvalue	p.adjust	geneID	Count
CC	GO:0005578	proteinaceous extracellular matrix	28/683	365/18399	0.00024621	0.07164718	COL14A1/COL17A1/HAPLN3/COL19A1/SERPINF1/TECTA/MMP3/MMP8/FLRT1/WISP1/ENAM/FRAS1/WNT16/FREM3/ELN/CHI3L1/COL5A3/COL4A3/ADAMTS14/ADAMTS19/MMP10/VWF/LRRN3/TNFRSF11B/KAZALD1/MFAP4/MATN3/ITGA6	28
CC	GO:0034702	ion channel complex	23/683	288/18399	0.00049174	0.07164718	CHRNE/CHRNA10/TRPC4/KCND1/KCNG2/KCNE3/KCNQ5/LRRC8E/ANO1/GRID2/GRIK5/ABCC9/GABRA2/GABRA5/SCN1A/SCN3B/SCN3A/GRIN2C/GRIN2D/GRIN3A/CLIC6/CLIC2/CATSPER1	23
CC	GO:1902495	transmembrane transporter complex	25/683	325/18399	0.0004987	0.07164718	CHRNE/CHRNA10/TRPC4/KCND1/KCNG2/KCNE3/KCNQ5/LRRC8E/ANO1/GRID2/GRIK5/ABCB6/ABCC9/GABRA2/GABRA5/SCN1A/SCN3B/SCN3A/GRIN2C/GRIN2D/GRIN3A/UQCC3/CLIC6/CLIC2/CATSPER1	25
CC	GO:1990351	transporter complex	25/683	332/18399	0.00068024	0.07329627	CHRNE/CHRNA10/TRPC4/KCND1/KCNG2/KCNE3/KCNQ5/LRRC8E/ANO1/GRID2/GRIK5/ABCB6/ABCC9/GABRA2/GABRA5/SCN1A/SCN3B/SCN3A/GRIN2C/GRIN2D/GRIN3A/UQCC3/CLIC6/CLIC2/CATSPER1	25
CC	GO:0101003	ficolin-1-rich granule membrane	8/683	60/18399	0.00160995	0.13877781	SLC11A1/SERPINB12/NCKAP1L/ENPP4/ATP6V0C/CD93/PKP1/NFASC	8
CC	GO:0098802	plasma membrane receptor complex	15/683	177/18399	0.00253432	0.18204886	CHRNE/CHRNA10/RAMP1/CARD11/GRID2/GRIK5/ACVR1C/IL6/TLR1/GRIN2C/GRIN2D/GRIN3A/ITGB4/ITGB8/ITGA6	15
CC	GO:0005788	endoplasmic reticulum lumen	21/683	298/18399	0.00388676	0.23931312	COL14A1/C3/COL17A1/COL19A1/EBI3/EDN1/CYP2W1/ENAM/COL25A1/APOE/MGAT4A/BCHE/IL6/COL5A3/COL4A3/GHRL/CES1/MELTF/IGFBP5/MATN3/IL12A	21
CC	GO:0017146	NMDA selective glutamate receptor complex	3/683	11/18399	0.00672195	0.32590943	GRIN2C/GRIN2D/GRIN3A	3
CC	GO:0034706	sodium channel complex	4/683	21/18399	0.00680553	0.32590943	GRIK5/SCN1A/SCN3B/SCN3A	4
CC	GO:0043235	receptor complex	21/683	325/18399	0.0101341	0.43677987	CHRNE/ADRB2/CHRNA10/RAMP1/CARD11/GRID2/GRIK5/FLT4/ACVR1C/IL6/GABRA2/GABRA5/NR1H3/PLXNA4/TLR1/GRIN2C/GRIN2D/GRIN3A/ITGB4/ITGB8/ITGA6	21
CC	GO:0001518	voltage-gated sodium channel complex	3/683	14/18399	0.0136496	0.47861007	SCN1A/SCN3B/SCN3A	3
CC	GO:0044420	extracellular matrix component	10/683	120/18399	0.01391592	0.47861007	COL14A1/COL17A1/SERPINF1/FRAS1/FREM3/ELN/COL5A3/COL4A3/MFAP4/ITGA6	10
CC	GO:0097060	synaptic membrane	19/683	295/18399	0.01443603	0.47861007	CHRNE/CHRNA10/SNCAIP/TMEM108/BAALC/ANK1/GRID2/GRIK5/GABRA2/GABRA5/SYP/CNKSR2/NDUFS7/GRIN2C/GRIN2D/GRIN3A/DLGAP2/EPHA7/RIMS1	19
CC	GO:0030285	integral component of synaptic vesicle membrane	3/683	15/18399	0.01659897	0.50912388	TMEM163/GABRA2/SYP	3
CC	GO:0033267	axon part	13/683	181/18399	0.01771893	0.50912388	SERPINF1/L1CAM/TMEM108/MGARP/NRG1/ANK1/GRIK5/SLC1A2/SCN1A/SYP/UCN/HAP1/NFASC	13
CC	GO:0030673	axolemma	3/683	16/18399	0.01987621	0.53431783	NRG1/ANK1/SLC1A2	3
CC	GO:0045211	postsynaptic membrane	15/683	225/18399	0.02107518	0.53431783	CHRNE/CHRNA10/TMEM108/BAALC/ANK1/GRID2/GRIK5/GABRA2/GABRA5/CNKSR2/GRIN2C/GRIN2D/GRIN3A/DLGAP2/EPHA7	15
CC	GO:0030175	filopodium	8/683	96/18399	0.02629834	0.58544602	TRPV4/ACPP/PPP1R9A/CXADR/LCP1/ACTA2/CD302/ITGA6	8
CC	GO:0034703	cation channel complex	14/683	212/18399	0.02711827	0.58544602	TRPC4/KCND1/KCNG2/KCNE3/KCNQ5/GRIK5/ABCC9/SCN1A/SCN3B/SCN3A/GRIN2C/GRIN2D/GRIN3A/CATSPER1	14
CC	GO:0008328	ionotropic glutamate receptor complex	5/683	46/18399	0.02716687	0.58544602	GRID2/GRIK5/GRIN2C/GRIN2D/GRIN3A	5
CC	GO:0044304	main axon	6/683	63/18399	0.0290586	0.59639312	NRG1/ANK1/SLC1A2/SCN1A/UCN/NFASC	6
CC	GO:0098878	neurotransmitter receptor complex	5/683	48/18399	0.03196607	0.62624432	GRID2/GRIK5/GRIN2C/GRIN2D/GRIN3A	5
CC	GO:0034707	chloride channel complex	5/683	49/18399	0.03455175	0.64746977	ANO1/GABRA2/GABRA5/CLIC6/CLIC2	5
CC	GO:0070820	tertiary granule	11/683	163/18399	0.0408761	0.67918917	SLC11A1/MMP8/SERPINB12/NCKAP1L/ENPP4/CXCL1/ATP6V0C/METTL7A/CD93/PKP1/NFASC	11
CC	GO:0032809	neuronal cell body membrane	3/683	21/18399	0.04118619	0.67918917	FLRT1/KCNE3/GABRA5	3

CC	GO:0044298	cell body membrane	3/683	21/18399	0.04118619	0.67918917	FLRT1/KCNE3/GABRA5	3
CC	GO:0005581	collagen trimer	7/683	88/18399	0.04507474	0.67918917	COL14A1/COL17A1/COL19A1/COL25A1/COL5A3/COL4A3/C1QL3	7
CC	GO:0016528	sarcoplasm	6/683	70/18399	0.0452783	0.67918917	ANK1/JPH2/FABP3/CLEC18B/GSTM2/MRVI1	6
CC	GO:0098563	intrinsic component of synaptic vesicle membrane	3/683	22/18399	0.04641385	0.67918917	TMEM163/GABRA2/SYP	3
CC	GO:0070382	exocytic vesicle	11/683	167/18399	0.04727535	0.67918917	TRIM9/SNCAIP/TMEM163/SLC18A2/SLC40A1/SYN2/STX11/GABRA2/SYP/SYTL3/HAP1	11

Additional Table 13 GO molecular function analysis of filtered mRNAs

ONTOLOGY	GOID	Description	GeneRatio	BgRatio	pvalue	p.adjust	geneID	Count
MF	GO:0005125	cytokine activity	23/646	218/17258	7.74E-06	0.00276242	CXCL11/TNFSF10/TNFSF13/IL1A/IL1B/INHA/EBI3/EDN1/NRG1/AREG/IL6/IL7/LIF/CXCL6/CXCL8/CXCL1/CXCL3/CXCL5/CCL7/TNFRSF11B/CSF3/CCL20/IL12A	23
MF	GO:0048018	receptor ligand activity	37/646	454/17258	8.15E-06	0.00276242	CXCL11/TNFSF10/TNFSF13/IL1A/IL1B/INHA/EBI3/EDN1/ADA2/ERFE/EREG/PTHLH/SFRP2/NRG1/NRG2/NRG4/AREG/FNDC5/AMH/IL6/IL7/LIF/CXCL6/CXCL8/CXCL1/CXCL3/CXCL5/SPX/UCN/GHRL/CCL7/TNFRSF11B/PSPN/CSF3/CCL20/EPHA7/IL12A	37
MF	GO:0030545	receptor regulator activity	38/646	483/17258	1.38E-05	0.00276242	CXCL11/TNFSF10/TNFSF13/IL1A/IL1B/INHA/EBI3/EDN1/ADA2/ERFE/EREG/PTHLH/SFRP2/NRG1/NRG2/NRG4/AREG/FNDC5/AMH/IL6/IL7/LIF/CXCL6/CXCL8/CXCL1/CXCL3/CXCL5/WFIKKN1/SPX/UCN/GHRL/CCL7/TNFRSF11B/PSPN/CSF3/CCL20/EPHA7/IL12A	38
MF	GO:0045236	CXCR chemokine receptor binding	6/646	16/17258	1.56E-05	0.00276242	CXCL11/CXCL6/CXCL8/CXCL1/CXCL3/CXCL5	6
MF	GO:0008009	chemokine activity	8/646	46/17258	0.00027339	0.02748107	CXCL11/CXCL6/CXCL8/CXCL1/CXCL3/CXCL5/CCL7/CCL20	8
MF	GO:0022836	gated channel activity	26/646	332/17258	0.00033158	0.02748107	CHRNE/CHRNA10/TRPV4/KCND1/KCNG2/KCNE3/KCNQ5/ANO1/ASIC3/JPH2/GRID2/GRIK5/GABRA2/GABRA5/SCN1A/SCN3B/SCN3A/P2RX6/GRIN2C/GRIN2D/GRIN3A/PIEZO2/CLIC6/CLIC2/CATSPER1/GPR89B	26
MF	GO:0005231	excitatory extracellular ligand-gated ion channel activity	8/646	48/17258	0.0003702	0.02748107	CHRNE/CHRNA10/GRID2/GRIK5/P2RX6/GRIN2C/GRIN2D/GRIN3A	8
MF	GO:0005230	extracellular ligand-gated ion channel activity	10/646	75/17258	0.00046517	0.02748107	CHRNE/CHRNA10/GRID2/GRIK5/GABRA2/GABRA5/P2RX6/GRIN2C/GRIN2D/GRIN3A	10
MF	GO:0043178	alcohol binding	10/646	75/17258	0.00046517	0.02748107	TRPC4/RBP4/RBP1/APOE/NR1H3/SYP/CETP/LRAT/PROM2/OSBP2	10
MF	GO:0022824	transmitter-gated ion channel activity	8/646	50/17258	0.00049322	0.02748107	CHRNE/CHRNA10/GRID2/GRIK5/GABRA2/GRIN2C/GRIN2D/GRIN3A	8
MF	GO:0022835	transmitter-gated channel activity	8/646	50/17258	0.00049322	0.02748107	CHRNE/CHRNA10/GRID2/GRIK5/GABRA2/GRIN2C/GRIN2D/GRIN3A	8
MF	GO:0005520	insulin-like growth factor binding	6/646	28/17258	0.00050026	0.02748107	HTRA4/WISP1/IGFBP5/KAZALD1/ITGB4/ITGA6	6
MF	GO:0004970	ionotropic glutamate receptor activity	5/646	19/17258	0.00054341	0.02748107	GRID2/GRIK5/GRIN2C/GRIN2D/GRIN3A	5
MF	GO:0005234	extracellularly glutamate-gated ion channel activity	5/646	19/17258	0.00054341	0.02748107	GRID2/GRIK5/GRIN2C/GRIN2D/GRIN3A	5
MF	GO:0005201	extracellular matrix structural constituent	10/646	78/17258	0.00063874	0.03014845	COL14A1/HAPLN3/COL19A1/TECTA/ENAM/ELN/CHI3L1/COL5A3/COL4A3/MATN3	10
MF	GO:0005216	ion channel activity	30/646	425/17258	0.00069167	0.03025376	CHRNE/CHRNA10/TRPC4/TRPV4/KCND1/KCNG2/KCNE3/KCNQ5/LRRC8E/SLC40A1/ANO1/ASIC3/JPH2/GRID2/GRIK5/ABCC9/GABRA2/GABRA5/SCN1A/SCN3B/SCN3A/P2RX6/GRIN2C/GRIN2D/GRIN3A/PIEZO2/CLIC6/CLIC2/CATSPER1/GPR89B	30
MF	GO:0015267	channel activity	32/646	466/17258	0.00074207	0.03025376	CHRNE/CHRNA10/TRPC4/TRPV4/KCND1/KCNG2/KCNE3/KCNQ5/LRRC8E/SLC40A1/ANO1/ASIC3/JPH2/GRID2/GRIK5/ABCC9/GABRA2/GABRA5/SCN1A/SCN3B/SCN3A/BCL2A1/P2RX6/GJB7/GRIN2C/GRIN2D/GRIN3A/PIEZO2/CLIC6/CLIC2/CATSPER1/GPR89B	32
MF	GO:0022803	passive transmembrane transporter activity	32/646	467/17258	0.00076916	0.03025376	CHRNE/CHRNA10/TRPC4/TRPV4/KCND1/KCNG2/KCNE3/KCNQ5/LRRC8E/SLC40A1/ANO1/ASIC3/JPH2/GRID2/GRIK5/ABCC9/GABRA2/GABRA5/SCN1A/SCN3B/SCN3A/BCL2A1/P2RX6/GJB7/GRIN2C/GRIN2D/GRIN3A/PIEZO2/CLIC6/CLIC2/CATSPER1/GPR89B	32
MF	GO:0022838	substrate-specific channel activity	30/646	435/17258	0.00100299	0.03737468	CHRNE/CHRNA10/TRPC4/TRPV4/KCND1/KCNG2/KCNE3/KCNQ5/LRRC8E/SLC40A1/ANO1/ASIC3/JPH2/GRID2/GRIK5/ABCC9/GABRA2/GABRA5/SCN1A/SCN3B/SCN3A/P2RX6/GRIN2C/GRIN2D/GRIN3A/PIEZO2/CLIC6/CLIC2/CATSPER1/GPR89B	30
MF	GO:0015245	fatty acid transporter activity	4/646	13/17258	0.00106137	0.03757264	MFSD2A/SLCO2A1/FABP3/SLC27A5	4

MF	GO:0008083	growth factor activity	15/646	162/17258	0.00113973	0.03842505	INHA/ADA2/EREG/NRG1/NRG2/NRG4/AREG/AMH/IL6/IL7/LIF/CXCL1/PSPN/CSF3/IL12A	15
MF	GO:0042379	chemokine receptor binding	8/646	58/17258	0.00135494	0.04360441	CXCL11/CXCL6/CXCL8/CXCL1/CXCL3/CXCL5/CCL7/CCL20	8
MF	GO:0008499	UDP-galactose:beta-N-acetylglucosamine beta-1,3-galactosyltransferase activity	4/646	14/17258	0.0014422	0.04439455	B3GALT2/B3GALT1/B3GALT5/B3GNT4	4
MF	GO:0005261	cation channel activity	23/646	314/17258	0.00174445	0.05146139	CHRNE/CHRNA10/TRPC4/TRPV4/KCND1/KCNG2/KCNE3/KCNQ5/SLC40A1/ANO1/ASIC3/JPH2/GRIK5/ABCC9/SCN1A/SCN3B/SCN3A/P2RX6/GRIN2C/GRIN2D/GRIN3A/PIEZO2/CATSPER1	23
MF	GO:0005319	lipid transporter activity	13/646	141/17258	0.0024669	0.06573686	SLC10A4/RBP4/TMEM30B/APOE/MFSD2A/SLCO2A1/ABCB4/FABP3/SPNS2/CETP/PITPNM3/SLC27A5/ATP10B	13
MF	GO:0048531	beta-1,3-galactosyltransferase activity	4/646	16/17258	0.00247041	0.06573686	B3GALT2/B3GALT1/B3GALT5/B3GNT4	4
MF	GO:0005126	cytokine receptor binding	20/646	266/17258	0.00250691	0.06573686	CXCL11/TNFSF10/TNFSF13/IL1A/IL1B/INHA/EBI3/AMH/IL6/IL7/LIF/CXCL6/CXCL8/CXCL1/CXCL3/CXCL5/CCL7/CSF3/CCL20/IL12A	20
MF	GO:0008066	glutamate receptor activity	5/646	27/17258	0.00294555	0.07448045	GRID2/GRIK5/GRIN2C/GRIN2D/GRIN3A	5
MF	GO:0019838	growth factor binding	12/646	130/17258	0.00352661	0.08609797	HTRA4/WISP1/FLT4/A2M/ACVR1C/WFIKKN1/S100A13/IGFBP5/KAZALD1/HAP1/ITGB4/ITGA6	12
MF	GO:0004222	metalloendopeptidase activity	11/646	115/17258	0.00389625	0.09195151	PAPLN/MMP3/MMP8/TMPRSS6/KEL/ADAMTS14/ADAMTS19/MMP10/TLL2/ADAM28/ADAM33	11
MF	GO:0001664	G-protein coupled receptor binding	19/646	260/17258	0.00432576	0.09879484	C3/CXCL11/RAMP1/EDN1/ADA2/WNT16/CXCL6/CXCL8/CXCL1/CXCL3/CXCL5/UCN/NECAB2/GHRL/GNAZ/CCL7/CCL20/GPRC5B/ITGB4	19
MF	GO:0015485	cholesterol binding	6/646	43/17258	0.00503575	0.11141589	APOE/NR1H3/SYP/CETP/PROM2/OSBP2	6
MF	GO:0015276	ligand-gated ion channel activity	12/646	139/17258	0.00602901	0.12554528	CHRNE/CHRNA10/ASIC3/JPH2/GRID2/GRIK5/GABRA2/GABRA5/P2RX6/GRIN2C/GRIN2D/GRIN3A	12
MF	GO:0022834	ligand-gated channel activity	12/646	139/17258	0.00602901	0.12554528	CHRNE/CHRNA10/ASIC3/JPH2/GRID2/GRIK5/GABRA2/GABRA5/P2RX6/GRIN2C/GRIN2D/GRIN3A	12
MF	GO:0061135	endopeptidase regulator activity	14/646	177/17258	0.00682657	0.13526148	C3/SERPINE3/SERPINF1/PAPLN/SERPINB12/BIRC3/SFRP2/NLRC4/A2M/WFIKKN1/COL4A3/SPINT2/SPINT1/HMSD	14
MF	GO:0086080	protein binding involved in heterotypic cell-cell adhesion	3/646	11/17258	0.0068777	0.13526148	DSC2/CXADR/NFASC	3
MF	GO:0005496	steroid binding	9/646	92/17258	0.00748345	0.13953101	PAQR5/HSD11B2/ESR1/APOE/NR1H3/SYP/CETP/PROM2/OSBP2	9
MF	GO:0005244	voltage-gated ion channel activity	15/646	198/17258	0.00768603	0.13953101	KCND1/KCNG2/KCNE3/KCNQ5/ANO1/SCN1A/SCN3B/SCN3A/GRIN2C/GRIN2D/GRIN3A/CLIC6/CLIC2/CATSPER1/GPR89B	15
MF	GO:0022832	voltage-gated channel activity	15/646	198/17258	0.00768603	0.13953101	KCND1/KCNG2/KCNE3/KCNQ5/ANO1/SCN1A/SCN3B/SCN3A/GRIN2C/GRIN2D/GRIN3A/CLIC6/CLIC2/CATSPER1/GPR89B	15
MF	GO:0004867	serine-type endopeptidase inhibitor activity	9/646	93/17258	0.00801867	0.14030831	SERPINE3/SERPINF1/PAPLN/SERPINB12/A2M/WFIKKN1/SPINT2/SPINT1/HMSD	9
MF	GO:0004497	monooxygenase activity	9/646	94/17258	0.00858253	0.14030831	CYP4F3/CYP2W1/CYP4X1/AGMO/FMO2/FMO3/CYP11A1/CYP1A1/CYP27A1	9
MF	GO:0032934	sterol binding	6/646	48/17258	0.00866409	0.14030831	APOE/NR1H3/SYP/CETP/PROM2/OSBP2	6
MF	GO:0005178	integrin binding	10/646	111/17258	0.00874837	0.14030831	ICAM5/WISP1/SFRP2/NRG1/MADCAM1/CXADR/COL4A3/VWF/LCP1/ITGA6	10
MF	GO:0005542	folic acid binding	3/646	12/17258	0.0089179	0.14030831	FTCD/GNMT/FTCDNL1	3
MF	GO:0031994	insulin-like growth factor I binding	3/646	12/17258	0.0089179	0.14030831	IGFBP5/ITGB4/ITGA6	3
MF	GO:0099094	ligand-gated cation channel activity	8/646	80/17258	0.01002526	0.15430186	CHRNE/CHRNA10/ASIC3/JPH2/GRIK5/GRIN2C/GRIN2D/GRIN3A	8
MF	GO:0008237	metallopeptidase activity	14/646	186/17258	0.01035614	0.15600316	PAPLN/MMP3/MMP8/TMPRSS6/KEL/ADAMTS14/ADAMTS19/MMP10/TLL2/ADAM28/ADAM33/CPB2/CPA5/CPA4	14
MF	GO:0043225	ATPase-coupled anion transmembrane transporter activity	3/646	13/17258	0.01127486	0.16630417	ABCC2/ABCC6/ABCC9	3
MF	GO:0004866	endopeptidase inhibitor activity	13/646	171/17258	0.0122209	0.17657951	C3/SERPINE3/SERPINF1/PAPLN/SERPINB12/BIRC3/NLRC4/A2M/WFIKKN1/COL4A3/SPINT2/SPINT1/HMSD	13

MF	GO:0098631	cell adhesion mediator activity	5/646	38/17258	0.01307493	0.18514099	DSC2/MADCAM1/CXADR/EPCAM/NFASC	5
MF	GO:0019841	retinol binding	3/646	14/17258	0.01395649	0.19374899	RBP4/RBP1/LRAT	3
MF	GO:0005507	copper ion binding	6/646	55/17258	0.01644908	0.22396053	SNAI3/IL1A/AOC2/SCO2/SOD3/S100A13	6
MF	GO:0005548	phospholipid transporter activity	6/646	56/17258	0.01785861	0.23656451	TMEM30B/MFSD2A/ABCB4/CETP/PITPNM3/ATP10B	6
MF	GO:0030414	peptidase inhibitor activity	13/646	180/17258	0.01804306	0.23656451	C3/SERPINE3/SERPINF1/PAPLN/SERPINB12/BIRC3/NLRC4/A2M/WFIKKN1/COL4A3/SPINT2/SPINT1/HMSD	13
MF	GO:0046873	metal ion transmembrane transporter activity	26/646	449/17258	0.01887147	0.24292727	SLC10A4/SLC11A1/CHRNA10/TRPC4/TRPV4/KCND1/KCNG2/KCNE3/KCNQ5/SLC40A1/ASIC3/JPH2/GRIK5/SLC5A2/SLC1A2/ABCC9/SLC34A3/SCN1A/SCN3B/SCN3A/GRIN2C/GRIN2D/GRIN3A/ATP2C2/CLDN16/CATSPER1	26
MF	GO:0048038	quinone binding	3/646	16/17258	0.0203141	0.25682829	VKORC1/AOC2/NDUFS7	3
MF	GO:0043492	ATPase activity, coupled to movement of substances	10/646	129/17258	0.02311831	0.28715375	ATP6V1C2/ABCB6/ABCB4/ABCC2/ABCC6/ABCC9/ATP6V0C/ATP6AP1L/ATP10B/ATP2C2	10
MF	GO:0035250	UDP-galactosyltransferase activity	4/646	30/17258	0.02462161	0.30016121	B3GALT2/B3GALT1/B3GALT5/B3GNT4	4
MF	GO:0042625	ATPase coupled ion transmembrane transporter activity	7/646	77/17258	0.02501343	0.30016121	ATP6V1C2/ABCC2/ABCC6/ABCC9/ATP6V0C/ATP6AP1L/ATP2C2	7
MF	GO:0005272	sodium channel activity	5/646	45/17258	0.02573771	0.30370495	ASIC3/GRIK5/SCN1A/SCN3B/SCN3A	5
MF	GO:0022853	active ion transmembrane transporter activity	10/646	132/17258	0.02659957	0.30856562	SLC10A4/ATP6V1C2/SLC1A2/ABCC2/ABCC6/ABCC9/SLC34A3/ATP6V0C/ATP6AP1L/ATP2C2	10
MF	GO:0042626	ATPase activity, coupled to transmembrane movement of substances	9/646	114/17258	0.02730206	0.30856562	ATP6V1C2/ABCB6/ABCB4/ABCC2/ABCC6/ABCC9/ATP6V0C/ATP6AP1L/ATP2C2	9
MF	GO:0098632	cell-cell adhesion mediator activity	4/646	31/17258	0.02745711	0.30856562	DSC2/CXADR/EPCAM/NFASC	4
MF	GO:0016820	hydrolase activity, acting on acid anhydrides, catalyzing transmembrane movement of substances	9/646	116/17258	0.03010289	0.33136558	ATP6V1C2/ABCB6/ABCB4/ABCC2/ABCC6/ABCC9/ATP6V0C/ATP6AP1L/ATP2C2	9
MF	GO:0005544	calcium-dependent phospholipid binding	5/646	47/17258	0.03042198	0.33136558	RPH3AL/C2CD4D/SYT17/SYTL3/ANXA8L1	5
MF	GO:0030594	neurotransmitter receptor activity	8/646	99/17258	0.03218147	0.34196627	CHRNE/CHRNA10/GRID2/GRIK5/GABRA2/GRIN2C/GRIN2D/GRIN3A	8
MF	GO:0016289	CoA hydrolase activity	3/646	19/17258	0.03236122	0.34196627	NUDT7/THEM5/ACOT1	3
MF	GO:0061134	peptidase regulator activity	14/646	216/17258	0.03297354	0.34331273	C3/SERPINE3/SERPINF1/PAPLN/SERPINB12/BIRC3/SFRP2/NLRC4/A2M/WFIKKN1/COL4A3/SPINT2/SPINT1/HMSD	14
MF	GO:0008378	galactosyltransferase activity	4/646	34/17258	0.03709021	0.36985726	B3GALT2/B3GALT1/B3GALT5/B3GNT4	4
MF	GO:0008395	steroid hydroxylase activity	4/646	34/17258	0.03709021	0.36985726	CYP2W1/CYP11A1/CYP1A1/CYP27A1	4
MF	GO:0016709	oxidoreductase activity, acting on paired donors, with incorporation or reduction of molecular oxygen, NAD(P)H as one donor, and incorporation of one atom of oxygen	4/646	34/17258	0.03709021	0.36985726	CYP4F3/FMO2/FMO3/CYP1A1	4
MF	GO:0005179	hormone activity	9/646	121/17258	0.03796825	0.37335449	INHA/EDN1/ERFE/PTHLH/FNDC5/AMH/SPX/UCN/GHRL	9
MF	GO:0015399	primary active transmembrane transporter activity	9/646	123/17258	0.04147331	0.38661999	ATP6V1C2/ABCB6/ABCB4/ABCC2/ABCC6/ABCC9/ATP6V0C/ATP6AP1L/ATP2C2	9
MF	GO:0015405	P-P-bond-hydrolysis-driven transmembrane transporter activity	9/646	123/17258	0.04147331	0.38661999	ATP6V1C2/ABCB6/ABCB4/ABCC2/ABCC6/ABCC9/ATP6V0C/ATP6AP1L/ATP2C2	9
MF	GO:0001614	purinergic nucleotide receptor activity	3/646	21/17258	0.04204765	0.38661999	P2RY6/P2RY2/P2RX6	3
MF	GO:0016502	nucleotide receptor activity	3/646	21/17258	0.04204765	0.38661999	P2RY6/P2RY2/P2RX6	3
MF	GO:0046961	proton-transporting ATPase activity, rotational mechanism	3/646	21/17258	0.04204765	0.38661999	ATP6V1C2/ATP6V0C/ATP6AP1L	3

Additional Table 14 Candidate miRNAs binding to circ_0002538 predicted by RNAhybrid, miRanda and TargetScan

circRNA	miRNA	miRanda	targetscan	RNAhybrid
hsa_circ_0002538	hsa-miR-519e-5p	0	1	1
hsa_circ_0002538	hsa-miR-3659	0	1	1
hsa_circ_0002538	hsa-miR-4659a-3p	1	0	1
hsa_circ_0002538	hsa-miR-548q	0	1	1
hsa_circ_0002538	hsa-let-7g-3p	1	1	0
hsa_circ_0002538	hsa-miR-449c-5p	0	1	1
hsa_circ_0002538	hsa-miR-3691-5p	1	0	1
hsa_circ_0002538	hsa-miR-513c-5p	1	1	1
hsa_circ_0002538	hsa-miR-376b-3p	0	1	1
hsa_circ_0002538	hsa-miR-298	1	1	1
hsa_circ_0002538	hsa-miR-6858-5p	0	1	1
hsa_circ_0002538	hsa-miR-6501-5p	0	1	1
hsa_circ_0002538	hsa-miR-1910-3p	1	1	1
hsa_circ_0002538	hsa-miR-548as-3p	1	1	1
hsa_circ_0002538	hsa-miR-6826-3p	0	1	1
hsa_circ_0002538	hsa-miR-211-5p	1	0	1
hsa_circ_0002538	hsa-miR-181c-3p	1	1	1
hsa_circ_0002538	hsa-miR-145-3p	1	1	1
hsa_circ_0002538	hsa-miR-4677-5p	0	1	1
hsa_circ_0002538	hsa-miR-4650-3p	0	1	1
hsa_circ_0002538	hsa-miR-6831-5p	1	1	1
hsa_circ_0002538	hsa-miR-548ay-3p	0	1	1
hsa_circ_0002538	hsa-miR-6770-5p	0	1	1
hsa_circ_0002538	hsa-miR-6879-5p	1	0	1
hsa_circ_0002538	hsa-miR-3689a-5p	1	0	1
hsa_circ_0002538	hsa-miR-3154	0	1	1
hsa_circ_0002538	hsa-miR-1185-5p	0	1	1
hsa_circ_0002538	hsa-miR-4632-5p	1	0	1
hsa_circ_0002538	hsa-miR-3689b-5p	1	0	1
hsa_circ_0002538	hsa-miR-6873-5p	1	0	1
hsa_circ_0002538	hsa-miR-6758-5p	1	1	1
hsa_circ_0002538	hsa-miR-3127-3p	0	1	1
hsa_circ_0002538	hsa-miR-4446-5p	0	1	1
hsa_circ_0002538	hsa-miR-489-3p	1	1	1
hsa_circ_0002538	hsa-miR-4436b-3p	1	0	1
hsa_circ_0002538	hsa-miR-7978	0	1	1
hsa_circ_0002538	hsa-miR-3927-3p	0	1	1
hsa_circ_0002538	hsa-miR-6878-5p	1	0	1
hsa_circ_0002538	hsa-miR-4458	1	0	1
hsa_circ_0002538	hsa-miR-4451	0	1	1
hsa_circ_0002538	hsa-miR-4453	0	1	1
hsa_circ_0002538	hsa-miR-4456	0	1	1
hsa_circ_0002538	hsa-miR-6827-5p	1	0	1
hsa_circ_0002538	hsa-miR-450b-5p	0	1	1
hsa_circ_0002538	hsa-miR-204-5p	1	0	1
hsa_circ_0002538	hsa-miR-130a-5p	1	1	1
hsa_circ_0002538	hsa-miR-4301	0	1	1
hsa_circ_0002538	hsa-miR-197-5p	1	1	1
hsa_circ_0002538	hsa-miR-3670	0	1	1
hsa_circ_0002538	hsa-miR-574-5p	1	1	1
hsa_circ_0002538	hsa-miR-877-3p	0	1	1
hsa_circ_0002538	hsa-miR-4504	0	1	1
hsa_circ_0002538	hsa-miR-376a-3p	0	1	1
hsa_circ_0002538	hsa-miR-6777-3p	0	1	1
hsa_circ_0002538	hsa-miR-589-5p	0	1	1
hsa_circ_0002538	hsa-miR-3913-3p	0	1	1
hsa_circ_0002538	hsa-miR-3118	0	1	1
hsa_circ_0002538	hsa-miR-4299	0	1	1
hsa_circ_0002538	hsa-miR-1304-5p	0	1	1
hsa_circ_0002538	hsa-miR-3162-5p	1	0	1
hsa_circ_0002538	hsa-miR-127-5p	0	1	1
hsa_circ_0002538	hsa-let-7a-2-3p	1	1	0
hsa_circ_0002538	hsa-miR-5197-3p	0	1	1
hsa_circ_0002538	hsa-miR-146b-5p	0	1	1
hsa_circ_0002538	hsa-miR-185-5p	1	0	1
hsa_circ_0002538	hsa-miR-4769-3p	1	1	0

hsa_circ_0002538	hsa-miR-22-5p	0	1	1
hsa_circ_0002538	hsa-miR-10526-3p	0	1	1
hsa_circ_0002538	hsa-miR-3925-5p	1	1	1
hsa_circ_0002538	hsa-miR-3059-5p	0	1	1
hsa_circ_0002538	hsa-miR-6817-5p	1	1	1
hsa_circ_0002538	hsa-miR-2116-5p	0	1	1
hsa_circ_0002538	hsa-miR-892c-5p	0	1	1
hsa_circ_0002538	hsa-miR-4689	0	1	1
hsa_circ_0002538	hsa-miR-6885-3p	0	1	1
hsa_circ_0002538	hsa-miR-605-3p	1	1	1
hsa_circ_0002538	hsa-miR-6735-5p	1	0	1
hsa_circ_0002538	hsa-miR-4659b-5p	0	1	1
hsa_circ_0002538	hsa-miR-4306	1	0	1
hsa_circ_0002538	hsa-miR-4658	1	1	1
hsa_circ_0002538	hsa-miR-3610	1	0	1
hsa_circ_0002538	hsa-miR-616-5p	1	1	0
hsa_circ_0002538	hsa-miR-6782-5p	1	0	1
hsa_circ_0002538	hsa-miR-548ag	0	1	1
hsa_circ_0002538	hsa-miR-1267	0	1	1
hsa_circ_0002538	hsa-miR-3689e	1	0	1
hsa_circ_0002538	hsa-miR-4661-3p	0	1	1
hsa_circ_0002538	hsa-miR-6808-5p	1	1	1
hsa_circ_0002538	hsa-miR-384	0	1	1
hsa_circ_0002538	hsa-miR-4659b-3p	1	0	1
hsa_circ_0002538	hsa-miR-3907	0	1	1
hsa_circ_0002538	hsa-miR-6511a-5p	1	1	1
hsa_circ_0002538	hsa-miR-6884-3p	0	1	1
hsa_circ_0002538	hsa-miR-616-3p	1	0	1
hsa_circ_0002538	hsa-miR-138-5p	1	1	1
hsa_circ_0002538	hsa-miR-6780a-3p	0	1	1
hsa_circ_0002538	hsa-miR-2117	0	1	1
hsa_circ_0002538	hsa-miR-3164	1	1	1
hsa_circ_0002538	hsa-miR-3714	0	1	1
hsa_circ_0002538	hsa-miR-142-3p	1	0	1
hsa_circ_0002538	hsa-miR-6808-3p	0	1	1
hsa_circ_0002538	hsa-miR-3680-5p	1	0	1
hsa_circ_0002538	hsa-miR-4786-3p	0	1	1
hsa_circ_0002538	hsa-miR-744-3p	0	1	1
hsa_circ_0002538	hsa-miR-4695-5p	1	0	1
hsa_circ_0002538	hsa-miR-4758-5p	0	1	1
hsa_circ_0002538	hsa-miR-6880-5p	1	0	1
hsa_circ_0002538	hsa-miR-3132	1	1	1
hsa_circ_0002538	hsa-miR-146a-5p	0	1	1
hsa_circ_0002538	hsa-miR-6856-5p	1	1	1
hsa_circ_0002538	hsa-miR-8070	0	1	1
hsa_circ_0002538	hsa-miR-4423-5p	1	1	1
hsa_circ_0002538	hsa-miR-136-5p	1	1	1
hsa_circ_0002538	hsa-miR-6755-5p	0	1	1
hsa_circ_0002538	hsa-miR-6745	1	0	1
hsa_circ_0002538	hsa-miR-4289	1	1	1
hsa_circ_0002538	hsa-miR-134-5p	0	1	1
hsa_circ_0002538	hsa-miR-6832-5p	1	1	1
hsa_circ_0002538	hsa-miR-2682-5p	0	1	1
hsa_circ_0002538	hsa-miR-6893-5p	1	1	1
hsa_circ_0002538	hsa-miR-576-3p	0	1	1
hsa_circ_0002538	hsa-miR-6760-5p	1	0	1
hsa_circ_0002538	hsa-miR-507	0	1	1
hsa_circ_0002538	hsa-miR-3935	0	1	1
hsa_circ_0002538	hsa-miR-499a-3p	0	1	1
hsa_circ_0002538	hsa-miR-4732-5p	0	1	1
hsa_circ_0002538	hsa-miR-942-5p	0	1	1
hsa_circ_0002538	hsa-miR-6790-5p	1	1	1
hsa_circ_0002538	hsa-miR-1238-5p	0	1	1
hsa_circ_0002538	hsa-miR-7843-3p	0	1	1

circ_0002538: hsa_circ_0002538; circRNA: circular RNAs; miRNA: microRNA.

Additional Table 15 The candidate miRNAs binding to PLLP predicted by miRDB, miRTarBase, miRWalk and TargetScan

miRNA	ID	GENE	miRDB	miRTarBase	miRWalk	TargetScan
hsa-miR-6785-5p	MIMAT0027470	PLLP	1	1	1	1
hsa-miR-1258	MIMAT0005909	PLLP	1	0	1	1
hsa-miR-1273e	MIMAT0018079	PLLP	0	1	1	1
hsa-miR-1289	MIMAT0005879	PLLP	1	0	1	1
hsa-miR-1295b-5p	MIMAT0022293	PLLP	0	1	1	1
hsa-miR-138-5p	MIMAT0000430	PLLP	1	0	1	1
hsa-miR-1470	MIMAT0007348	PLLP	1	0	1	1
hsa-miR-149-3p	MIMAT0004609	PLLP	1	1	1	0
hsa-miR-181a-2-3p	MIMAT0004558	PLLP	1	0	1	1
hsa-miR-1827	MIMAT0006767	PLLP	0	1	1	1
hsa-miR-185-3p	MIMAT0004611	PLLP	1	0	1	1
hsa-miR-186-3p	MIMAT0004612	PLLP	1	0	1	1
hsa-miR-18a-5p	MIMAT0000072	PLLP	1	0	1	1
hsa-miR-25-5p	MIMAT0004498	PLLP	0	1	1	1
hsa-miR-302f	MIMAT0005932	PLLP	0	1	1	1
hsa-miR-30c-1-3p	MIMAT0004674	PLLP	0	1	1	1
hsa-miR-3122	MIMAT0014984	PLLP	0	1	1	1
hsa-miR-3714	MIMAT0018165	PLLP	0	1	1	1
hsa-miR-3909	MIMAT0018183	PLLP	1	0	1	1
hsa-miR-3910	MIMAT0018184	PLLP	0	1	1	1
hsa-miR-3937	MIMAT0018352	PLLP	0	1	1	1
hsa-miR-3975	MIMAT0019360	PLLP	0	1	1	1
hsa-miR-4251	MIMAT0016883	PLLP	1	0	1	1
hsa-miR-4283	MIMAT0016914	PLLP	1	0	1	1
hsa-miR-4291	MIMAT0016922	PLLP	1	0	1	1
hsa-miR-4473	MIMAT0019000	PLLP	1	0	1	1
hsa-miR-450a-1-3p	MIMAT0022700	PLLP	0	1	1	1
hsa-miR-454-3p	MIMAT0003885	PLLP	1	0	1	1
hsa-miR-4667-3p	MIMAT0019744	PLLP	1	0	1	1
hsa-miR-4671-3p	MIMAT0019753	PLLP	1	0	1	1

hsa-miR-4673	MIMAT0019755	PLLP	1	0	1	1
hsa-miR-4728-5p	MIMAT0019849	PLLP	1	1	1	0
hsa-miR-4768-5p	MIMAT0019920	PLLP	1	0	1	1
hsa-miR-512-3p	MIMAT0002823	PLLP	1	0	1	1
hsa-miR-548az-3p	MIMAT0025457	PLLP	1	0	1	1
hsa-miR-582-3p	MIMAT0004797	PLLP	1	0	1	1
hsa-miR-6504-3p	MIMAT0025465	PLLP	1	0	1	1
hsa-miR-6509-3p	MIMAT0025475	PLLP	1	0	1	1
hsa-miR-6513-5p	MIMAT0025482	PLLP	0	1	1	1
hsa-miR-654-3p	MIMAT0004814	PLLP	1	0	1	1
hsa-miR-6739-5p	MIMAT0027379	PLLP	1	0	1	1
hsa-miR-6799-5p	MIMAT0027498	PLLP	0	1	1	1
hsa-miR-6829-5p	MIMAT0027558	PLLP	1	0	1	1
hsa-miR-6883-5p	MIMAT0027666	PLLP	1	1	1	0
hsa-miR-7113-5p	MIMAT0028123	PLLP	1	0	1	1
hsa-miR-7162-5p	MIMAT0028234	PLLP	1	0	1	1
hsa-miR-887-5p	MIMAT0026720	PLLP	0	1	1	1
hsa-miR-940	MIMAT0004983	PLLP	0	1	1	1

PLLP: Plasmolipin.

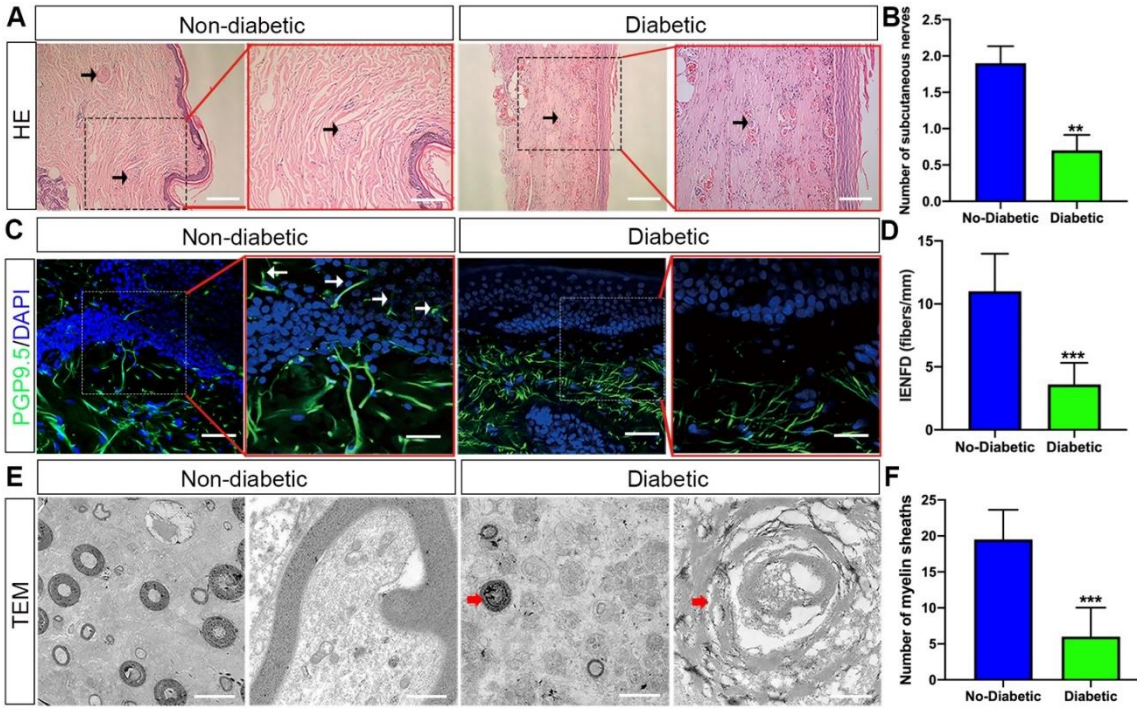

Additional Figure 1 Confirmation of DPN in the collected peripheral nerve tissues.

(A, B) HE staining showed that the number of subcutaneous nerves (arrows) in the skin 10 cm above the lateral malleolus of patients with diabetes was decreased compared with that of patients without diabetes. The arrows point to subcutaneous nerves. Scale bars: 200 μm; 100 μm (high-magnification images). (C, D) The IF micrographs showed IENFD (arrows) in the skin of patients with diabetes was decreased than that of patients without diabetes. The images on the right are the high-magnification images in the square of the images on the left. The arrows pointed to PGP9.5 positive nerve fibers. Scale bars: 50 μm; 25 μm (high-magnification images). (E, F) TEM showed that the number of axons and intact myelin sheaths were decreased in the sural nerves of patients with diabetes. Arrows indicate abnormal myelin sheaths. Scale bars: 10 μm (left); 1 μm (right). Data are expressed as mean ± SD (n = 10). **P < 0.01, **P < 0.001, *vs*. no-diabetes (independent-sample t-test). HE: Hematoxylin and eosin; IENFD: intraepidermal nerve fiber density; IF: immunofluorescence staining; PGP9.5: protein gene product 9.5; TEM: transmission electron microscopy.

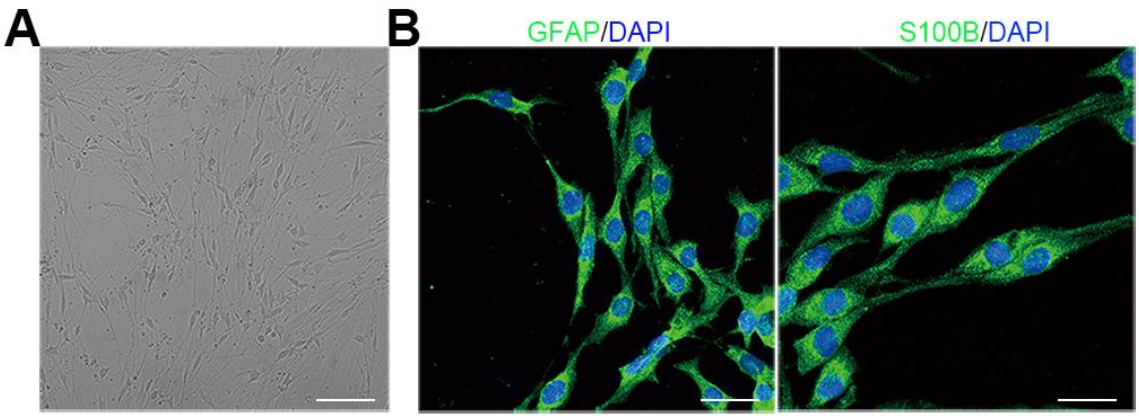

Additional Figure 2 Identification of SCs isolated from sural nerves of patients.

(A) The isolated SCs exhibited a long spindle shape under an optical microscope. Scale bar: 200 μm. (B) The positive SC markers, S100B (Fluor® 488) and GFAP (Fluor® 488), indicated that the isolated cells were SCs. Scale bars: 50 μm. DAPI: 2-(4-Amidinophenyl)-6-indolecarbamidine dihydrochloride; GFAP: glial fibrillary acidic protein; IF: immunofluorescence; S100B: S100 calcium binding protein B.

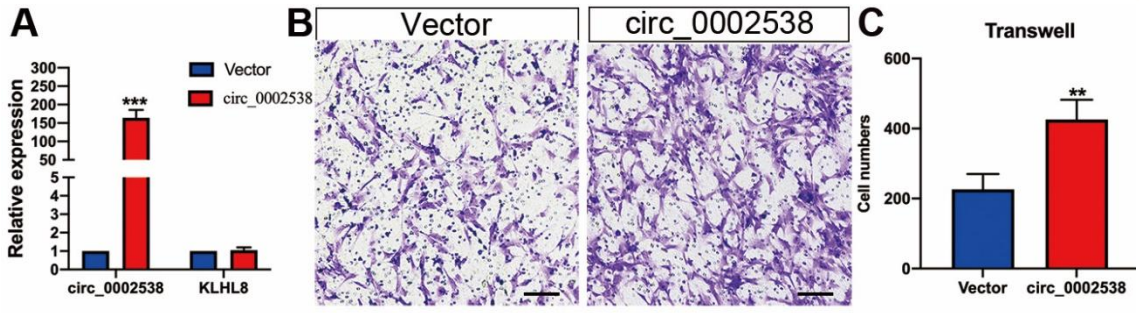

Additional Figure 3 Overexpression of circ_0002538 promotes SC migration.

(A) As assessed by RT-PCR, circ_0002538 was increased in circ_0002538-overexpressing SCs, while KLHL8 mRNA did not change significantly. Y-axis: fold changes of RNA expressions compared with the vector group. (B, C) Migration assays showed that overexpression of circ_0002538 increased the number of SCs that migrated to the lower chamber. Scale bars: 100 μm. All bar graphs represent the average of three independent replicates, and the error bars are the SD. $^{**}P < 0.01$, $^{***}P < 0.001$, *vs.* vector group (independent-sample *t*-test). KLHL8: Kelch-like family member 8; RT-PCR: Real-time polymerase chain reaction; SCs: Schwann cells.

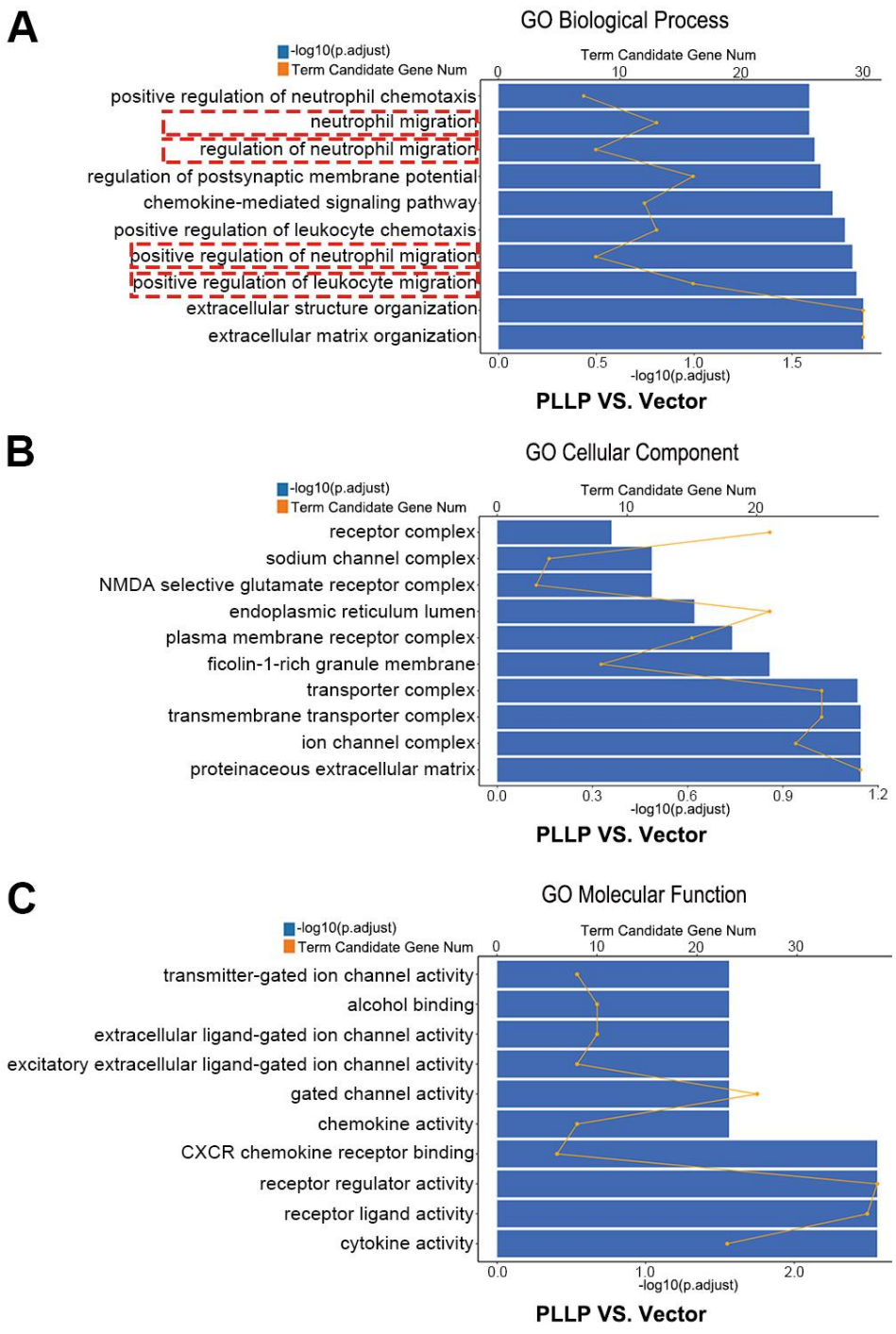

Additional Figure 4 The filtered mRNAs in the mRNA-sequencing results of the PLLP-overexpressing SCs and the control SCs were further analyzed with GO enrichment analysis.

(A) GO biological process analysis. The red dotted box highlighted the interesting biological process. (B) GO cellular component analysis. (C) GO molecular function analysis. GO: Gene Ontology; PLLP: plasmolipin; SCs: Schwann cells.